NIES-GOSAT2-ALG-20191008-012-00

GOSAT-2 TANSO-FTS-2 SWIR L2 Retrieval Algorithm Theoretical Basis Document

December 2020

National Institute for Environmental Studies
GOSAT-2 Project

YOSHIDA Yukio[1)]
OSHIO Haruki[1)]

1) Center for Global Environmental Research, National Institute for Environmental Studies

CONTENTS

1. Introduction

This Algorithm Theoretical Basis Document (ATBD) describes the algorithms to retrieve chlorophyll fluorescence as well as column-averaged dry-air mole fractions of carbon dioxide (CO_2), methane (CH_4), and carbon monoxide (CO) from the SWIR radiance spectrum data observed by TANSO-FTS-2 onboard GOSAT-2 (TANSO-FTS-2 L1B Product), and generate "TANSO-FTS-2 SWIR L2 Chlorophyll Fluorescence and Proxy-method Product" and "TANSO-FTS-2 SWIR L2 Column-averaged Dry-air Mole Fraction Product".

1.1 Scope of the Algorithm

Figure 1.1-1 shows the whole processing flow of GOSAT-2 data analysis. The scope of application in this ATBD is the yellow-colored part in the figure.

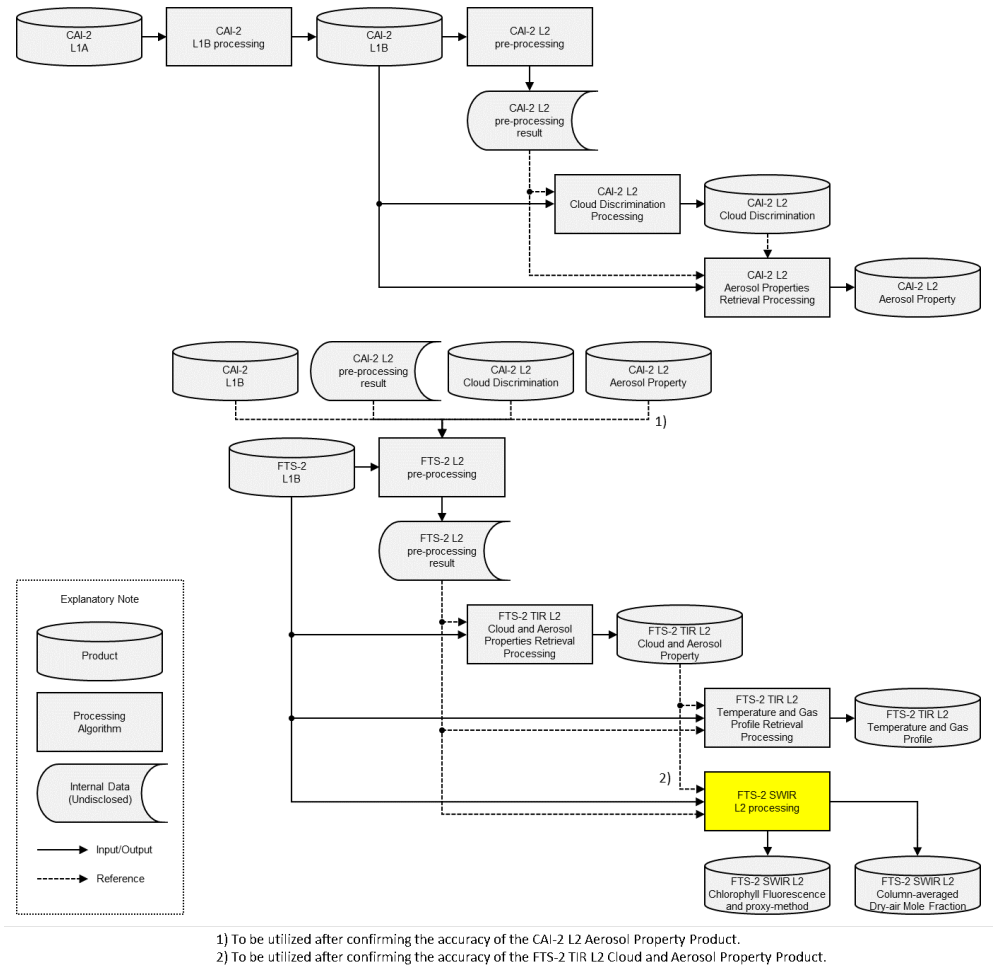

Figure 1.1-1. The scope of the algorithm described in this ATBD in the processing flow of GOSAT-2 data analysis.

1.2 Baseline Documents

Related documents of the ATBD are as follows.

(1) Algorithm Theoretical Basis Document for Greenhouse gases Observing SATellite-2 (GOSAT-2)

(2) GOSAT-2/TANSO-FTS-2 Level 1 Product Description Document

(3) GOSAT-2 TANSO-FTS-2 L2 Pre-processing Algorithm Theoretical Basis Document

(4) GOSAT-2 TANSO-FTS-2 TIR L2 Cloud and Aerosol Property Retrieval Processing Algorithm Theoretical Basis Document

(5) NIES GOSAT-2 Product Format Descriptions (Product edition)

- Vol. 4: GOSAT-2 TANSO-FTS-2 SWIR L2 Chlorophyll Fluorescence and Proxy-method Product
- Vol. 5: GOSAT-2 TANSO-FTS-2 SWIR L2 Column-averaged Dry-air Mole Fraction Product
- Vol. 6: GOSAT-2 TANSO-FTS-2 TIR L2 Cloud and Aerosol Product

2. Backgrounds

2.1 Overview of Observation Instruments

GOSAT-2 carries two sensors: Thermal And Near-infrared Sensor for carbon Observation-Fourier Transform Spectrometer 2 (TANSO-FTS-2, hereinafter, "FTS-2") and TANSO-Cloud and Aerosol Imager 2 (TANSO-CAI-2, hereinafter, "CAI-2"). FTS-2 is a Fourier transform spectrometer which has three bands in the short wavelength infrared (SWIR) regions and two bands in the thermal infrared (TIR) regions. It observes any points up to ±40° in the along track (AT) direction and ±35° in the cross track (CT) direction, within 15.8 mrad of the instantaneous field of view (IFOV) (equivalent to a circle with a diameter of about 9.7 km at the nadir point of the satellite), by using the two-axis pointing control mechanisms (Note: the range of the angle corresponds to the range of the angle of viewing vector, but not to the range of motor-rotation angle around the point mechanism's axis). CAI-2 is an electronic scanning imager which has each five bands of forward and backward viewing (±20°) from the nadir point of the satellite in the along track direction from ultraviolet to short wavelength infrared bands, 10 bands in total. It observes the 920-km field of view (FOV) in the cross track direction with spatial resolution of 0.46 km or 0.92 km. The specifications of FTS-2 and CAI-2 are summarized in Table 2.1-1 and Table 2.1-2, respectively.

FTS-2 introduces light observed from arbitrary directions into the interferometer via the pointing mechanism. The interference light is split into the wavenumber region of each band by multiple dichroic mirrors and bandpass filters. The three SWIR bands are further divided into two polarization components by the polarization beam splitter and an interferogram is recorded by the detector. The time necessary to acquire an interferogram is 4.024 sec. The pointing mechanism is also used to point to the same point during the interferogram acquisition. In addition, observations over ocean are made pointing in the direction of the specular reflection point (sunglint observation mode), since the reflectance of water is low except around the specular reflection point.

FTS-2 performs the solar irradiation calibration on the orbit using a diffuser plate, and also performs the instrument line shape function calibration, blackbody calibration, and deep space calibration by pointing its pointing mechanism to the internal calibration source. In addition, the lunar calibration is carried out at the night side by pointing the satellite body in the opposite direction to the earth's center.

CAI-2 has a wide FOV in the cross-track direction of the satellite orbit to observe spatial distributions of clouds and aerosols. Over the ocean, high reflectance around the specular reflection point making it difficult to discriminate clouds. CAI-2 observes same location from the two directions, forward and backward, and even if one of the viewing directions approaches to the specular reflectance point, the other is deviated from the point, so that the accuracy of the cloud discrimination can improve.

The FTS-2 TIR is operated in both day side and night side while the operations of the FTS-2 SWIR and CAI-2 are limited to the day side area on the ground. FTS-2 also equips a high-resolution monitoring camera (CAM) to check the FTS-2 FOV, which is not a mission instrument but takes images interlocking with the interferogram acquisition in the day side.

Table 2.1-1. Specifications of TANSO-FTS-2.

	Band 1	Band 2	Band 3	Band 4	Band 5
Polarization observation	Yes	Yes	Yes	No	No
Spectral coverage [cm^{-1}]	12950 - 13250	5900 - 6400	4200 - 5200	1188 - 1800	700 - 1188
FWHM of the instrument line shape function	< 0.4 cm^{-1}	< 0.27 cm^{-1}	< 0.27 cm^{-1}	< 0.27 cm^{-1}	< 0.27 cm^{-1}
Sampling step	< 0.2 cm^{-1}	< 0.2 cm^{-1}	< 0.2 cm^{-1}	< 0.2 cm^{-1}	< 0.2 cm^{-1}
Interval time of data acquisition	Approx. 4.67 sec. (Time required for interferogram acquisition: 4.024 sec.)				
IFOV	15.8 mrad (Diameter projected on the earth's surface at the nadir point of the satellite: approx. 9.7 km)				
FOV	±40° (Along track direction), ±35° (Cross track direction)				

Table 2.1-2. Specifications of TANSO-CAI-2.

	Band 1 / 6	Band 2 / 7	Band 3 / 8	Band 4 / 9	Band 5 / 10
Optical Tube	Tube 1	Tube 2	Tube 3	Tube 4	Tube 5
Viewing direction	Forward viewing (+20° in AT direction) / Backward viewing (-20° in AT direction)				
Center wavelength [μm]	0.343 / 0.380	0.443 / 0.550	0.674	0.869	1.63
Wavelength width [μm]	< 0.02	< 0.02	< 0.02	< 0.02	< 0.09
Resolution	0.46 km				0.92 km
Effective pixels	2048				958
Swath	920 km				

3. Input and Output Data

3.1 Input Data

The input data for FTS-2 SWIR L2 processing is FTS-2 L1B Product. FTS-2 L1B Product consists of “Common file” that stores information common to SWIR and TIR, “SWIR file” that stores SWIR information, and “TIR file” that stores TIR information. One scene data of FTS-2 L1B Product is defined as one span data divided one revolution data into four, starting at ascending node. Scene 01 stores data from ascending node to the end of night side observation. Scene 02 stores data from the start of day side observation to descending node. Scene 03 stores data from descending node to the end of day side observation. Scene 04 stores data from the start of night side observation to next ascending node. The place where day side observation and night side observation are switched depends on season. Because the operation of FTS-2 SWIR is limited to day side, FTS-2 L1B SWIR files exist only Scenes 02 and 03. FTS-2 SWIR L2 processing only uses the SWIR file. In the following part, “FTS-2 L1B Product” shall refer to its SWIR file. Table 3.1-1 shows the list of input data for FTS-2 SWIR L2 processing. Note that some part of the processing were already done in the FTS-2 L2 pre-processing (see Subsection 3.3.1). How to calculate these values are described in “GOSAT-2 TANSO-FTS-2 L2 Pre-processing Algorithm Theoretical Basis Document” (Section 1.2 (3)). Also note that Table 3.1-1 does not contain any data that is simply copied into the output data described in Section 3.2.

Table 3.1-1. Dataset of FTS-2 L1B SWIR file for FTS-2 SWIR L2 processing.

Dataset name	Explanation	Unit
SoundingAttribute		
numSoundings	Number of observation data stored in file.	
observationTime	FTS-2 observation time. The central time of interferogram acquisition time of 4.024 sec.	
QualityInfo		
soundingQualityFlag	Quality of each observation point on a four level scale: Good/Fair/Poor/NG	
dataInvalidFlag	The flag which indicates if the observation is “valid”.	
IMC_StabilityFlag	IMC stability flag.	
missingFlag	Missing data flag.	
saturationFlag	Interferogram saturation flag.	
spikeFlag	Spike flag.	
scanStabilityFlag	Scan stability flag.	
SNR	Simplified calculated SNR.	
interferogramQualityFlag	Interferogram quality flag.	
spectrumQualityFlag	Spectrum quality flag.	
SatelliteGeometry		
yawSteeringFlag	Yaw steering flag indicates the execution of yaw steering.	
SoundingGeometry		
solarDistance	Distance from the sun to observation point at observation time.	AU
SoundingData		
WavenumberInfo		
numWN	Number of spectrum data.	
beginWN	Beginning wavenumber of spectrum data.	cm^{-1}
deltaWN	Interval of wavenumber of spectrum data.	cm^{-1}
RawSpectrum		
band1P	Band 1P spectrum data before sensitivity correction.	V/cm^{-1}
band1S	Band 1S spectrum data before sensitivity correction.	V/cm^{-1}
band2P	Band 2P spectrum data before sensitivity correction.	V/cm^{-1}
band2S	Band 2S spectrum data before sensitivity correction.	V/cm^{-1}
band3P	Band 3P spectrum data before sensitivity correction.	V/cm^{-1}
band3S	Band 3S spectrum data before sensitivity correction.	V/cm^{-1}

3.2 Output Data

From the FTS-2 SWIR L2 processing, “FTS-2 SWIR L2 Chlorophyll Fluorescence and Proxy-method Product” and “FTS-2 SWIR L2 Column-averaged Dry-air Mole Fraction Product” are generated.

3.2.1 FTS-2 SWIR L2 Chlorophyll Fluorescence and Proxy-method Product

FTS-2 SWIR L2 Chlorophyll Fluorescence and Proxy-method Product includes solar-induced chlorophyll fluorescence, XCH_4 (proxy), XCO (proxy), and several parameters related to optical path length modifications, those calculated from the six individual retrieval results obtained under the assumption of cloud- and aerosol-free condition. For details of the included dataset, refer to the document, “NIES GOSAT-2 Product File Format Description (Product edition) Vol. 4: GOSAT-2 TANSO-FTS-2 SWIR L2 Chlorophyll Fluorescence and Proxy-method Product”.

3.2.2 FTS-2 SWIR L2 Column-averaged Dry-air Mole Fraction Product

FTS-2 SWIR L2 Column-averaged Dry-air Mole Fraction Product includes XCO_2, XCH_4, XCO, and XH_2O simultaneously retrieved by so-called full-physics method for cases where the effect of optical path length modification due to clouds and aerosols is relatively small. For details of the included dataset, refer to the document, “NIES GOSAT-2 Product File Format Description (Product edition) Vol. 5: GOSAT-2 TANSO-FTS-2 SWIR L2 Column-averaged Dry-air Mole Fraction Product”.

3.3 Reference Data and Intermediate Output File

3.3.1 Reference Data for Retrieval Component

The reference data used in the retrieval component of the FTS-2 SWIR L2 processing are listed in Table 3.3.1-1

Table 3.3.1-1. Reference data used in the retrieval component of FTS-2 SWIR L2 processing.

Reference data	Reference items
FTS-2 L2 pre-processing result [1)]	Following variables corresponding to the center of FTS-2 IFOV after Ortho-correction. Solar zenith angle [deg.] and azimuth angle [deg.], satellite zenith angle [deg.] and azimuth angle [deg.]. Angle between radiative transfer reference plane and scan mirror reflection reference plane [deg.], incident angle to scan mirror [deg.], angle between scan mirror reflection reference plane and FTS-2 detector reference plane [deg.], angle between polarization plane of observation light and radiative transfer reference plane [deg.]. Doppler velocity for the sun and the satellite [m/s]. Total number of grid points and number of land-grid points within FTS-2 IFOV-area for land/sea mask data. Cloud determination result by CAI-2 L2 Cloud Discrimination Product. Cloud determination result by each polarization component of FTS-2 2 μm band. Following variables corresponding to FTS-2 observation time and space. The number of layers in each vertical profile and the type of aerosol are based on the source data. Surface pressure [hPa], surface wind speed (east-west wind, north-south wind) [m/s], and variance of surface wind speed [$(m/s)^2$]. Vertical profiles of pressure [hPa], temperature [K], geopotential height [m], and gravitational acceleration [m/s^2]. Vertical profiles of concentrations [ppm] and variance-covariance matrix [ppm^2] of H_2O, CO_2, O_3, N_2O, CO, CH_4. Aerosol mass mixing ratio profile [kg/kg].
FTS-2 SWIR instrument characteristics [2)]	Time-dependent degradation factor, complex refractive index of scan mirror, instrument line shape function, optical efficiency of FTS-2 without scan mirror [$V/cm^{-1}/(W/cm^2/str/cm^{-1})$].

Reference data	Reference items
Optical thickness for reference spectrum [3)]	Absorption optical thickness of the US standard atmosphere with increased CO_2 concentration of 380 ppm.
Solar irradiance data [4)]	Solar irradiance spectrum [$W/cm^2/cm^{-1}$] at a distance of one astronomical unit from the sun
LUT for molecular absorption cross-section [5)]	Look-up table (LUT) for molecular absorption cross-section [cm^2/molecules] over the range of relevant wavenumber, temperatures, and pressures.
LUT for scattering properties of aerosol [6)]	LUT for mass extinction coefficient [cm^2/g], mass scattering coefficient [cm^2/g], and scattering phase matrix, corresponding to the aerosol components of the aerosol transport model, SPRINTARS, over the relevant wavelength and relative humidity.
LUT for scattering properties of cloud [7)]	LUT for cirrus extinction coefficient normalized by ice water content [m^2/g], single scattering albedo, and scattering phase matrix over the relevant wavelength and effective particle size of ice particles.

1) See "GOSAT-2 TANSO-FTS-2 L2 Pre-processing Algorithm Theoretical Basis Document" (Section 1.2 (3)) for details.

2) Source information are stored in "TANSO-FTS-2 instrument characteristic information" available via GOSAT-2 Product Archive (https://prdct.gosat-2.nies.go.jp/). The provided information are used as is for the time-dependent degradation factor (RAD_Time_Wave_Deg) and the complex refractive index of scan mirror (SCANNER_REFRACTION), and pre-processed for the instrument line shape function (ILSF) and the optical efficiency of FTS-2 without scan mirror. The provided P- and S-polarization components ILSF (ILSF_P and ILSF_S) are adjusted to come to a peak at the wavenumber difference of 0 cm^{-1} and normalized with the integrated value of 1 for FTS-2 SWIR L2 processing. These normalized ILSF for P- and S-polarization components are averaged and used as ILSF for total intensity. The optical efficiency of FTS-2 without scan mirror is the reciprocal of the provided radiance conversion coefficient (Rad_CNV).

3) The optical thickness is calculated using LUT for molecular absorption cross-section shown in Table 3.3.1-1. The wavenumber interval is determined according the LUT.

4) The Solar Pseudo-Transmittance Spectrum (Disk-Integrated Spectrum, 2015 version) (Toon, 2015b) is used as the solar Fraunhofer line model.

5) Table 3.3.1-2 shows line parameters and references to calculate the LUT for molecular absorption cross-section. The LUT has 70 pressure grid points between 0.06 hPa and 1040 hPa in a logarithmic scale, and 10 temperature grid points for each pressure are set in the width of 90 K at an interval of 10 K each centering the temperature value of the U.S. standard atmosphere. For continuous absorption, the LUT has only 21 temperature grid points between 150 K and 350 K at

interval of 10 K.

6) The LUT for scattering properties of aerosol has 18 wavelength grid points at 0.3, 0.35, 0.4, 0.45, 0.5, 0.55, 0.6, 0.65, 0.7, 0.75, 0.8, 0.9, 1.0, 1.25, 1.5, 1.75, 2.0, and 2.5 μm. To consider the aerosol hygroscopic growth effect, the LUT also has 8 relative humidity grid points at 0.0, 0.5, 0.7, 0.8, 0.9, 0.95, 0.98, and 0.99. Scattering properties of hygroscopic aerosols are prepared for each relative humidity value, therefore, the LUT contains scattering properties for a total of 75 aerosol components of all 19 aerosol species treated by SPRINTARS.
7) Only cirrus cloud is considered in the FTS-2 SWIR L2 processing. The LUT of scattering properties of cloud contains the scattering properties extracted based on the General Habit Mixture V3.6 from the Ice Cloud Bulk Scattering Models by Baum et al. (2014). The number of wavelength grid points is 70 in the ranges 0.55, 0.75-0.78, 1.56-1.73, 1.92-2.38 μm at 0.01 μm intervals, whereas the number of effective particle size grid points is 23 ranging from 10 to 120 μm at 5 μm intervals.

Table 3.3.1-2. Line parameters and references used for the calculation of LUT for molecular absorption cross-section. LM, CIA, and SDV denotes line mixing, collision induced absorption, and speed-dependent Voigt, respectively.

FTS-2 Band	Gas	Line parameter	Reference
1	O_2	ABSCO V5.0 (LM, CIA)	Drouin et al. (2017)
	O_3 continuum	MT_CKD	Mlawer et al. (2012)
2	H_2O	ATM line list	Toon (2015a)
	CO_2	Lamouroux et al. (2010) (LM)	Lamouroux et al. (2010)
	CH_4	$^{12}CH_4$ $2\nu_3$ (SDV + LM) others HITRAN 2016	Devi et al. (2015, 2016) Gordon et al. (2017)
	H_2O continuum	MT_CKD	Mlawer et al. (2012)
3	H_2O	ATM line list	Toon (2015a)
	CO_2	Lamouroux et al. (2010) (LM)	Lamouroux et al. (2010)
	CO	$^{12}C^{16}O$ 2ν (SDV + LM) others HITRAN 2016	Devi et al. (2012) Gordon et al. (2017)
	CH_4	ATM line list	Toon (2015a)
	H_2O continuum	MT_CKD	Mlawer et al. (2012)

3.3.2 Processing Results by Retrieval Component

The processing results by the retrieval component of FTS-2 SWIR L2 processing are listed in Table 3.3.2-1. The processing results by the retrieval (SIF & proxy method) and the retrieval (full-physics method) are used as input in the post-processing component (chlorophyll fluorescence

and proxy method) and the post-processing component (column-averaged dry-air mole fraction), respectively.

Table 3.3.2-1. Processing results by the retrieval component of FTS-2 SWIR L2 processing.

Category	Output data
Retrieval result	Land fraction within the FTS-2 IFOV-area and SNR for polarization synthesized spectrum for each sounding. Pre-screening and iteration convergence results for each retrieval and each sounding. When sounding passed the pre-screening, following variables are stored. Number of iterations, state vector, flag indicating whether or not each state vector element satisfies the constraint condition, chi-squared, and mean squared of the residual spectrum for each sub-band. Furthermore, when state vector includes gas concentration, following variables are stored. Pressure at each boundary of Main-layer, pressure weighting function, total column amount of dry-air for retrieval state as well as a priori state. Retrieved value, a priori value, DFS, uncertainty for retrieval state, and column averaging kernel of each retrieved column-averaged dry-air mole fraction of gas.
Post-processing result for retrieval (SIF & proxy method)	Retrieved zero-level offset, maximum radiance within the sub-band used, and SNR obtained in the retrieval (Band1_SIF). Retrieved XCH_4 (proxy method), its quality flag, and XCO_2 (model value). Retrieved XCO (proxy method) and its quality flag. Surface pressure difference, ratios of retrieved H_2O or CO_2 or CH_4 in Band 2 and Band 3.
Copied from FTS-2 L1B product	FTS-2 observation time, quality of each observation point, IMC stability flag, missing data flag, interferogram saturation flag, spike flag, scan stability flag, interferogram quality flag, spectrum quality flag, yaw steering flag.
Copied from FTS-2 L2 pre-processing result	Average of radiance normalized with noise level for each polarization component used in the FTS-2 2 μm band cloud determination.

* A sub-band refers to each wavenumber range of the observed spectrum used in the retrieval processing.

4. FTS-2 SWIR L2 Processing Algorithm

4.1 Overview of Algorithm

From the FTS-2 SWIR L2 processing, FTS-2 SWIR L2 Chlorophyll Fluorescence and Proxy-method Product and FTS-2 SWIR L2 Column-averaged Dry-air Mole Fraction Product are obtained.

FTS-2 SWIR L2 Chlorophyll Fluorescence and Proxy-method Product includes the six individual retrieval results processed under the assumption of cloud- and aerosol-free condition. These six retrievals are collectively named the "retrieval (SIF & proxy method)". Six different wavenumber ranges, two each from the three FTS-2 SWIR bands correspond to six independent retrievals. From FTS-2 Band 1, solar-induced chlorophyll fluorescence (SIF) and surface pressure are retrieved using Fraunhofer lines in the wavenumber range where O_2 absorption is negligibly small and the O_2 A-band, respectively. From FTS-2 Band 2, XCO_2 and XCH_4 are retrieved from the 1.6 μm CO_2 band and 1.67 μm CH_4 band, respectively. From FTS-2 Band 3, XCO_2 and XH_2O, and XCO, XCH_4, and XH_2O are retrieved using the 2.08 μm CO_2 band and 2.3 μm CO band, respectively. SIF is a weak radiation emitted by chlorophylls during the photosynthesis process and appeared as the variation in fractional depth (filling in) of the Fraunhofer lines in the satellite observed spectrum. SIF can be retrieved from satellite observed spectrum by utilizing this filling-in signal (Frankenberg et al., 2011b). However, the retrieved filling-in signal (hereinafter, "FS") from satellite observed spectrum consists not only SIF but also additive signal due to uncharacterized instrument characteristics (hereinafter, "US"; undesirable signal), therefore, US has to be subtracted from FS to obtain SIF (hereinafter, "SIF radiance correction"). US can be evaluated from the retrieved FS over ice/snow and/or barren areas where SIF is expected to be negligibly small. Since US can be time-dependent, the SIF radiance correction is applied on a monthly basis as the minimum period to obtain enough data for US evaluation. Except for SIF retrieval, other five retrievals utilize atmospheric absorption bands. Since these retrievals are processed under the assumption of cloud- and aerosol-free condition, the retrieved column-averaged dry-air mole fractions include some effects from optical path length modifications. If column-averaged dry-air mole fraction of some gas species (Xgas) can be obtained in a relatively high accuracy using a model-based calculation or other methods, that gas can be used as an optical path length proxy by comparing the retrieved Xgas to the prior knowledge. Since the degree of optical path length modification is considered to be similar between the nearby wavelength, the evaluated optical path length proxy can be utilized to target gas retrieval. This method is called "proxy method", and CO_2 retrieved from the 1.6 μm CO_2 band is often utilized as the optical path length proxy to obtain XCH_4 from the 1.67 μm CH_4 band (Frankenberg et al., 2011a, Parker et al., 2011, etc.). In addition, the difference between retrieved and a priori values of surface pressure obtained under the assumption of cloud- and aerosol-free condition as well as the ratio of retrieved Xgas in Band 2 and Band 3 are

expected to reflect the degree of optical path length modification due to clouds and aerosols. These are useful as cloud and aerosol information from the FTS-2 observation itself. By using them together with cloud information from CAI-2, which may have different observation times and viewing direction, it leads to a better understanding of the state within the FTS-2 IFOV. Considering these points, the FTS-2 SWIR L2 Chlorophyll Fluorescence and Proxy-method Product contains retrieval results for all FTS-2 SWIR observations.

On the other hand, the FTS-2 SWIR L2 Column-averaged Dry-air Mole Fraction Product includes simultaneously retrieved XCO_2, XCH_4, XH_2O, and XCO taking into account clouds and aerosols and utilizing the several wavenumber ranges. This retrieval is named as the "retrieval (full-physics method)" after the way of the treatment of the optical path length modification. In the full-physics method, the optical path length modification due to cloud and aerosol is described by the atmospheric scattering processes using the forward model. Different from the proxy method, the full-physics method has an advantage that there is no limitations for the gas species to retrieve but has a disadvantage of being sensitive to the optical path length modifications due to clouds and aerosol scattering compared to the proxy method. Therefore, FTS-2 SWIR observations that are strongly affected by clouds and/or aerosols are not processed by the retrieval (full-physics method), and retrieval results for converged cases are stored in the FTS-2 SWIR L2 Column-averaged Dry-air Mole Fraction Product.

Differences in the wavenumber range of observed spectra, state vector elements, and treatment of clouds and aerosols can be treated as differences in retrieval settings, and the Maximum A Posteriori (MAP) retrieval method (Rodgers, 2000) is used for all retrieval processing. The overview flow of retrieval component, post-processing component (chlorophyll fluorescence and proxy method), and post-processing component (column-averaged dry-air mole fraction) are shown in Figures 4.1-1, 4.1-2, and 4.1-3, respectively.

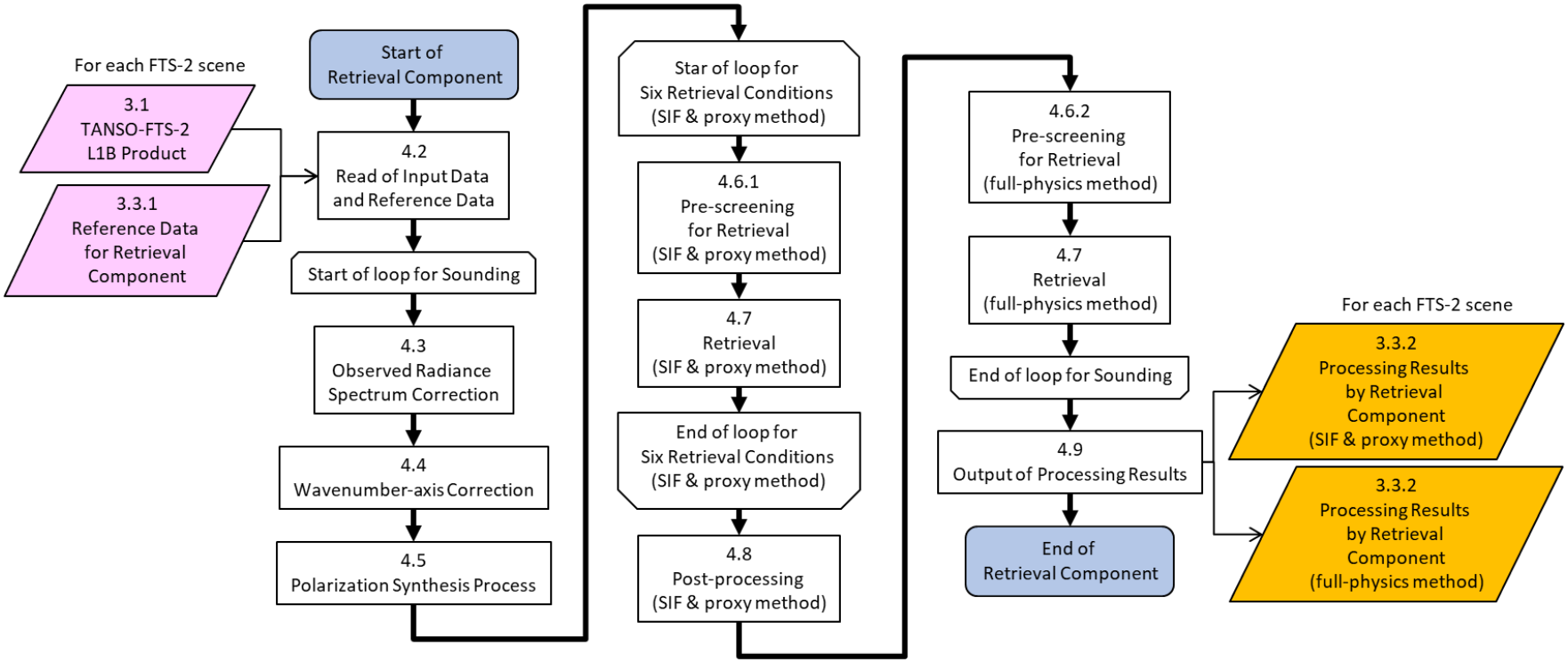

Figure 4.1-1. Overview flow of FTS-2 SWIR L2 Processing: Retrieval Component. The processing is performed for each scene of FTS-2 L1B Product.

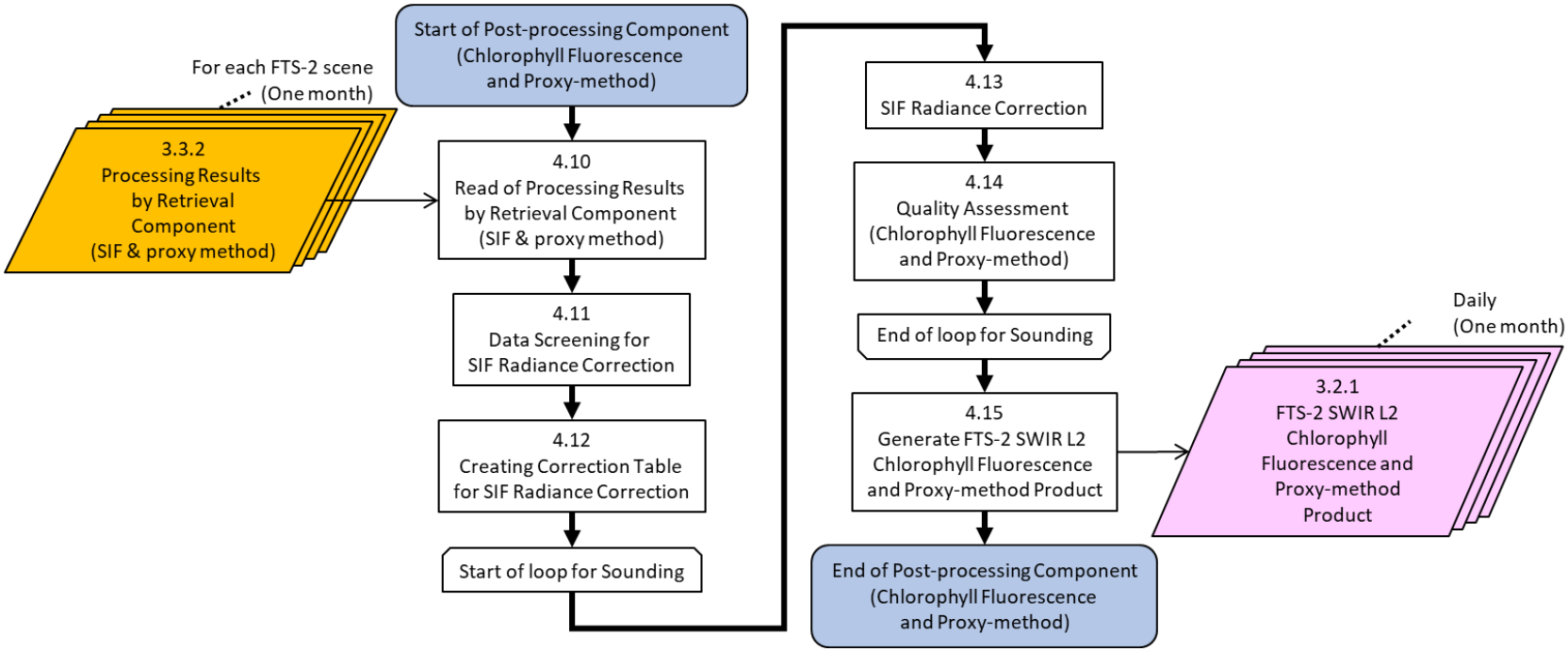

Figure.4.1-2. Overview flow of FTS-2 SWIR L2 Processing: Post-processing Component (Chlorophyll Fluorescence and Proxy-method). The processing is performed on a monthly basis and generates daily SWIR L2 products.

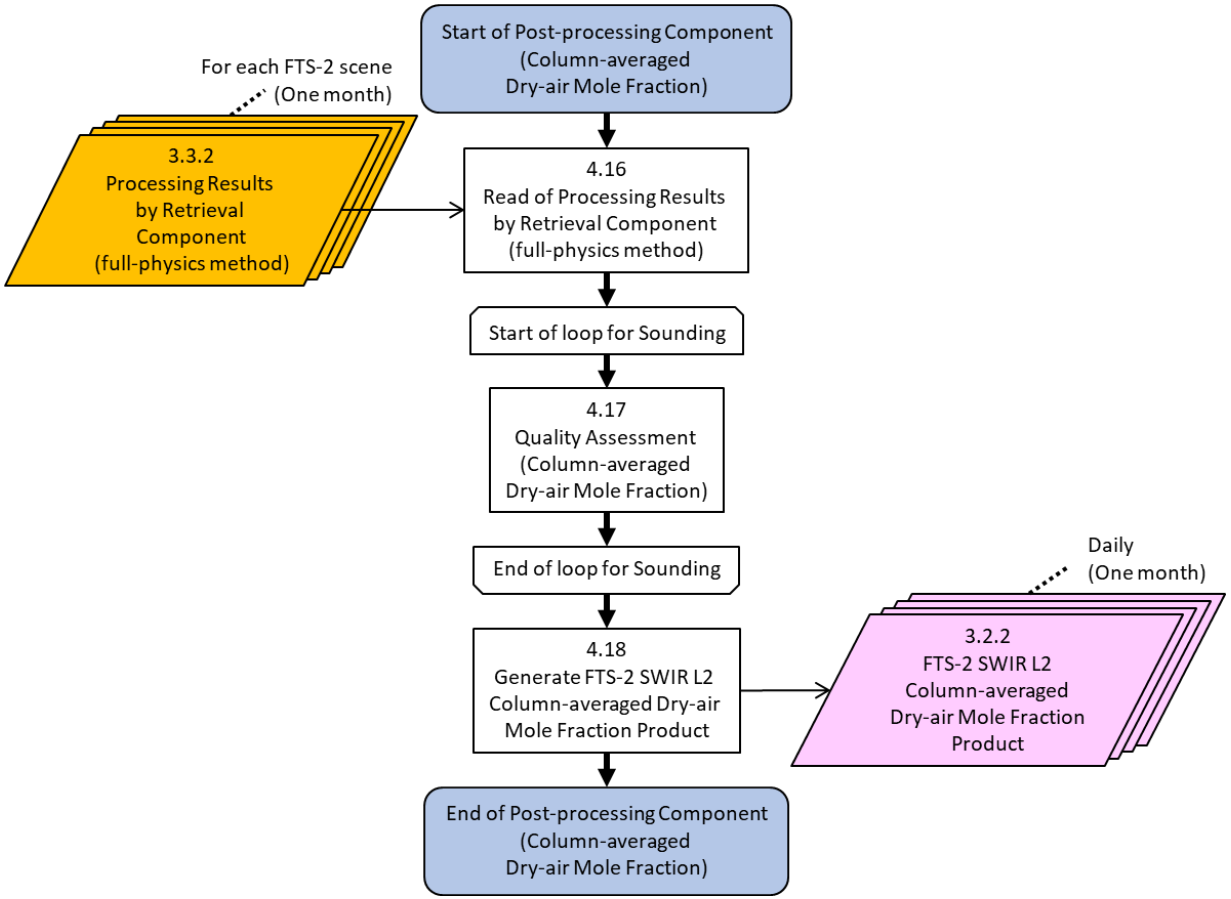

Figure.4.1-3. Overview flow of FTS-2 SWIR L2 Processing: Post-processing Component (Column-averaged Dry-air Mole Fraction). The processing is performed on a monthly basis and generates daily SWIR L2 products.

4.2 Read of Input Data and Reference Data

The input data shown in Section 3.1 (FTS-2 L1B Product) and the reference data shown in Subsection 3.3.1 are read out.

4.3 Observed Radiance Spectrum Correction

Apply necessary corrections for radiance value of the observed spectrum. In the case of FTS-2, the channeling as seen in TANSO-FTS Band 2S has not been confirmed, therefore, only degradation correction is applied. The spectra before and after each correction are denoted by $S_0(\nu)$ and $S_{corr}(\nu)$, respectively, where ν is a wavenumber.

4.3.1 Degradation Correction

After the launch of GOSAT-2, the sensitivity of FTS-2 is expected to change over the years. The solar irradiance and lunar calibration data obtain in orbit and the vicarious calibration data are used for evaluation of the sensitivity change of FTS-2. For the period after the satellite launch until the first sensitivity change evaluation result is obtained, the sensitivity is treated as unchanged from before the launch.

The sensitivity change of FTS-2 is expressed as a function for the number of days (t [day]) elapsed since the reference date (YYYY.MM.DD = 2019.02.05). First evaluation result was released on 2019.04.23 and it was revised on 2019.08.01 and 2020.05.25 (Figure 4.3.1-1). The degradation model itself has been updated with the revision, and the degradation model of revision 2020.05.25 is given by Eq. (4.3.1-1). Degradation is corrected by Eq. (4.3.1-2). The values for the coefficients a_1, a_2, a_3, a_4, d, e, and f are shown in the FTS-2 SWIR instrument characteristics (Table 3.3.1-1). Note, the sensitivity gap due to the change in the FTS-2 temperature setting on July 12, 2019 (Suto et al., 2020) was incorporated in the revision 2020.05.25.

$$C_{degradation}\left(\nu,t\right)=\left(a_1+a_2\cdot\nu+a_3\cdot\nu^2+a_4\cdot\nu^3\right)\cdot\left[d+e\cdot\exp\left(-\frac{t}{f}\right)\right] \tag{4.3.1-1}$$

$$S_{corr}\left(\nu\right)=\frac{S_0\left(\nu\right)}{C_{degradation}\left(\nu,t\right)} \tag{4.3.1-2}$$

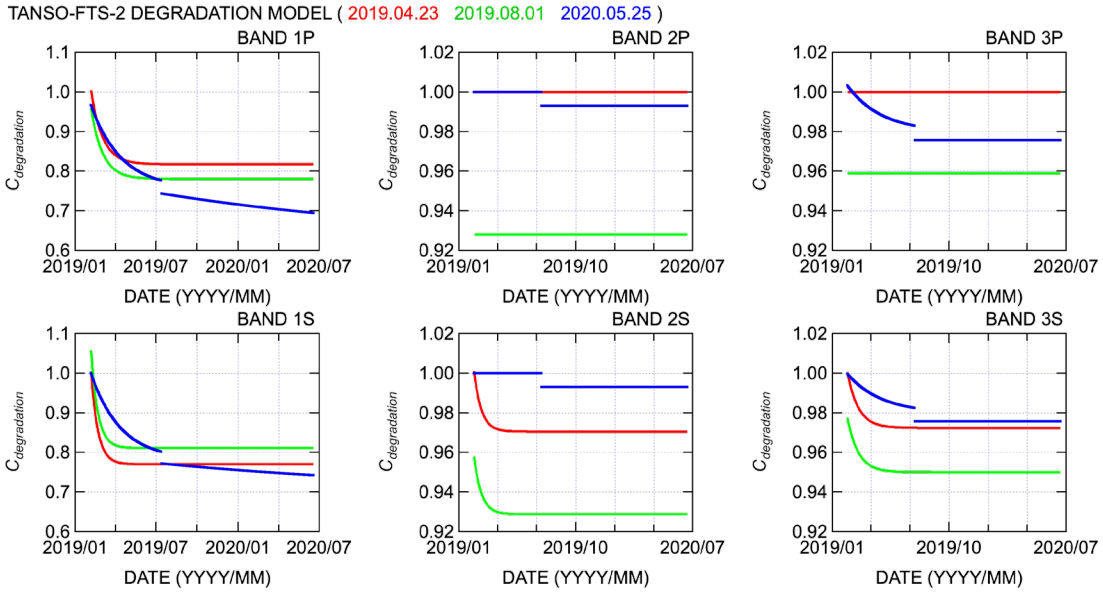

Figure 4.3.1-1. Degradation model of TANSO-FTS-2.

4.4 Wavenumber-axis Correction

The beginning wavenumber and wavenumber interval of the spectrum data stored in FTS-2 L1B Product are nominal values. However, the actual values of each sounding are expected to vary slightly due to the self-apodization, temperature dependence of the sampling laser's wavelength, and the misalignment of FTS-2. For this reason, the wavenumber-axis correction is performed.

The wavenumber grid of a Fourier transform spectrometer (FTS) is defined as an integral multiple of the wavenumber interval $\Delta\nu$. Since the nominal wavenumber interval $\Delta\nu_0$ stored in FTS-2 L1B Product and the actual wavenumber interval $\Delta\nu_{cor}$ are related by the Eq. (4.4-1) using the correction coefficient ρ, the wavenumber grid of FTS-2 is given by Eq. (4.4-2) using the beginning wavenumber ν_s stored in FTS-2 L1B Product.

$$\Delta\nu_{cor} = \rho \cdot \Delta\nu_0 \tag{4.4-1}$$

$$\nu_{cor,i} = \rho \cdot \left[\nu_s + (i-1) \cdot \Delta\nu_0\right] \qquad i = 1,2,3,... \tag{4.4-2}$$

The correction coefficient ρ is determined for each band by iterative calculation using the Golden Section Search method to maximize the cross correlation coefficient $C(\rho)$ between the observed spectrum S_{obs} stored in FTS-2 L1B Product and the calculated reference spectrum S_{ref}. The wavenumber range used is the same as in Table 2.1-1.

$$C(\rho) = \sum_{i=i_{sta}}^{i_{end}} \left[S_{ref,P}\left(\nu_{sat,i}\right) \cdot S_{obs,P}\left(\nu_{cor,i}\right) + S_{ref,S}\left(\nu_{sat,i}\right) \cdot S_{obs,S}\left(\nu_{cor,i}\right) \right] \tag{4.4-3}$$

where the subscripts P and S denote respective polarization components, and i_{sta} and i_{end} denote the indexes corresponding to the beginning and ending points of the wavenumber range, respectively.

The reference spectrum S_{ref} is obtained by a convolution integral of the monochromatic radiance spectrum I with the FTS-2 instrument line shape function *ILS*. ILSF is shown in the FTS-2 SWIR instrument characteristics (Table 3.3.1-1).

$$\begin{aligned} S_{ref,P/S}\left(\nu_{sat,i}\right) &= ILS_{P/S}\left(\nu_{sat,i},\nu\right) \otimes I(\nu) \\ &= \int_{-\infty}^{\infty} ILS_{P/S}\left(\nu_{sat,i}-\nu\right) \cdot I(\nu) d\nu \\ &= \sum_{j=-N_w}^{N_w} ILS_{P/S,i}\left(-j\cdot\delta\nu\right) \cdot I\left(\nu_{sat,i}+j\cdot\delta\nu\right) \end{aligned} \tag{4.4-4}$$

$$\begin{aligned} & ILS_{P/S,i}\left(-j\cdot\delta\nu\right) \\ &= \frac{\nu_{END}-\nu_{sat,i}}{\nu_{END}-\nu_{STA}} \cdot ILS_{P/S,\nu_{STA}}\left(-j\cdot\delta\nu\right) + \frac{\nu_{sat,i}-\nu_{STA}}{\nu_{END}-\nu_{STA}} \cdot ILS_{P/S,\nu_{END}}\left(-j\cdot\delta\nu\right) \end{aligned} \tag{4.4-5}$$

where $\otimes$ denotes a convolution integral, $\delta\nu$ is the integration step size of the convolution integral and should be a value closest to 0.01 cm^{-1} that satisfies the condition $\Delta\nu_0 = n_w \cdot \delta\nu$ (n_w is an integer value). An integer value N_w is determined so that the convolution integral half width $N_w \cdot \delta\nu$ becomes about 20 cm^{-1}. Among the wavenumber for which the ILSF is provided, ν_{STA} and ν_{END} are those satisfy the condition $\nu_{STA} \le \nu_{sat,ista}$, $\nu_{sat,iend} \le \nu_{END}$ and are closest to $\nu_{sat,ista}$ and $\nu_{sat,iend}$, respectively.

The monochromatic radiance spectrum I is calculated using the solar zenith angle θ_0, satellite zenith angle θ_1, Doppler velocity relative to the sun $v_{dop,sun}$, and Doppler velocity relative to the satellite $v_{dop,sat}$ calculated in the FTS-2 L2 pre-processing, as well as the distance between the sun and the observation point $D_{sun\text{-}obs}$ [AU] stored in FTS-2 L1B Product as:

$$I\left(\nu_{sat,k}\right) = \frac{F_0\left(\nu_{sun,k}\right)}{D_{sun-obs}^2} \cdot \exp\left[-\left(\frac{1}{\cos\theta_0} + \frac{1}{\left|\cos\theta_1\right|} \right) \cdot \tau\left(\nu_{srf,k}\right) \right] \tag{4.4-6}$$

$$\nu_{sat,k} = \left(1 + \frac{v_{dop,sat}}{c}\right) \cdot \nu_{srf,k} \tag{4.4-7}$$

$$\nu_{sun,k} = \left(1 - \frac{v_{dop,sun}}{c}\right) \cdot \nu_{srf,k} \tag{4.4-8}$$

where the subscript k denotes an element that corresponds to the monochromatic radiance spectrum.

F_0 is solar irradiance at a distance of one astronomical unit from the sun (Table 3.3.1-1) and obtained from the solar irradiance data by performing a four-point Lagrange interpolation (Eq. (4.4-9)), where τ is the optical thickness for reference spectrum shown in Table 3.3.1-1. In the convolution integral of Eq. (4.4-4), the monochromatic radiance spectrum is obtained from that calculated by Eq. (4.4-6) by performing a four-point Lagrange interpolation (Eq. (4.4-9)).

$$\begin{aligned} I(\nu) = & \frac{(\nu-\nu_k)\cdot(\nu-\nu_{k+1})\cdot(\nu-\nu_{k+2})}{(\nu_{k-1}-\nu_k)\cdot(\nu_{k-1}-\nu_{k+1})\cdot(\nu_{k-1}-\nu_{k+2})} \cdot I(\nu_{k-1}) \\ & + \frac{(\nu-\nu_{k-1})\cdot(\nu-\nu_{k+1})\cdot(\nu-\nu_{k+2})}{(\nu_k-\nu_{k-1})\cdot(\nu_k-\nu_{k+1})\cdot(\nu_k-\nu_{k+2})} \cdot I(\nu_k) \\ & + \frac{(\nu-\nu_{k-1})\cdot(\nu-\nu_k)\cdot(\nu-\nu_{k+2})}{(\nu_{k+1}-\nu_{k-1})\cdot(\nu_{k+1}-\nu_k)\cdot(\nu_{k+1}-\nu_{k+2})} \cdot I(\nu_{k+1}) \\ & + \frac{(\nu-\nu_{k-1})\cdot(\nu-\nu_k)\cdot(\nu-\nu_{k+1})}{(\nu_{k+2}-\nu_{k-1})\cdot(\nu_{k+2}-\nu_k)\cdot(\nu_{k+2}-\nu_{k+1})} \cdot I(\nu_{k+2}) \end{aligned} \tag{4.4-9}$$

where $I(\nu_k)$ is a solar irradiance datum or a monochromatic radiance spectrum, and ν_k corresponds a wavenumber grid which satisfy the condition $\nu_k \leq \nu \leq \nu_{k+1}$.

4.5 Polarization Synthesis Process

Since computational costs of a radiative transfer calculation in vector mode is high, the forward model uses a radiative transfer code in scalar mode. For this reason, the total radiance spectra of the light incident into FTS-2 is calculated from the observed spectra of two polarization components.

The Stokes vector $\mathbf{I}_{P/S}$ of the light observed by FTS-2 can be expressed as below using the Muller matrices those describing the reflection of the scan mirror, the optical efficiency of FTS-2, and the polarization beam splitter, the rotation matrix of the polarization reference plane, and the Stokes vector of light incident into FTS-2 $\mathbf{I}_{in}$. The observed spectra of P- and S-polarization components and the total radiance spectra incident into FTS-2 are the first elements of $\mathbf{I}_{P/S}$ and $\mathbf{I}_{in}$, respectively. Note that the Mueller matrices and Stokes vector are the function of wavenumber, ν is omitted from the following equations.

$$\mathbf{I}_P = \mathbf{M}_{BS,P} \cdot \mathbf{M}_{opt} \cdot \mathbf{L}(\theta_{PM-DET}) \cdot \mathbf{M}_{phase}(\theta_{in}) \cdot \mathbf{M}_{PM}(\theta_{in}) \cdot \mathbf{L}(\theta_{RT-PM}) \cdot \mathbf{I}_{in} \tag{4.5-1}$$

$$\mathbf{I}_S = \mathbf{M}_{BS,S} \cdot \mathbf{M}_{opt} \cdot \mathbf{L}(\theta_{PM-DET}) \cdot \mathbf{M}_{phase}(\theta_{in}) \cdot \mathbf{M}_{PM}(\theta_{in}) \cdot \mathbf{L}(\theta_{RT-PM}) \cdot \mathbf{I}_{in} \tag{4.5-2}$$

$$\mathbf{L}(\theta) = \begin{pmatrix} 1 & 0 & 0 & 0 \\ 0 & \cos 2\theta & \sin 2\theta & 0 \\ 0 & -\sin 2\theta & \cos 2\theta & 0 \\ 0 & 0 & 0 & 1 \end{pmatrix} \tag{4.5-3}$$

$$\mathbf{M}_{PM}(\theta) = \begin{pmatrix} M_{PM,1}(\theta) & M_{PM,2}(\theta) & 0 & 0 \\ M_{PM,2}(\theta) & M_{PM,1}(\theta) & 0 & 0 \\ 0 & 0 & M_{PM,3}(\theta) & 0 \\ 0 & 0 & 0 & M_{PM,3}(\theta) \end{pmatrix} \tag{4.5-4}$$

$$\begin{cases} M_{PM,1}(\theta) = \dfrac{R_{//}(\theta) + R_{\perp}(\theta)}{2} \\ M_{PM,2}(\theta) = \dfrac{R_{//}(\theta) - R_{\perp}(\theta)}{2} \\ M_{PM,3}(\theta) = \sqrt{R_{//}(\theta) \cdot R_{\perp}(\theta)} \end{cases} \tag{4.5-5}$$

$$\mathbf{M}_{phase}(\theta) = \begin{pmatrix} 1 & 0 & 0 & 0 \\ 0 & 1 & 0 & 0 \\ 0 & 0 & \cos\delta(\theta) & \sin\delta(\theta) \\ 0 & 0 & -\sin\delta(\theta) & \cos\delta(\theta) \end{pmatrix} \tag{4.5-6}$$

$$\begin{cases} R_{//}(\theta) = r_{//}(\theta) \cdot r_{//}(\theta) \\ R_{\perp}(\theta) = r_{\perp}(\theta) \cdot r_{\perp}(\theta) \\ \delta(\theta) = \tan^{-1}\left\{ \dfrac{\mathrm{Im}\left[r_{//}(\theta) \cdot r_{\perp}(\theta) \right]}{\mathrm{Re}\left[r_{//}(\theta) \cdot r_{\perp}(\theta) \right]} \right\} \end{cases} \tag{4.5-7}$$

$$\begin{cases} r_{//}(\theta) = \dfrac{m^2 \cdot \cos\theta - \sqrt{m^2 - \sin^2\theta}}{m^2 \cdot \cos\theta + \sqrt{m^2 - \sin^2\theta}} \\ r_{\perp}(\theta) = \dfrac{\cos\theta - \sqrt{m^2 - \sin^2\theta}}{\cos\theta + \sqrt{m^2 - \sin^2\theta}} \end{cases} \tag{4.5-8}$$

$$\mathbf{M}_{BS,P} \cdot \mathbf{M}_{opt} = W_P \cdot \begin{pmatrix} 1 & 1 & 0 & 0 \\ 1 & 1 & 0 & 0 \\ 0 & 0 & 0 & 0 \\ 0 & 0 & 0 & 0 \end{pmatrix} \tag{4.5-9}$$

$$\mathbf{M}_{BS,S} \cdot \mathbf{M}_{opt} = W_S \cdot \begin{pmatrix} 1 & -1 & 0 & 0 \\ -1 & 1 & 0 & 0 \\ 0 & 0 & 0 & 0 \\ 0 & 0 & 0 & 0 \end{pmatrix} \tag{4.5-10}$$

$$\mathbf{I} = \begin{pmatrix} I \\ Q \\ U \\ V \end{pmatrix} \tag{4.5-11}$$

where $\theta_{RT\text{-}PM}$ is the angle between radiative transfer reference plane and scan mirror reference plane, θ_{in} is the incident angle to scan mirror, $\theta_{PM\text{-}DET}$ is the angle between scan mirror reflection reference plane and FTS-2 detector reference plane, and those are shown in the FTS-2 L2 pre-processing result (Table 3.3.1-1). Also, m is the complex refractive index of the scan mirror, and W_p and W_s are the optical efficiency of FTS-2 shown in the FTS-2 SWIR instrument characteristics (Table 3.3.1-1).

By rearrange Eqs. (4.5-1) and (4.5-2), the observed spectra of P- and S-polarization components are given by Eqs. (4.5-12) and (4.5-13), respectively.

$$S_P = ILS_{P,i} \otimes \left(A_P \cdot I_{in} + B_P \cdot Q_{in} + C_P \cdot U_{in} + D_P \cdot V_{in} \right) \tag{4.5-12}$$

$$S_S = ILS_{S,i} \otimes \left(A_S \cdot I_{in} + B_S \cdot Q_{in} + C_S \cdot U_{in} + D_S \cdot V_{in} \right) \tag{4.5-13}$$

$$A_P = W_P \cdot \left[R_{//}(\theta_{in}) \cdot \cos^2 \theta_{PM-DET} + R_{\perp}(\theta_{in}) \cdot \sin^2 \theta_{PM-DET} \right] \tag{4.5-14}$$

$$\begin{aligned} B_P = {} & W_P \cdot \left[R_{//}(\theta_{in}) \cdot \cos^2 \theta_{PM-DET} - R_{\perp}(\theta_{in}) \cdot \sin^2 \theta_{PM-DET} \right] \cdot \cos 2\theta_{RT-PM} \\ & - W_P \cdot \sqrt{R_{//}(\theta_{in}) \cdot R_{\perp}(\theta_{in})} \cdot \cos \delta(\theta_{in}) \cdot \sin 2\theta_{PM-DET} \cdot \sin 2\theta_{RT-PM} \end{aligned} \tag{4.5-15}$$

$$\begin{aligned} C_P = {} & W_P \cdot \left[R_{//}(\theta_{in}) \cdot \cos^2 \theta_{PM-DET} - R_{\perp}(\theta_{in}) \cdot \sin^2 \theta_{PM-DET} \right] \cdot \sin 2\theta_{RT-PM} \\ & + W_P \cdot \sqrt{R_{//}(\theta_{in}) \cdot R_{\perp}(\theta_{in})} \cdot \cos \delta(\theta_{in}) \cdot \sin 2\theta_{PM-DET} \cdot \cos 2\theta_{RT-PM} \end{aligned} \tag{4.5-16}$$

$$D_P = W_P \cdot \sqrt{R_{//}(\theta_{in}) \cdot R_{\perp}(\theta_{in})} \cdot \sin \delta(\theta_{in}) \cdot \sin 2\theta_{PM-DET} \tag{4.5-17}$$

$$A_S = W_S \cdot \left[R_{//}(\theta_{in}) \cdot \sin^2 \theta_{PM-DET} + R_{\perp}(\theta_{in}) \cdot \cos^2 \theta_{PM-DET} \right] \tag{4.5-18}$$

$$\begin{aligned} B_S = {} & W_S \cdot \left[R_{//}(\theta_{in}) \cdot \sin^2 \theta_{PM-DET} - R_{\perp}(\theta_{in}) \cdot \cos^2 \theta_{PM-DET} \right] \cdot \cos 2\theta_{RT-PM} \\ & + W_S \cdot \sqrt{R_{//}(\theta_{in}) \cdot R_{\perp}(\theta_{in})} \cdot \cos \delta(\theta_{in}) \cdot \sin 2\theta_{PM-DET} \cdot \sin 2\theta_{RT-PM} \end{aligned} \tag{4.5-19}$$

$$\begin{aligned} C_S = {} & W_S \cdot \left[R_{//}(\theta_{in}) \cdot \sin^2 \theta_{PM-DET} - R_{\perp}(\theta_{in}) \cdot \cos^2 \theta_{PM-DET} \right] \cdot \sin 2\theta_{RT-PM} \\ & - W_S \cdot \sqrt{R_{//}(\theta_{in}) \cdot R_{\perp}(\theta_{in})} \cdot \cos \delta(\theta_{in}) \cdot \sin 2\theta_{PM-DET} \cdot \cos 2\theta_{RT-PM} \end{aligned} \tag{4.5-20}$$

$$D_S = -W_S \cdot \sqrt{R_{//}(\theta_{in}) \cdot R_{\perp}(\theta_{in})} \cdot \sin \delta(\theta_{in}) \cdot \sin 2\theta_{PM-DET} \tag{4.5-21}$$

To calculate four Stokes parameters from the two observation components, some assumptions are needed. In atmospheric radiative transfer, the Stopes parameter V_{in} is sufficiently small and can be ignored. By means of a single-scattering approximation, the Stokes parameter Q_{in} and U_{in} are related as expressed in Eq. (4.5-22) using the angle between polarization plane of observation light and radiative transfer reference plane χ_{ss} calculated in the FTS-2 L2 pre-processing.

$$\frac{U_{in}}{Q_{in}} = \tan 2\chi_{ss} \tag{4.5-22}$$

In addition to the above, assume that the difference between ILSF for P- and S-polarization component can be ignored, and the wavenumber dependencies denoted by $A_{P/S}$ ~ $D_{P/S}$ in Eqs. (4.5-14) ~ (4.5-21) can also be ignored in the range of the convolution integral. Then, the total intensity spectra convolved by the ILSF are given by Eq. (4.5-23). Further, the corresponding observation error variance and SNR are given by Eqs. (4.5-24) and (4.5-25), respectively.

$$S_{synth} = ILS_i \otimes I_{in} = \frac{\left(B_S + C_S \cdot \tan 2\chi_{ss}\right)\cdot S_P - \left(B_P + C_P \cdot \tan 2\chi_{ss}\right)\cdot S_S}{\left(B_S + C_S \cdot \tan 2\chi_{ss}\right)\cdot A_P - \left(B_P + C_P \cdot \tan 2\chi_{ss}\right)\cdot A_S} \quad (4.5\text{-}23)$$
$$= C_{synth,P} \cdot S_P - C_{synth,S} \cdot S_S$$

$$\sigma^2_{synth} = \left(C_{synth,P} \cdot \sigma_P\right)^2 + \left(C_{synth,S} \cdot \sigma_S\right)^2 \quad (4.5\text{-}24)$$

$$C_{synth,P/S} = \frac{B_{S/P} \cdot \cos 2\chi_{ss} + C_{S/P} \cdot \sin 2\chi_{ss}}{\left(B_S \cdot \cos 2\chi_{ss} + C_S \cdot \sin 2\chi_{ss}\right)\cdot A_P - \left(B_P \cdot \cos 2\chi_{ss} + C_P \cdot \sin 2\chi_{ss}\right)\cdot A_S} \quad (4.5\text{-}25)$$

$$\sigma_{P/S} = \frac{Max\left(S_{P/S}\right)}{SNR_{P/S}} \quad (4.5\text{-}26)$$

$$SNR_{synth} = \frac{Max\left(S_{synth}\right)}{\sigma_{synth}} \quad (4.5\text{-}27)$$

where $Max(S)$ is the maximum value of the observed spectrum S within the band.

In the equations, the wavenumber notation ν is omitted; however, since the optical efficiency of FTS-2 W_p and W_s are evaluated based on the pre-launch calibration data obtained by the actual FTS-2 instrument, the nominal wavenumber grid of the FTS-2 with no additional correction applied is used. In contrast, the complex refractive index of scan mirror is evaluated based on the data obtained independently but not by the actual FTS-2 instrument, and thus, the corrected wavenumber grid is used. For the interpolation in the wavenumber direction, the spline interpolation is employed.

4.6 Pre-screening

According to the pre-screening conditions, select the soundings to be processed in the retrieval processing. For the soundings identified as not for the processing, the corresponding retrieval processing is not performed, and missing values are stored in the corresponding retrieval results. Note that the following pre-screening conditions are subject to change depending on the quality evaluation results.

4.6.1 Pre-screening for Retrieval (SIF & proxy method)

Select the soundings for the retrieval (SIF & proxy method). The objectives of the retrieval (SIF & proxy method) are not only the retrieval of chlorophyll fluorescence and the proxy-method based column-averaged dry-air mole fractions but also to obtain several information related to optical path length modification. Therefore, all FTS-2 SWIR soundings are basically subject to process, however, considering the processing stability, the soundings falls in any of the following conditions are excluded from the processing.

When missing data flag (FTS-2 L1B Product: QualityInfo/missingFlag) of the band used for the retrieval is NOT “Normal (No data loss)”.

When saturation flag (FTS-2 L1B Product: QualityInfo/saturationFlag) of the band used for the retrieval is NOT “DN saturation detection = Normal”.

When interferogram quality flag (FTS-2 L1B Product: QualityInfo/interferogramQualityFlag) of the band used for the retrieval is NOT “Normal”.

When spectrum quality flag (FTS-2 L1B Product: QualityInfo/spectrumQualityFlag) of the band used for the retrieval is NOT “Normal”.

When solar zenith angle calculated in the FTS-2 L2 pre-processing is over 80°.

4.6.2 Pre-screening for Retrieval (full-physics method)

Select the soundings for the retrieval (full-physics method). The target of the retrieval (full-physics method) are FST-2 SWIR soundings which are relatively less affected by clouds and aerosols, therefore, the soundings falls in any of the following conditions are excluded from the processing.

- When quality flag of each observation point (FTS-2 L1B Product: QualityInfo/soundingQualityflag) is “Poor” or “NG”.
- When data invalid flag (FTS-2 L1B Product: QualityInfo/dataInvalidFlag) is NOT “Valid”.
- When IMC stability flag (FTS-2 L1B Product: QualityInfo/IMC_StabilityFlag) is NOT “Stable”.
- When scan stability flag (FTS-2 L1B Product: QualityInfo/scanStabilityFlag) is NOT “Stable”.

  When missing data flag (FTS-2 L1B Product: QualityInfo/missingFlag) of the band used

for the retrieval is NOT “Normal (No data loss)”.

When saturation flag (FTS-2 L1B Product: QualityInfo/saturationFlag) of the band used for the retrieval is NOT “DN saturation detection = Normal”.

When spike flag (FTS-2 L1B Product: QualityInfo/spikeFlag) of the band used for the retrieval is NOT “Normal (no spike)”.

When interferogram quality flag (FTS-2 L1B Product: QualityInfo/interferogramQualityFlag) of the band used for the retrieval is NOT “Normal”.

When spectrum quality flag (FTS-2 L1B Product: QualityInfo/spectrumQualityFlag) of the band used for the retrieval is NOT “Normal”.

When SNR_{synth} (Eq. (4.5-27)) of Band 1 is less than 70.

- When solar zenith angle calculated in the FTS-2 L2 pre-processing is over 70°.
- When land fraction f_{LAND} [%] (Eq. (4.6.2-1)) is greater than 10% and less than 60%.
- When cloud determination result by CAI-2 L2 Cloud Discrimination Product calculated in the FTS-2 L2 pre-processing is “cloud present”.
- When one of the cloud determination result of FTS-2 2 μm band by polarization component calculated in the FTS-2 L2 pre-processing is “cloud present”.

$$f_{LAND} = \frac{N_{LSmsk\_land}}{N_{LSmsk\_total}} \cdot 100 \tag{4.6.2-1}$$

where N_{LSmsk_land} and N_{LSmsk_total} are number of land grid points and total number of grid points within FTS-2 IFOV-area, respectively, for land/sea mask data calculated in the FTS-2 L2 pre-processing.

4.7 Retrieval Processing

As stated previously, retrievals (SIF & proxy method) and (full-physics method) are both performed utilizing the MAP analysis method described in the following Subsection 4.7.1. Each retrieval setting such as state vector elements and wavenumber range of the radiance spectra are summarized in Subsection 4.7.2. Further, the vertical grids, the forward model utilized in the MAP analysis method, a priori and optical properties of state vector elements, and the formulation of Jacobian are described in the Subsections 4.7.3, 4.7.4, 4.7.5, and 4.7.6, respectively.

4.7.1 MAP Analysis Method

According to the Maximum A Posteriori (MAP) analysis method, the optimal estimate of state vector **x**, which represents a unknown parameters to be retrieved, is the value of **x** that minimizes the cost function $J(\mathbf{x})$ as expressed in Eq. (4.7.1-1) below.

$$J(\mathbf{x}) = \left[\mathbf{y} - \mathbf{F}(\mathbf{x},\mathbf{c})\right]^T \cdot \mathbf{S}_\varepsilon^{-1} \cdot \left[\mathbf{y} - \mathbf{F}(\mathbf{x},\mathbf{c})\right] + \left(\mathbf{x} - \mathbf{x}_a\right)^T \cdot \mathbf{S}_a^{-1} \cdot \left(\mathbf{x} - \mathbf{x}_a\right) \tag{4.7.1-1}$$

where **y** is a observed radiance spectrum, **F**(**x**, **c**) is a forward model, **c** is a variable not included in the state vector but necessary for the forward model description, $\mathbf{x}_a$ is the a priori state vector, $\mathbf{S}_a$ is the variance-covariance matrix of $\mathbf{x}_a$, and $\mathbf{S}_\varepsilon$ is the variance-covariance matrix of observation error and forward model.

In the FTS-2 SWIR L2 processing, the solution **x** is constrained under the following condition.

$$\mathbf{x}_{\min} \le \mathbf{x} \le \mathbf{x}_{\max} \tag{4.7.1-2}$$

Then, **x** is iteratively obtained using the Levenberg-Marquardt method as expressed in Eq. (4.7.1-3). Note that for the FTS-2 SWIR L2 processing, various schemes are employed in reference to Nakagawa and Oyanagi (1982).

$$\mathbf{x}_{i+1} = \mathbf{x}_i + \left(\mathbf{K}_i^T \cdot \mathbf{S}_\varepsilon^{-1} \cdot \mathbf{K}_i + \mathbf{S}_a^{-1} + \lambda \cdot \mathbf{D}^2\right)^{-1} \cdot \left\{\mathbf{K}_i^T \cdot \mathbf{S}_\varepsilon^{-1} \cdot \left[\mathbf{y} - \mathbf{F}(\mathbf{x}_i)\right] - \mathbf{S}_a^{-1} \cdot \left(\mathbf{x}_i - \mathbf{x}_a\right)\right\} \tag{4.7.1-3}$$

where the subscript i denotes the number of iterations, $\mathbf{K} = \partial\mathbf{F}(\mathbf{x})/\partial\mathbf{x}$ is a Jacobian, **D** is a diagonal matrix introduced to stabilize the iteration process, and λ refers to a coefficient of which value is adjusted so that the value of the cost function decreases in each step of the iteration

Eq. (4.7.1-3) is not solved directly but using the Cholesky decomposition of $\mathbf{S}_\varepsilon$ and $\mathbf{S}_a$ (Eqs.

(4.7.1-6) and (4.7.1-7)), rearranged into Eqs. (4.7.1-4) and (4.7.1-5), and solved with respect to ($\mathbf{x}_{i+1}$ - $\mathbf{x}_a$) using the DGELSS of LAPACK, where the coefficient λ has the initial value of zero and will be updated every time calculating Eq. (4.7.1-5) using the method described below.

$$\begin{aligned}&\left(\mathbf{K}_i^T \cdot \mathbf{S}_\varepsilon^{-1} \cdot \mathbf{K}_i + \mathbf{S}_a^{-1} + \lambda \cdot \mathbf{D}^2\right) \cdot \left(\mathbf{x}_{i+1} - \mathbf{x}_a\right) \\ &= \mathbf{K}_i^T \cdot \mathbf{S}_\varepsilon^{-1} \cdot \left[\mathbf{y} - \mathbf{F}\left(\mathbf{x}_i\right) + \mathbf{K}_i \cdot \left(\mathbf{x}_i - \mathbf{x}_a\right)\right] + \lambda \cdot \mathbf{D}^2 \cdot \left(\mathbf{x}_i - \mathbf{x}_a\right)\end{aligned} \tag{4.7.1-4}$$

$$\begin{pmatrix} \widetilde{\mathbf{K}}_i \\ \mathbf{T}_{ainv} \\ \sqrt{\lambda}\mathbf{D} \end{pmatrix} \cdot \left(\mathbf{x}_{i+1} - \mathbf{x}_a\right) = \begin{pmatrix} \widetilde{\mathbf{y}}_i + \widetilde{\mathbf{K}}_i \cdot \left(\mathbf{x}_i - \mathbf{x}_a\right) \\ 0 \\ \sqrt{\lambda} \cdot \mathbf{D} \cdot \left(\mathbf{x}_i - \mathbf{x}_a\right) \end{pmatrix} \tag{4.7.1-5}$$

$$\mathbf{S}_\varepsilon = \mathbf{T}_\varepsilon^T \cdot \mathbf{T}_\varepsilon \tag{4.7.1-6}$$

$$\mathbf{S}_a^{-1} = \mathbf{T}_{ainv}^T \cdot \mathbf{T}_{ainv} \tag{4.7.1-7}$$

$$\mathbf{D}^2 = diag\left(\mathbf{A}^T \cdot \mathbf{A}\right) \tag{4.7.1-8}$$

$$\mathbf{A} = \begin{pmatrix} \widetilde{\mathbf{K}}_i \\ \mathbf{T}_{ainv} \end{pmatrix} \tag{4.7.1-9}$$

$$\widetilde{\mathbf{y}}_i = \mathbf{T}_\varepsilon^{-T} \cdot \left[\mathbf{y} - \mathbf{F}\left(\mathbf{x}_i\right)\right] \tag{4.7.1-10}$$

$$\widetilde{\mathbf{K}}_i = \mathbf{T}_\varepsilon^{-T} \cdot \mathbf{K}_i \tag{4.7.1-11}$$

In updating the state vector through an iterative process under the constraint condition of Eq. (4.7.1-2), the trust region method is applied to the variation of the solutions to stabilize the convergence, and the coefficient λ is adjusted so that the cost function (Eq. (4.7.1-1)) decreases.

First, obtain the solution satisfying the constraint condition of Eq. (4.7.1-2). Let the correction vector calculated from ($\mathbf{x}_{i+1}$ - $\mathbf{x}_a$), which obtained by Eq. (4.7.1-5) be denoted by $\Delta\mathbf{x}_1$, and the correction vector scaled with a reduction factor α to satisfy the condition of Eq. (4.7.1-2) be denoted by $\Delta\mathbf{x}_2$.

$$\Delta\mathbf{x}_1 = \left(\mathbf{x}_{i+1} - \mathbf{x}_a\right) + \mathbf{x}_a - \mathbf{x}_i \tag{4.7.1-12}$$

$$\Delta\mathbf{x}_2 = \alpha \cdot \Delta\mathbf{x}_1 \tag{4.7.1-13}$$

The reduction factor α is calculated by the following procedure. To determine α, each element of state vector $\mathbf{x}$ denoted by $x(j)$, is categorized into the two groups $\mathbf{x}_E$ and $\mathbf{x}_S$, which indicate

satisfying the condition of Eq. (4.7.1-2) with equality signs and inequality signs, respectively. The procedure described below is executed every time α is re-determined.

(1) Assume that all the variables belong to $\mathbf{x}_S$.

(2) Solve Eq. (4.7.1-5) and calculate Eq. (4.7.1-12).

(3) Consider all the state vector elements $x(j)$ that belong to $\mathbf{x}_S$ and satisfy the condition $x(j) + \Delta x_1(j) < x_{min}(j)$ (i.e., $\Delta x_1(j) < 0$). Obtain the maximum positive number α_1 (< 1) that satisfies the conditions $x(j) + \alpha_1 \cdot \Delta x_1(j) \geq x_{min}(j)$.

(4) Consider all the state vector elements $x(j)$ that belong to $\mathbf{x}_S$ and satisfy the condition $x(j) + \Delta x_1(j) > x_{max}(j)$ (i.e., $\Delta x_1(j) > 0$). Obtain the maximum positive number α_2 (< 1) that satisfies the conditions $x(j) + \alpha_2 \cdot \Delta x_1(j) \leq x_{max}(j)$.

(5) Define $\alpha = \min(\alpha_1, \alpha_2)$ and move the state vector elements corresponding to α to the group of $\mathbf{x}_E$.

(6) If $\alpha = 0$, it means that an element, which should belong to the group $\mathbf{x}_E$, was included in the group $\mathbf{x}_S$. In this case, the column in the Jacobian matrix corresponding to the state vector element that gives this α will be replaces with zero. Then return to the step (2).

(7) Calculate Eq. (4.7.1-13) using the obtained positive number α.

The process to update the coefficient λ is described below. Eq. (4.7.1-3) can be rearranged to Eqs. (4.7.1-14) ~ (4.7.1-16), where Eq. (4.7.1-19) express a singular-value decomposition of the matrix $\mathbf{A} \cdot \mathbf{D}^{-1}$.

$$\left(\mathbf{A}^T \cdot \mathbf{A} + \lambda \cdot \mathbf{D}^2\right) \cdot \Delta\mathbf{x} = \mathbf{b} \tag{4.7.1-14}$$

$$\left[\left(\mathbf{A} \cdot \mathbf{D}^{-1}\right)^T \cdot \left(\mathbf{A} \cdot \mathbf{D}^{-1}\right) + \lambda \cdot \mathbf{I}\right] \cdot \mathbf{D} \cdot \Delta\mathbf{x} = \mathbf{D}^{-1} \cdot \mathbf{b} \tag{4.7.1-15}$$

$$\left(\mathbf{\Lambda}^2 + \lambda \cdot \mathbf{I}\right) \cdot \mathbf{V}^T \cdot \mathbf{D} \cdot \Delta\mathbf{x} = \mathbf{V}^T \cdot \mathbf{D}^{-1} \cdot \mathbf{b} \tag{4.7.1-16}$$

$$\mathbf{b} = \tilde{\mathbf{K}}_i^T \cdot \tilde{\mathbf{y}}_i - \mathbf{S}_a^{-1} \cdot \left(\mathbf{x} - \mathbf{x}_a\right) \tag{4.7.1-17}$$

$$\Delta\mathbf{x} = \mathbf{x}_{i+1} - \mathbf{x}_i \tag{4.7.1-18}$$

$$\mathbf{A} \cdot \mathbf{D}^{-1} = \mathbf{U} \cdot \mathbf{\Lambda} \cdot \mathbf{V}^T \tag{4.7.1-19}$$

Using $\mathbf{V} \cdot \mathbf{V}^T = \mathbf{I}$ and eq. (4.7.1-16), the variation of the solution $|\mathbf{D} \cdot \Delta\mathbf{x}|$ is expressed as Eq. (4.7.1-20).

$$\left|\mathbf{D} \cdot \Delta\mathbf{x}\right| = \left|\mathbf{V}^T \cdot \mathbf{D} \cdot \Delta\mathbf{x}\right| = \left|\left(\mathbf{\Lambda}^2 + \lambda \cdot \mathbf{I}\right)^{-1} \cdot \mathbf{V}^T \cdot \mathbf{D}^{-1} \cdot \mathbf{b}\right| \tag{4.7.1-20}$$

Let the radius of the trust region for the variation of the solution be δ.

$$\left|\mathbf{D}\cdot\Delta\mathbf{x}_2\right| = \left|\left(\mathbf{\Lambda}^2 + \lambda\cdot\mathbf{I}\right)^{-1}\cdot\mathbf{V}^T\cdot\mathbf{D}^{-1}\cdot\mathbf{b}\right| \le \delta \qquad (4.7.1\text{-}21)$$

Then, the minimum value of λ (≥ 0) satisfying the above condition can be derived numerically from Eq. (4.7.1-21), where the initial value of δ is the value obtained by calculating the right side of Eq. (4.7.1-21) using the solution initially obtained by solving Eq. (4.7.1-5).

$$\delta = \left|\mathbf{D}\cdot\Delta\mathbf{x}_1\right| \qquad (4.7.1\text{-}22)$$

Using the obtained correction vector $\Delta\mathbf{x}_2$, update the solution $\mathbf{x}_i$. Before processing the next iteration step, evaluate the impact of the non-linearity of the forward model, and update the radius δ of the trust region. Let consider the parameter r given by Eq. (4.7.1-23).

$$r = \frac{J\left(\mathbf{x}_i + \Delta\mathbf{x}_2\right) - J\left(\mathbf{x}_i\right)}{J'\left(\mathbf{x}_i + \Delta\mathbf{x}_2\right) - J\left(\mathbf{x}_i\right)} = \frac{J\left(\mathbf{x}_i + \Delta\mathbf{x}_2\right) - J\left(\mathbf{x}_i\right)}{-\Delta\mathbf{x}_2^T\cdot\left(\widetilde{\mathbf{K}}_i^T\cdot\widetilde{\mathbf{K}}_i + \mathbf{S}_a^{-1} + 2\cdot\lambda\cdot\mathbf{D}^2\right)\cdot\Delta\mathbf{x}_2} \qquad (4.7.1\text{-}23)$$

where $J'(\mathbf{x}_i+\Delta\mathbf{x}_2)$ represents the cost function evaluated assuming that the forward model is linear ($\mathbf{F}(\mathbf{x}_i+\Delta\mathbf{x}_2) = \mathbf{F}(\mathbf{x}_i) + \mathbf{K}_i\cdot\Delta\mathbf{x}_2$).

When $r > 10^{-4}$, adopt the correction vector $\Delta\mathbf{x}_2$ and move to the next iteration step, where with max(0.5, min(2, 0.5 / | r - 1 |)) of greater than 1, and increase of δ will be requested. In cases where the increase of δ is requested more than twice, or where max(0.5, min(2, 0.5 / | r - 1 |)) is less than 1; multiply δ by max(0.5, min(2, 0.5 / | r - 1 |)). The reason why δ is not increased on the initial request to prevent the oscillation of δ.

When $r \le 10^{-4}$, the correction vector $\Delta\mathbf{x}_2$ is rejected and Eq. (4.7.1-5) is solved again multiplying min(δ', δ) by 0.5, where δ' is the δ calculated from Eq. (4.7.1-22) using the latest $\Delta\mathbf{x}_1$. This case indicates that the solution is diverging. If the divergence is repeated more than the specified number of times without progressing the iteration steps, the retrieval process terminates with no solution.

Note that the updated δ will never exceed the initial value of δ.

Finally, the condition of terminating the iterative process is described below. When satisfying the both Eqs. (4.7.1-24) and (4.7.1-25), the solution is determined to have converged. The former condition indicates that the variation of spectrum residual is small enough, and the latter indicates that the variation of the solution is small enough.

$$\frac{\left|J\left(\mathbf{x}_{i+1}\right)-J\left(\mathbf{x}_{i}\right)\right|}{m}<f_{tol} \tag{4.7.1-24}$$

$$\frac{\left|\left(\mathbf{x}_{i+1}-\mathbf{x}_{i}\right)^{T}\cdot\mathbf{S}^{-1}\cdot\left(\mathbf{x}_{i+1}-\mathbf{x}_{i}\right)\right|}{n}<x_{tol} \tag{4.7.1-25}$$

$$\mathbf{S}=\left(\widetilde{\mathbf{K}}_{i}^{T}\cdot\widetilde{\mathbf{K}}_{i}+\mathbf{S}_{a}^{-1}\right)^{-1} \tag{4.7.1-26}$$

where m is the number of elements of the observed radiance spectrum $\mathbf{y}$, and n is the number of elements of the state vector $\mathbf{x}$.

The iterative process terminates when the solution is converged or when the solution does not converge even after reaching the specified maximum number of iterations as well as when the solution diverges even after reaching the specified maximum number of repeated divergences as mentioned above. The maximum numbers of iterations, the maximum number of repeated divergences, f_{tol}, and x_{tol} are specified for each retrieval.

<A posteriori processing after iterative process>

After the iterative process ends, the following calculations are carried out, however, Eqs. (4.7.1-31) ~ (4.7.1-43) are calculated only when the column-averaged dry-air mole fraction is retrieved. The subscripts x and c denote the elements corresponding to and not corresponding to the gas species to be retrieved, respectively, whereas for the vectors and matrices, the subscripts refer to the submatrices consisting of the corresponding elements.

- Mean squared of the residual spectrum (MRS)

$$\chi_{SB}^{2}=\frac{\widetilde{\mathbf{y}}_{SB}^{T}\cdot\widetilde{\mathbf{y}}_{SB}}{m_{SB}} \tag{4.7.1-27}$$

where the subscript SB denotes the target sub-band and the vector consists only of the corresponding elements.

- Error covariance matrix

$$\mathbf{S}=\left(\widetilde{\mathbf{K}}^{T}\cdot\widetilde{\mathbf{K}}+\mathbf{S}_{a}^{-1}\right)^{-1} \tag{4.7.1-28}$$

- Averaging kernel matrix

$$\mathbf{AK}=\widetilde{\mathbf{G}}\cdot\widetilde{\mathbf{K}} \tag{4.7.1-29}$$

$$\widetilde{\mathbf{G}}=\mathbf{S}\cdot\widetilde{\mathbf{K}}^{T} \tag{4.7.1-30}$$

- Pressure weighting function

$$\left(\mathbf{h}\right)_j = h_j = \frac{w_{dry,j}}{\sum_j w_{dry,j}} \tag{4.7.1-31}$$

where the subscript j denote a vertical grid.

- Column-averaged dry-air mole fraction

$$X_x = \mathbf{h}^T \cdot \mathbf{x}_x \tag{4.7.1-32}$$

- DFS (degree of freedom for signals) of column-averaged dry-air mole fraction

$$DFS_x = trace\left(\mathbf{AK}_{xx}\right) \tag{4.7.1-33}$$

$$\mathbf{AK}_{xx} = \widetilde{\mathbf{G}}_x \cdot \widetilde{\mathbf{K}}_x \tag{4.7.1-34}$$

- Column averaging kernel of column-averaged dry-air mole fraction

$$\left(\mathbf{a}_x\right)_j = a_{x,j} = \left(\mathbf{h}^T \cdot \mathbf{AK}_{xx}\right)_j \cdot \frac{1}{h_j} \tag{4.7.1-35}$$

- Retrieval noise of column-averaged dry-air mole fraction

$$\mathbf{S}_{m,x} = \widetilde{\mathbf{G}}_x \cdot \widetilde{\mathbf{G}}_x{}^T \tag{4.7.1-36}$$

$$\sigma_{m,x} = \sqrt{\mathbf{h}^T \cdot \mathbf{S}_{m,x} \cdot \mathbf{h}} \tag{4.7.1-37}$$

- Smoothing error of column-averaged dry-air mole fraction

$$\mathbf{S}_{s,x} = \left(\mathbf{AK}_{xx} - \mathbf{I}\right) \cdot \mathbf{S}_{a,xx} \cdot \left(\mathbf{AK}_{xx} - \mathbf{I}\right)^T \tag{4.7.1-38}$$

$$\sigma_{s,x} = \sqrt{\mathbf{h}^T \cdot \mathbf{S}_{s,x} \cdot \mathbf{h}} \tag{4.7.1-39}$$

- Interference error of column-averaged dry-air mole fraction

$$\mathbf{S}_{i,x} = \mathbf{AK}_{xc} \cdot \mathbf{S}_{a,xc} \cdot \mathbf{AK}_{xc}^T \tag{4.7.1-40}$$

$$\sigma_{i,x} = \sqrt{\mathbf{h}^T \cdot \mathbf{S}_{i,x} \cdot \mathbf{h}} \tag{4.7.1-41}$$

$$\mathbf{AK}_{xc} = \widetilde{\mathbf{G}}_x \cdot \widetilde{\mathbf{K}}_c \tag{4.7.1-42}$$

- Uncertainty of column-averaged dry-air mole fraction

$$\sigma_x = \sqrt{\sigma_{m,x}^2 + \sigma_{s,x}^2 + \sigma_{i,x}^2} \tag{4.7.1-43}$$

Note:

$$\begin{aligned}
\mathbf{S} &= \left(\widetilde{\mathbf{K}}^T \cdot \widetilde{\mathbf{K}} + \mathbf{S}_a^{-1}\right)^{-1} \\
&= \left(\widetilde{\mathbf{K}}^T \cdot \widetilde{\mathbf{K}} + \mathbf{S}_a^{-1}\right)^{-1} \cdot \left(\widetilde{\mathbf{K}}^T \cdot \widetilde{\mathbf{K}} + \mathbf{S}_a^{-1}\right) \cdot \left(\widetilde{\mathbf{K}}^T \cdot \widetilde{\mathbf{K}} + \mathbf{S}_a^{-1}\right)^{-1} \\
&= \left(\widetilde{\mathbf{K}}^T \cdot \widetilde{\mathbf{K}} + \mathbf{S}_a^{-1}\right)^{-1} \cdot \widetilde{\mathbf{K}}^T \cdot \widetilde{\mathbf{K}} \cdot \left(\widetilde{\mathbf{K}}^T \cdot \widetilde{\mathbf{K}} + \mathbf{S}_a^{-1}\right)^{-1} \\
&\quad + \left(\widetilde{\mathbf{K}}^T \cdot \widetilde{\mathbf{K}} + \mathbf{S}_a^{-1}\right)^{-1} \cdot \mathbf{S}_a^{-1} \cdot \left(\widetilde{\mathbf{K}}^T \cdot \widetilde{\mathbf{K}} + \mathbf{S}_a^{-1}\right)^{-1} \\
&= \widetilde{\mathbf{G}} \cdot \widetilde{\mathbf{G}}^T + \left(\mathbf{AK} - \mathbf{I}\right) \cdot \mathbf{S}_a \cdot \left(\mathbf{AK} - \mathbf{I}\right)^T \\
&= \begin{pmatrix} \widetilde{\mathbf{G}}_x \\ \widetilde{\mathbf{G}}_c \end{pmatrix} \cdot \begin{pmatrix} \widetilde{\mathbf{G}}_x^T & \widetilde{\mathbf{G}}_c^T \end{pmatrix} \\
&\quad + \begin{pmatrix} \mathbf{AK}_{xx} - \mathbf{I} & \mathbf{AK}_{xc} \\ \mathbf{AK}_{cx} & \mathbf{AK}_{cc} - \mathbf{I} \end{pmatrix} \cdot \begin{pmatrix} \mathbf{S}_{a,xx} & 0 \\ 0 & \mathbf{S}_{a,cc} \end{pmatrix} \cdot \begin{pmatrix} \left(\mathbf{AK}_{xx} - \mathbf{I}\right)^T & \mathbf{AK}_{cx}^T \\ \mathbf{AK}_{xc}^T & \left(\mathbf{AK}_{cc} - \mathbf{I}\right)^T \end{pmatrix} \\
&= \begin{pmatrix} \mathbf{S}_{xx} & \mathbf{S}_{xc} \\ \mathbf{S}_{cx} & \mathbf{S}_{cx} \end{pmatrix}
\end{aligned} \tag{4.7.1-44}$$

$$\begin{aligned}
\mathbf{S}_{xx} &= \widetilde{\mathbf{G}}_x \cdot \widetilde{\mathbf{G}}_x^T + \left(\mathbf{AK}_{xx} - \mathbf{I}\right) \cdot \mathbf{S}_{a,xx} \cdot \left(\mathbf{AK}_{xx} - \mathbf{I}\right)^T + \mathbf{AK}_{xc} \cdot \mathbf{S}_{a,cc} \cdot \mathbf{AK}_{xc}^T \\
&= \mathbf{S}_{m,x} + \mathbf{S}_{s,x} + \mathbf{S}_{i,x}
\end{aligned} \tag{4.7.1-45}$$

4.7.2 Retrieval Setting

In each retrieval, the state vector $\mathbf{x}$ and its a priori value $\mathbf{x}_a$ are column vectors with unknown parameters to be retrieved placed in order. The variance-covariance matrix $\mathbf{S}_a$ for the a priori value is a matrix in which variance-covariance matrices of each unknown parameter are placed as expressed in Eqs. (4.7.2-1) ~ (4.7.2-3).

$$\mathbf{x} = \begin{pmatrix} \mathbf{x}_{gas1}^T & \mathbf{x}_{gas2}^T & \cdots & \mathbf{x}_{aer1}^T & \cdots & \mathbf{x}_{alb-SB1}^T & \mathbf{x}_{alb-SB2}^T & \cdots \end{pmatrix}^T \tag{4.7.2-1}$$

$$\mathbf{x}_a = \begin{pmatrix} \mathbf{x}_{a,gas1}^T & \mathbf{x}_{a,gas2}^T & \cdots & \mathbf{x}_{a,aer1}^T & \cdots & \mathbf{x}_{a,alb-SB1}^T & \mathbf{x}_{a,alb-SB2}^T & \cdots \end{pmatrix}^T \tag{4.7.2-2}$$

$$\mathbf{S}_a = \begin{pmatrix} \mathbf{S}_{a,gas1} & & & & & & \\ & \mathbf{S}_{a,gas2} & & 0 & & & \\ & & \ddots & & & & \\ & & & \mathbf{S}_{a,aer1} & & & \\ & & & & \ddots & & \\ & 0 & & & \mathbf{S}_{a,alb-SB1} & & \\ & & & & & \mathbf{S}_{a,alb-SB2} & \\ & & & & & & \ddots \end{pmatrix} \tag{4.7.2-3}$$

where the subscript *SB* denotes a sub-band.

Further, the observed radiance spectrum **y** and forward model **F**(**x**, **c**) are column vectors in which radiance spectra of each sub-band are placed in order, whereas the variance-covariance matrix $\mathbf{S}_\varepsilon$ is a matrix in which variance-covariance matrices of each sub-band are placed in order as expressed in Eqs. (4.7.2-4) ~ (4.7.2-6). Here, the polarization synthesized spectrum calculated by Eq. (4.5-23) is used as the observed radiance spectrum.

$$\mathbf{y} = \begin{pmatrix} \mathbf{y}_{SB1}^T & \mathbf{y}_{SB2}^T & \cdots \end{pmatrix}^T \tag{4.7.2-4}$$

$$\mathbf{F}(\mathbf{x},\mathbf{c}) = \begin{pmatrix} \mathbf{F}_{SB1}(\mathbf{x},\mathbf{c})^T & \mathbf{F}_{SB2}(\mathbf{x},\mathbf{c})^T & \cdots \end{pmatrix}^T \tag{4.7.2-5}$$

$$\mathbf{S}_\varepsilon = \begin{pmatrix} \mathbf{S}_{\varepsilon,SB1} & & 0 \\ & \mathbf{S}_{\varepsilon,SB2} & \\ 0 & & \ddots \end{pmatrix} \tag{4.7.2-6}$$

The contribution of forward model error on $\mathbf{S}_\varepsilon$ is empirically modeled as Eq. (4.7.2-7). This scaling is sometimes referred to as empirical noise. $\mathbf{S}_\varepsilon$ is the diagonal matrix with the variance $\sigma^2_{empirical,SB}$ as its diagonal elements.

$$\sigma^2_{empirical,SB} = \sigma^2_{synth,SB} \cdot \left[a_{0,SB} + a_{1,SB} \cdot SNR_{SB} + a_{2,SB} \cdot SNR_{SB}^2 \right] \tag{4.7.2-7}$$

where coefficients a_0, a_1, and a_2 are evaluated for each sub-band by fitting the lower envelope of the mean squared of the residual spectrum, obtained from the retrieval processing using a diagonal matrix $\mathbf{S}_\varepsilon$ with diagonal elements $\sigma^2_{synth,SB}$, as a function of SNR (Fig. 4.7.2-1).

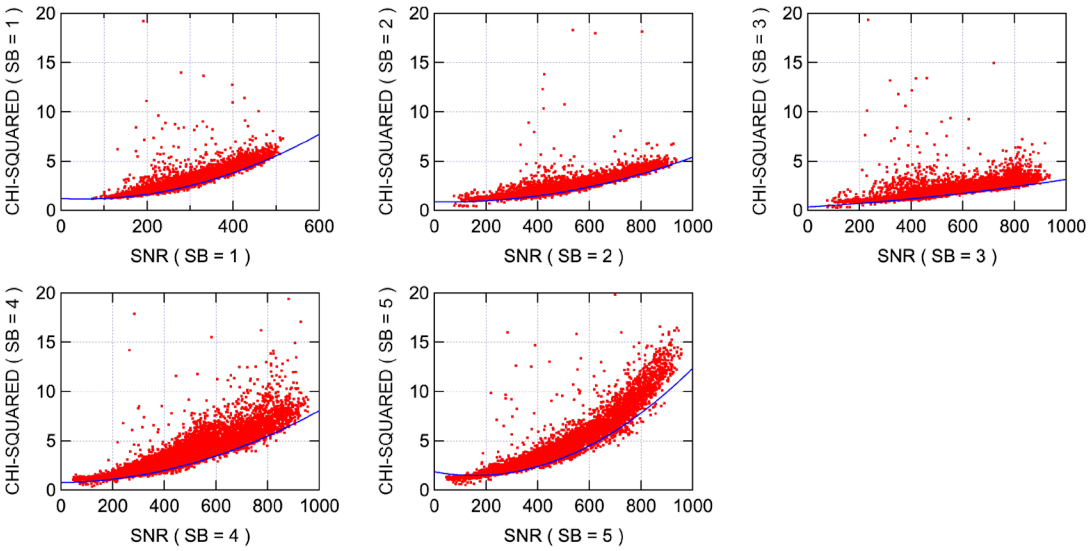

Figure 4.7.2-1. Example of the empirical noise. Red dots are the mean squared of the residual spectrum obtained from the retrieval using a diagonal matrix $\mathbf{S}_\varepsilon$ with diagonal elements $\sigma^2_{synth,SB}$, and the blue line shows the fitting function of the lower envelope of the mean squared of the residual spectrum as a function of SNR.

The wavenumber range and state vector elements for each individual retrieval are summarized in Tables 4.7.2-1 ~ 4.7.2-7. Note that the Lambertian surface is tentatively assumed, regardless the actual land fraction within the FTS-2 IFOV-area.

Table 4.7.2-1. Retrieval (SIF & proxy method): Band 1 Chlorophyll fluorescence

Item	Contents	Note
process ID	B1_SIF	
wavenumber range	13173 ~ 13227 cm^{-1}	polarization synthesized spectrum
state vector elements	zero-level offset	Equivalent to FS (= US + SIF) (see Sec. 4.1)
	surface albedo (2 wavenumber grid points)	zigzag approximation
	wavenumber dispersion correction factor	
forward model	no cloud and aerosol	

Table 4.7.2-2. Retrieval (SIF & proxy method): Band 1 Surface pressure

Item	Contents	Note
process ID	B1_Psrf	
wavenumber range	12950 ~ 13200 cm^{-1}	polarization synthesized spectrum
state vector elements	surface pressure	
	temperature shift	
	surface albedo (2 wavenumber grid points)	zigzag approximation
	wavenumber dispersion correction factor	
forward model	no cloud and aerosol	

Table 4.7.2-3. Retrieval (SIF & proxy method): Band 2 CO_2 1.6 μm band

Item	Contents	Note
process ID	B2_1590	
wavenumber range	6180 ~ 6380 cm^{-1}	polarization synthesized spectrum
state vector elements	CO_2 profile (15 layers)	layer-averaged dry-air mole fraction
	H_2O profile (15 layers)	layer-averaged dry-air mole fraction
	surface albedo (9 wavenumber grid points)	zigzag approximation
	wavenumber dispersion correction factor	
forward model	no cloud and aerosol	

Table 4.7.2-4. Retrieval (SIF & proxy method): Band 2 CH_4 1.67 μm band

Item	Contents	Note
process ID	B2_1660	
wavenumber range	5900 ~ 6150 cm^{-1}	polarization synthesized spectrum
state vector elements	CH_4 profile (15 layers)	layer-averaged dry-air mole fraction
	H_2O profile (15 layers)	layer-averaged dry-air mole fraction
	surface albedo (11 wavenumber grid points)	zigzag approximation
	wavenumber dispersion correction factor	
forward model	no cloud and aerosol	

Table 4.7.2-5. Retrieval (SIF & proxy method): Band 3 CO_2 2.08 μm band

Item	Contents	Note
process ID	B3_2060	
wavenumber range	4800 ~ 4900 cm^{-1}	polarization synthesized spectrum
state vector elements	CO_2 profile (15 layers)	layer-averaged dry-air mole fraction
	H_2O profile (15 layers)	layer-averaged dry-air mole fraction
	surface albedo (5 wavenumber grid points)	zigzag approximation
	wavenumber dispersion correction factor	
forward model	no cloud and aerosol	

Table 4.7.2-6. Retrieval (SIF & proxy method): Band 3 CO 2.3 μm band

Item	Contents	Note
process ID	B3_2350	
wavenumber range	4200 ~ 4300 cm^{-1}	polarization synthesized spectrum
state vector elements	CO profile (15 layers)	layer-averaged dry-air mole fraction
	CH_4 profile (15 layers)	layer-averaged dry-air mole fraction
	H_2O profile (15 layers)	layer-averaged dry-air mole fraction
	surface albedo (5 wavenumber grid points)	zigzag approximation
	wavenumber dispersion correction factor	
forward model	no cloud and aerosol	

Table 4.7.2-7. Retrieval (full-physics method): Column-averaged dry-air mole fraction

Item	Contents	Note
process ID	SWFP	
wavenumber range	SB1: 12950 ~ 13200 cm^{-1} SB2: 6180 ~ 6380 cm^{-1} SB3: 5900 ~ 6150 cm^{-1} SB4: 4800 ~ 4900 cm^{-1} SB5: 4200 ~ 4300 cm^{-1}	polarization synthesized spectrum The sub-bands (SBs) are numbered in the alignment order as 1, 2, 3, 4, and 5.
state vector elements	CO_2 profile (15 layers)	layer-averaged dry-air mole fraction
	CH_4 profile (15 layers)	layer-averaged dry-air mole fraction
	CO profile (15 layers)	layer-averaged dry-air mole fraction
	H_2O profile (15 layers)	layer-averaged dry-air mole fraction
	aerosol profile (15 layers, 2 types)	logarithm of the optical thickness at reference wavelength
	surface pressure	
	temperature shift	
	chlorophyll fluorescence (SIF at reference wavenumber)	
	chlorophyll fluorescence (slope for wavenumber)	
	surface albedo (2, 9, 11, 2, and 2 wavenumber grid points for SBs 1 ~ 5)	zigzag approximation
	wavenumber dispersion correction factor (each SB)	
forward model	no cloud	

4.7.3 Vertical Grid

For the FTS-2 SWIR L2 processing, the following three types of vertical grids are defined (Figure 4.7.3-1).

(a) Main-layer

The vertical grid created by evenly dividing the atmosphere by atmospheric pressure is defined as a Main-layer and is utilized to describe a unknown parameters when its vertical profile is retrieved, e.g., the layer-averaged (partial column-averaged) dry-air mole fraction of gas species and the optical thickness for each layer and each aerosol type. The number of layers of a Main-layer Nm is determined to be 15.

(b) Sub-layer

The molecular absorption cross-section is a function of pressure and temperature, and in order to accurately calculate the gas absorption optical thickness, vertical profiles of pressure and temperature inside the Main-layer need to be considered. Let each layer of the Main-layer further divide into Nd layers and defined them as Sub-layers, where the top layer of the Main-layer is evenly divided by the logarithm of the pressure and the other layers are evenly divided by the pressure. That is, each Sub-layer belongs to one of the Main-layers. Sub-layers are utilized only when calculating the gas absorption optical thickness of each layer of the Main-layer. The number of layers to be divided (Nd) is set to 12 layers, so the total number of Sub-layers Ns will be $Ns = Nm \cdot Nd = 180$ layers.

(c) RT-layer

In calculating a radiative transfer considering clouds in the FTS-2 SWIR L2 processing, the cloud-top and -bottom pressures are need to be added to the layer boundaries. A vertical grid in which the cloud-top and -bottom pressures are added to a Main-layer as layer boundaries is defined as an RT-layer. By adding a boundary, the pre-existing layer is divided into two layers, where the optical thickness of the existing layer is allocated in proportion to the pressure difference between the created two layers. However, in case that the boundary to be added is quite closed to the existing boundary (one of the distribution ratios proportional to the pressure difference is less than 10^{-6}), the boundary will not be added and will be substituted by the existing boundary. Therefore, the number of RT-layer Nr is not a fixed value but between Nm and (Nm + 2) layers, and each RT-layer belongs to one of the Main-layers. Note that, when “no cloud” is assumed in the retrieval, the RT-layer is equal to the Main-layer.

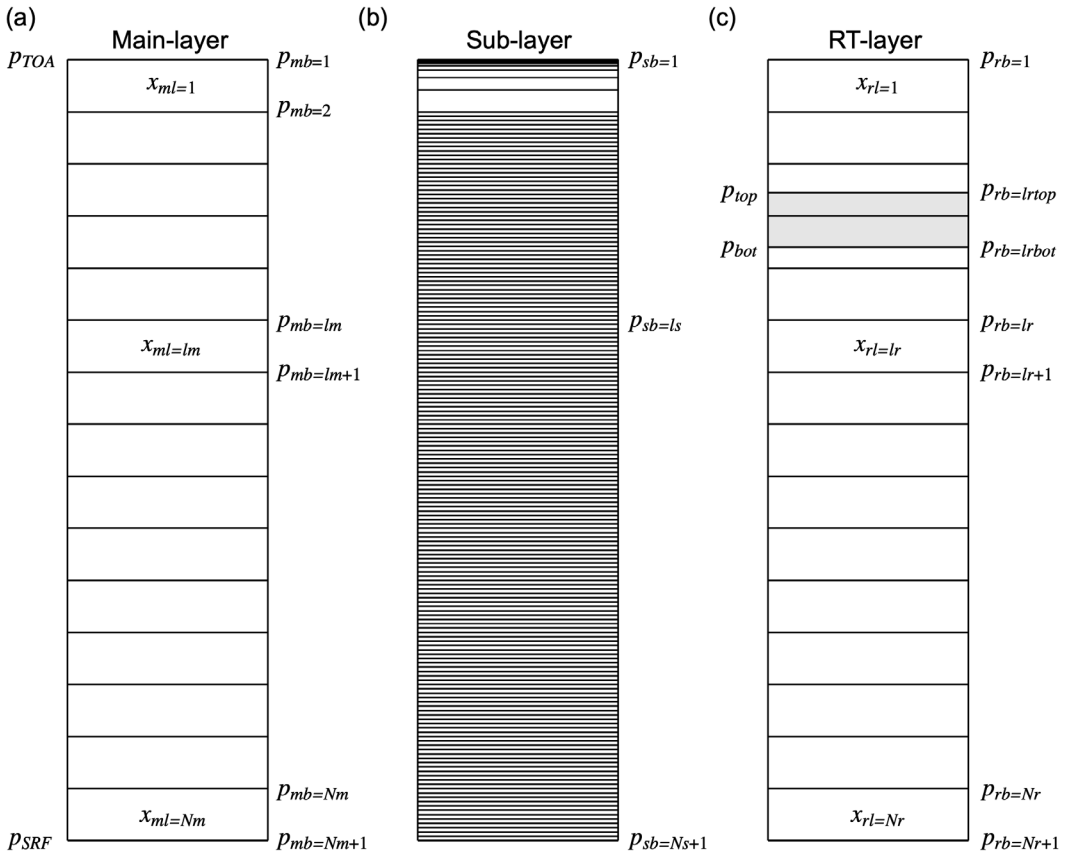

Figure 4.7.3-1. Vertical grids utilized in FTS-2 SWIR L2 processing. (a) Main-layer, (b) Sub-layer, and (c) RT-layer. x is an arbitrary parameter. The subscripts *mb*, *sb*, and *rb* denote the values at the boundaries of the Main-layer, Sub-layer, and RT-layer, respectively. The subscripts *ml*, *sl*, and *rl* denote the values within the Main-layer, Sub-layer, and RT-layer, respectively.

It is preferable that the pressure at the top of the atmosphere (TOA) p_{TOA} in a forward model is small enough to ignore the column amount outside the calculation boundaries but high enough to hold the local thermodynamic equilibrium (LTE). Hence, the pressure p_{TOA} is set to 0.1 hPa. Using this pressure, and the surface pressure p_{SRF}, the pressures at each boundary of a Main-layer and a Sub-layer are given by Eqs. (4.7.3-1) and (4.7.3-2), respectively.

$$p_{mb=lm} = \frac{Nm+1-lm}{Nm} \cdot p_{TOA} + \frac{lm-1}{Nm} \cdot p_{SRF} \qquad lm = 1,2,3,...Nm+1 \tag{4.7.3-1}$$

$$p_{sb=ls} = \begin{cases} p_{TOA} \cdot \left(1 + \dfrac{1}{Nm} \cdot \dfrac{p_{SRF} - p_{TOA}}{p_{TOA}}\right)^{(ls-1)/Nd} & 1 \le ls \le Nd \\ \dfrac{Ns+1-ls}{Ns} \cdot p_{TOA} + \dfrac{ls-1}{Ns} \cdot p_{SRF} & Nd+1 \le ls \le Ns+1 \end{cases} \tag{4.7.3-2}$$

The boundary elements corresponding to the cloud-top pressure p_{top} and the cloud-bottom pressure p_{bot} in a RT-layer are denoted by *lrtop* and *lrbot*, respectively. Let the element of the Main-layer to which the element of the RT-layer *lr* belongs be *lm*(*lr*), then the distribution ratio of the RT-layer to the Main-layer $frc_{RT}(lr)$ along with the addition of boundaries is given by Eq. (4.7.3-3).

$$frc_{RT}\left(lr\right)=\begin{cases}\dfrac{p_{rb=lr+1}-p_{rb=lr}}{p_{mb=lm(lr)+1}-p_{mb=lm(lr)}}=\dfrac{Nm\cdot\left(p_{rb=lr+1}-p_{rb=lr}\right)}{p_{SRF}-p_{TOA}} & lrtop-1\le lr\le lrbot\\ 1 & others\end{cases} \tag{4.7.3-3}$$

Likewise, the distribution ratio of the RT-layer to the optical thickness of cirrus clouds $frc_{CLD}(lr)$ is given by Eq. (4.7.3-4).

$$frc_{CLD}\left(lr\right)=\begin{cases}\dfrac{p_{rb=lr+1}-p_{rb=lr}}{p_{rb=lrbot}-p_{rb=lrtop}} & lrtop\le lr\le lrbot-1\\ 0 & others\end{cases} \tag{4.7.3-4}$$

4.7.4 Forward Model

The forward model consists of two parts. The first part is the radiative transfer calculation that computes the upward Stokes vector and the weighting functions at the top of the atmosphere. The second part is the instrument model that takes the instrument characteristics into account to calculate the theoretical radiance spectrum and the Jacobian from the obtained Stokes vector and weighting functions.

(a) Overview

The one-dimensional vector radiative transfer equation is expressed as Eq. (4.7.4-1).

$$\mu\cdot\frac{\partial\mathbf{I}\left(\tau,\mu,\phi\right)}{\partial\tau}=-\mathbf{I}\left(\tau,\mu,\phi\right)+\omega\cdot\int_{-1}^{1}d\mu'\int_{0}^{2\pi}d\phi'\mathbf{P}\left(\tau,\mu,\phi;\mu',\phi'\right)\cdot\mathbf{I}\left(\tau,\mu',\phi'\right)+\left(1-\omega\right)\cdot\mathbf{B}\left(\tau\right) \tag{4.7.4-1}$$

where $\mathbf{I}=(I, Q, U, V)^{\mathrm{T}}$ is a Stokes vector and the first element I is radiance. τ is the optical

thickness measured from TOA, μ is the cosine of the polar angle from $+\tau$ axis (a vertical downward axis), ϕ is an azimuth angle, ω is a single scattering albedo, **P** is a scattering phase matrix, and **B** is a thermal radiation vector.

As a method to calculate the upward Stokes vector at TOA by solving Eq. (4.7.4-1), the vector radiative transfer code, *pstar* (Ota et al., 2010) is employed. The source code of *pstar* is available from the following site: OpenCLASTR (https://ccsr.aori.u-tokyo.acjp/~clastr/). (Note: the version used here is *pstar4*, which is before the public release as of the time of this writing.)

In *pstar*, when solving the one-dimensional radiative transfer equation, the vertically inhomogeneous atmosphere is divided into multiple atmospheric layers each considered homogeneous, and the reflection, transmission, and emission matrices of each of the layers are calculated using the Discrete-Ordinate method. Then a Stokes vector at an arbitrary point and in an arbitrary direction is calculated using the Matrix Operator method. The TMS method (Nakajima and Tanaka, 1988) is used to enable an accurate radiance calculation even with a small number of streams. For more details, refer to Ota et al. (2010). With *pstar4*, used in the FTS-2 SWIR L2 processing, the weighting functions with respect to the absorption optical thickness for each layer, the scattering optical thickness due to molecules and particles (cloud and aerosol) for each layer, and the surface albedo or surface wind speed depend on the surface type are calculated simultaneously in addition to the Stokes vector.

In order to accurately consider the instrument characteristics in the subsequent instrument model, the wavenumber interval of Stokes vector and weighting functions should be sufficiently finer than the TANSO-FTS-2's sampling interval of 0.2 cm^{-1}. In the radiative transfer calculation, the wavenumber interval is set to 0.01 cm^{-1}, however, performing the *pstar* calculation with this interval size for all wavenumber points within the applicable wavenumber range (> 20,000 wavenumber points) requires a high calculation cost. For this reason, the highspeed radiative transfer calculation method by Duan et al. (2005) is employed in combination. Note that in Duan's calculation method, the wavenumber dependencies of the aerosol scattering properties and the surface albedo, so the method is specifically extended to take them also into consideration.

For chlorophyll fluorescence, the above mentioned highspeed radiative transfer calculation method is difficult to combine, and thus it is calculated using an approximation expression and added to the Stokes vector and weighting functions obtained by the highspeed radiative transfer calculation.

In the instrument model, a convolution integral of the instrument line shape function is performed with respect to the thus-obtained Stokes vector and weighting functions while considering the instrument characteristics of FTS-2.

Further details of the forward model are presented below. In the radiative transfer calculation, the detailed information on *pstar* itself is not provided but it left to Ota et al. (2010), and information

on the other parts will be explained.

(b) Radiative transfer calculation: Input and output of *pstar*

As stated above, in order to omit the detailed explanation about *pstar*, the input and output variables that are the interfaces of *pstar* are shown below.

<Input variables>

In each layer of RT-layer,

- Optical thickness $\tau_{rl}(\nu)$
- Optical thickness of Rayleigh scattering $\tau_{sca,m,rl}(\nu)$
- Optical thickness of scattering elements other than Rayleigh scattering by type $\tau_{sca,p,type,rl}(\nu)$
- Scattering phase matrix of scattering elements other than Rayleigh scattering by type $\mathbf{P}_{p,type,rl}(\Theta,\nu)$
  * Note: Θ is a scattering angle
- Depolarization factor of Rayleigh scattering $\delta_{rl}(\nu)$

For the case of surface reflectivity is homogeneous (Lambertian surface)

- Surface albedo $\alpha(\nu)$

For the case of surface reflectivity is calculated based on Cox-Munk model (Cox and Munk, 1954)

- Surface wind speed u_{10}
- Complex refractive index of water $m_{wat}(\nu)$

Irradiance of the incident light at TOA $f_0(\nu)$

Cosine of the angle between the incident light unit vector and $+\tau$ axis $\mu_0 = \cos(\theta_0)$

Cosine of the angle between the observation light unit vector and $+\tau$ axis $\mu_1 = -\cos(\theta_1)$

Relative azimuth angle between incident light unit vector and observation light unit vector $\phi = \phi_0 - \phi_1 + \pi$

where θ_0, ϕ_0, θ_1, and ϕ_1 are solar zenith and azimuth angle, satellite zenith and azimuth angle calculated in the FTS-2 L2 pre-processing, respectively.

<Output variables>

Stokes vector of emergent light to the satellite direction at TOA $\mathbf{I}_{RT}(\nu)$

Spherical albedo r

In each layer of RT-layer

- Weighting function with respect to the optical thickness of Rayleigh scattering

  $\partial\mathbf{I}_{RT}(\nu)/\partial\ln(\tau_{sca,m,rl}(\nu))$, $\partial r(\nu)/\partial\ln(\tau_{sca,m,rl}(\nu))$
- Weighting function with respect to the optical thickness of scattering elements other than

Rayleigh scattering by type

$$\partial \mathbf{I}_{RT}(\nu)/\partial \ln(\tau_{sca,p,type,rl}(\nu)),\ \partial r(\nu)/\partial \ln(\tau_{sca,p,type,rl}(\nu))$$

- Weighting function with respect to the absorption optical thickness

$$\partial \mathbf{I}_{RT}(\nu)/\ln(\partial \tau_{abs,rl}(\nu)),\ \partial r(\nu)/\ln(\partial \tau_{abs,rl}(\nu))$$

For the case of surface reflectivity is homogeneous (Lambertian surface)

- Weighting function with respect to surface albedo $\partial \mathbf{I}_{RT}(\nu)/\partial \alpha(\nu)$

For the case of surface reflectivity is calculated based on Cox-Munk model

- Weighting function with respect to surface wind speed $\partial \mathbf{I}_{RT}(\nu)/\partial u_{10}$

where the subscripts *sca* and *abs* denote scattering and absorption component, respectively, the subscripts *m* and *p* are a gas molecule and a set of aerosol and clouds (scattering elements other than Rayleigh scattering), respectively, and the subscript *type* is a type of aerosol and cloud.

The vector radiative transfer code, *pstar*, is a generic atmospheric radiative transfer code and is utilized under the following condition in the FTS-2 SWIR L2 processing.

- Among the Stokes parameter $\mathbf{I}_{RT}(\nu) = (I, Q, U, V)^{\mathrm{T}}$, only $I(\nu)$ is calculated.
- The number of streams is set at six for a hemisphere.
- Thermal radiation is not considered.
- Regardless the land fraction within the FTS-2 IFOV-area, homogeneous surface reflectivity (Lambertian surface) is assumed.

(c) Radiative transfer calculation: Highspeed radiative transfer calculation method

The idea underlying the highspeed radiative transfer calculation is to categorize the atmospheric parameters of tens of thousands of wavenumber points into groups by the several parameters that present a certain kind of similarities, and parameterize the radiance using the grouping parameters. The radiative transfer calculation is performed using *pstar* for the sample points extracted from the applicable wavenumber range, and after creating a table using grouping parameters, the Stokes vectors and weighting functions are calculated by interpolating the table for all the wavenumber points within the target wavenumber range, thereby reducing the computational cost significantly.

Let the optical thickness due to the gas absorption and scattering of the entire atmosphere be τ_{abs} and τ_{sca}, respectively, and each component up to the typical altitude z_{sca} where scattering events take place be τ'_{abs} and τ'_{sca}, respectively. In Duan et al. (2005), z_{sca} is defined as the altitude that satisfies the condition $\tau'_{sca} = \min(1, \tau_{sca}/2)$, and τ_{abs} and $\xi = \tau'_{abs} / \tau_{abs}$ are grouping parameters.

When treating the radiative transfer of solar irradiance incident on TOA, the upward Stokes vector at TOA, $\mathbf{I}_{RT} = (I, Q, U, V)^{\mathrm{T}}$ can be separated into a single scattering component $\mathbf{I}^{ss}$ and a multiple scattering component $\mathbf{I}^{ms}$.

$$\mathbf{I}_{RT}(\nu) = f_{sol}(\nu) \cdot \left[\mathbf{I}^{ss}(\nu) + \mathbf{I}^{ms}(\nu) \right] \tag{4.7.4-2}$$

$$\frac{\partial \mathbf{I}_{RT}(\nu)}{\partial x} = f_{sol}(\nu) \cdot \left[\frac{\partial \mathbf{I}^{ss}(\nu)}{\partial x} + \frac{\partial \mathbf{I}^{ms}(\nu)}{\partial x} \right] \tag{4.7.4-3}$$

where $f_{sol} = F_0 / (D_{sun\text{-}obs})^2$ is the solar irradiance incident on TOA (see Eq. (4.4-6) for F_0 and $D_{sun\text{-}obs}$), and x is either $\tau_{sca,m}$, $\tau_{sca,p,type}$, τ_{abs}, α, or u_{10}.

$\mathbf{I}^{ss}$ and $\partial\mathbf{I}^{ss}/\partial x$ can be calculated in a highspeed without being approximated, and hence are calculated strictly for each wavenumber points. Contrary, $\mathbf{I}^{ms}$ and $\partial\mathbf{I}^{ms}/\partial x$ are parameterized using the grouping parameters as in the following equations.

$$\mathbf{I}^{ms}(\tau_{abs}(\nu), \xi(\nu)) = \exp\{ g_{\mathbf{I}}(\tau_{abs}) - \beta_{\mathbf{I}}(\tau_{abs}) \cdot [\ln \xi - \ln \xi_0(\tau_{abs})] \} \tag{4.7.4-4}$$

$$\frac{\partial \mathbf{I}^{ms}(\tau_{abs}(\nu), \xi(\nu))}{\partial x} = g_x(\tau_{abs}) - \beta_x(\tau_{abs}) \cdot [\ln \xi - \ln \xi_0(\tau_{abs})] \tag{4.7.4-5}$$

where $\xi_0(\tau_{abs})$ is the average value of ξ at the optical thickness of τ_{abs}.

The table $\xi_0(\tau_{abs})$ can be created by appropriately setting reference points from the calculation wavenumber range, and the tables $g(\tau_{abs})$ and $\beta(\tau_{abs})$ can be created based on the radiative transfer calculation results for the reference points. Using the created tables, $\mathbf{I}^{ms}$ and $\partial\mathbf{I}^{ms}/\partial x$ can be calculated for all the wavenumber points within the calculation wavenumber range through table-interpolation. Here, the incident irradiance at TOA for radiative transfer calculation is set to $f_0 = 1$.

The Eqs. (4.7.4-4) and (4.7.4-5) are based on the assumption that the optical properties other than τ_{abs} are consistent within the calculation wavenumber range. Therefore, the calculation is performed on a sub-band basis, and the wavenumber dependencies of the cloud and aerosol scattering properties and the surface reflectivity within the sub-band are considered as described in the followings.

First, regarding the wavenumber dependencies of the cloud and aerosol optical thickness and the single scattering albedo, it is premised that the wavenumber range of each sub-band is set so that a linear approximation is obtained within the calculation wavenumber range. In addition, for the scattering phase matrix, the wavenumber dependency within the sub-band is ignored, but the scattering phase matrix for the wavenumber at the center of sub-band is used. Given these premises, the Stokes vector and weighting functions at an arbitrary wavenumber within the calculation wavenumber range are calculated by linearly interpolating the Stokes vector and weighting functions calculated using the optical properties at the both ends of the sub-band.

Next, the wavenumber dependency of the surface reflectivity is treated as explained below. Let

assume that the ground surface be a Lambertian surface with a reflectivity α. Using the Stokes vectors at TOA $\mathbf{I}_{RT,0}$ and $\mathbf{I}_{RT,m}$ for $\alpha = 0$, α_m, respectively, the radiance at TOA $\mathbf{I}_{RT,\alpha}$ for an arbitrary surface reflectivity α is expressed by the following equation (Liou, 2002).

$$\mathbf{I}_{RT,\alpha}(\nu) = \mathbf{I}_{RT,0}(\nu) + \left[\mathbf{I}_{RT,m}(\nu) - \mathbf{I}_{RT,0}(\nu)\right] \cdot \frac{1 - r(\nu)\cdot\alpha_m}{\alpha_m} \cdot \frac{\alpha(\nu)}{1 - r(\nu)\cdot\alpha(\nu)} \tag{4.7.4-6}$$

where r is a spherical albedo.

The weighting functions with respect to the surface albedo and each optical thickness are expressed by the Eqs. (4.7.4-7) and (4.7.4-8), respectively. Note that the same parameterization as Eqs. (4.7.4-4) and (4.7.4-5) is also applied to r and $\partial r/\partial x$.

$$\frac{\partial \mathbf{I}_{RT,\alpha}(\nu)}{\partial \alpha(\nu)} = \left[\mathbf{I}_{RT,m}(\nu) - \mathbf{I}_{RT,0}(\nu)\right] \cdot \frac{1 - r(\nu)\cdot\alpha_m}{\alpha_m} \cdot \frac{1}{\left[1 - r(\nu)\cdot\alpha(\nu)\right]^2} \tag{4.7.4-7}$$

$$\begin{aligned}\frac{\partial \mathbf{I}_{RT,\alpha}(\nu)}{\partial x} = {} & \frac{\partial \mathbf{I}_{RT,0}(\nu)}{\partial x} + \left[\frac{\partial \mathbf{I}_{RT,m}(\nu)}{\partial x} - \frac{\partial \mathbf{I}_{RT,0}(\nu)}{\partial x}\right] \cdot \frac{1 - r(\nu)\cdot\alpha_m}{\alpha_m} \cdot \frac{\alpha(\nu)}{1 - r(\nu)\cdot\alpha(\nu)} \\ & + \left[\mathbf{I}_{RT,m}(\nu) - \mathbf{I}_{RT,0}(\nu)\right] \cdot \frac{\alpha(\nu)\cdot\left[\alpha(\nu) - \alpha_m\right]}{\alpha_m \cdot \left[1 - r(\nu)\cdot\alpha(\nu)\right]^2} \cdot \frac{\partial r(\nu)}{\partial x}\end{aligned} \tag{4.7.4-8}$$

where x is either $\tau_{sca,m}$, $\tau_{sca,p,type}$, or τ_{abs}.

Based on the above, the following tables are prepared for each sub-band: for the case of surface reflectivity is homogeneous (Lambertian surface), tables corresponding to the four combination of the optical properties for the wavenumbers at both ends of the sub-band, and the surface reflectivity $\alpha = 0$, α_m; for the case of surface reflectivity is calculated based on Cox-Munk model, tables corresponding to the two optical properties at the wavenumber of the both ends of the sub-band. Using these tables, a highspeed radiative transfer calculation that takes into account the wavenumber dependencies of the cloud and aerosol scattering properties and surface reflectivity is performed.

(d) Radiative transfer calculation: Solar-induced chlorophyll fluorescence

Solar-induced chlorophyll fluorescence (SIF) can be measured from the wavenumber range of TANSO-FTS-2 Band 1. In the radiative transfer calculation, SIF is treated as an light source independent of sun light. Similar to Frankenberg et al. (2011b), SIF observed by the satellite $\mathbf{I}_{SIF}$ can be approximated by SIF at the surface $\mathbf{I}_{SIF,srf}$ attenuated by gas absorption. Also, since the polarization state of SIF is not known, it is treated as unpolarized ($\mathbf{I}_{SIF} = (I_{SIF}, 0, 0, 0)^{\mathrm{T}}$).

$$I_{SIF}(\nu) = I_{SIF,srf}(\nu) \cdot \exp\left[-\frac{\tau_{abs}(\nu)}{\mu_1}\right] \tag{4.7.4-9}$$

$$I_{SIF,srf}(\nu) = \begin{cases} SIF_{ref} \cdot \left[1 + SIF_{slp} \cdot (\nu - 13245)\right] & \textit{for Band 1} \\ 0 & \textit{for Band 2, 3} \end{cases} \tag{4.7.4-10}$$

where τ_{abs} is the optical thickness due to gaseous absorption, SIF_{ref} is the value of SIF signal at the reference wavelength (755 nm, corresponding wavenumber is 13245 cm^{-1}), and SIF_{slp} is the slope for wavenumber.

(e) Instrument model

The Stokes vector $\mathbf{I}_{mono}$ corrected from the Stokes vector at TOA ($\mathbf{I}_{RT}$ + $\mathbf{I}_{SIF}$) with the radiometric calibration adjustment factor $f_{\mathbf{I}}$, and zero-level offset $\mathbf{I}_{ZLO} = (I_{ZLO}, 0, 0, 0)^T$ is given by Eq. (4.7.4-11).

$$\mathbf{I}_{mono}(\nu) = \left[\mathbf{I}_{RT}(\nu) + \mathbf{I}_{SIF}(\nu)\right] \cdot f_{\mathbf{I}} + \mathbf{I}_{ZLO} \tag{4.7.4-11}$$

With respect to the wavenumber considering the wavenumber dispersion correction factor $\Delta\rho$,

$$\nu_{ret,i} = \rho \cdot (1 + \Delta\rho) \cdot \left[\nu_s + (i-1) \cdot \Delta\nu_0\right] \tag{4.7.4-12}$$

A convolution integral with ILSF is performed, yielding a forward model and a Jacobian.

$$\mathbf{F}(\mathbf{x}, \mathbf{c}) = ILS \otimes \mathbf{I}_{mono}(\nu) \tag{4.7.4-13}$$

$$\mathbf{K} = \frac{\partial \mathbf{F}(\mathbf{x}, \mathbf{c})}{\partial \mathbf{x}} = ILS \otimes \frac{\partial \mathbf{I}_{mono}(\nu)}{\partial \mathbf{x}} \tag{4.7.4-14}$$

Note, unless otherwise specified, $f_{\mathbf{I}} = 1.0$, $I_{ZLO} = 0.0$, and $\Delta\rho = 0.0$.

4.7.5 A Priori Value of State Vector and Related Optical Properties

4.7.5.1 A priori value of vertical profile of gas

The layer-averaged (partial column-averaged) dry-air mole fraction with respect to the Main-layer is included in the state vector element, and its a priori value is calculated as the ratio of the partial column amount of target gas to the partial column amount of dry-air.

<Column amount of dry-air>

Column amount of dry-air is calculated based on the vertical profiles of pressure p [hPa], gravitational acceleration g [m/s^2], and H_2O concentration C_{H2O} [ppm]. These values at the center of FTS-2 IFOV are calculated in the FTS-2 L2 pre-processing and given as values at the same vertical grid boundary from TOA to the surface. *No* is the number of layers of these data. The subscripts *ob*, *ol*, and *lo* denote the value at the boundary, value in the layer, and an element of the vertical grid, respectively. The subscripts *air*, *dry*, and H_2O denote air, dry-air, and water vapor, respectively.

Based on the hydrostatic equilibrium equation ($dp / dz = -\rho \cdot g$), the mass of air $m_{air,ol=lo}$ [kg/cm^2] of the layer *lo* is given by the Eq. (4.7.5.1-1).

$$m_{air,ol=lo} = \int \rho_{air} dz = \int \frac{10^{-2} dp}{g} = \frac{p_{ob=lo+1} - p_{ob=lo}}{g_{ol=lo}} \cdot 10^{-2} \tag{4.7.5.1-1}$$

$$g_{ol=lo} = \frac{g_{ob=lo+1} + g_{ob=lo}}{2} \tag{4.7.5-1-2}$$

where ρ is a mass density [kg/cm^3] and z is an altitude [km].

The mass density of air is the sum of the mass density of dry-air and that of water vapor.

$$\begin{aligned} \rho_{air,ol=lo} &= \rho_{dry,ol=lo} + \rho_{H_2O,ol=lo} = u \cdot \left(\mu_{dry} \cdot n_{dry,ol=lo} + \mu_{H_2O} \cdot n_{H_2O,ol=lo} \right) \\ &= u \cdot n_{dry,ol=lo} \cdot \left(\mu_{dry} + \mu_{H_2O} \cdot C_{H_2O,ol=lo} \cdot 10^{-6} \right) \end{aligned} \tag{4.7.5.1-3}$$

$$C_{H_2O,ol=lo} = \frac{n_{H_2O,ol=lo}}{n_{dry,ol=lo}} \cdot 10^6 = \frac{C_{H_2O,ob=lo} + C_{H_2O,ob=lo+1}}{2} \tag{4.7.5.1-4}$$

where u is the unified atomic mass unit [kg], μ is an average molecular weight, and n is a number density [molecules/cm^3].

Based on the above, the partial column amount of dry-air $w_{dry,ol=lo}$ [molecules/cm^2] in the layer *lo* is:

$$w_{dry,ol=lo} = \int n_{dry} dz = \int \frac{10^{-2} dp}{g \cdot u \cdot \left(\mu_{dry} + \mu_{H_2O} \cdot C_{H_2O} \cdot 10^{-6} \right)} = \frac{m_{air,ol=lo}}{u \cdot \left(\mu_{dry} + \mu_{H_2O} \cdot C_{H_2O,ol=lo} \cdot 10^{-6} \right)} \quad (4.7.5.1\text{-}5)$$

The partial column amount $W_{dry,ob=lo}$ integrated from TOA to the boundary surface $p_{ob=lo}$ is:

$$W_{dry,ob=lo} = \begin{cases} 0 & lo = 1 \\ W_{dry,ob=lo-1} + w_{dry,ol=lo-1} & 1 < lo \le No + 1 \end{cases} \quad (4.7.5.1\text{-}6)$$

The integrated partial column amount of dry-air from TOA to an arbitrary boundary surface p can be given by linearly interpolating $W_{dry,ob=lo}$ with respect to the pressure. Accordingly, the partial column amount of dry-air for the Main-layer *lm* and Sub-layer *ls* can be given by Eqs. (4.7.5.1-7) and (4.7.5.1-8), respectively.

$$w_{dry,ml=lm} = W_{dry,mb=lm+1} - W_{dry,mb=lm} \quad (4.7.5.1\text{-}7)$$

$$w_{dry,sl=ls} = W_{dry,sb=ls+1} - W_{dry,sb=ls} \quad (4.7.5.1\text{-}8)$$

Since all vertical grids, the lowest bottom is the earth's surface, the total column amount of dry-air is a constant value regardless of any vertical grids.

$$W_{dry,SRF} = W_{dry,ob=No+1} = W_{dry,mb=Nm+1} = W_{dry,sb=Ns+1} = W_{dry,rb=Nr+1} \quad (4.7.5.1\text{-}9)$$

<Remapping of gas concentration>

The source data of gas concentration used in the FTS-2 SWIR L2 processing are various, and each uses a different vertical grid (see “GOSAT-2 TANSO-FTS-2 L2 Pre-processing Algorithm Theoretical Basis Document” for more detail). Similar to the column amount of dry-air, consider calculating the layer-averaged dry-air mole fraction of each gas component with respect to each of the Main- and Sub-layers so that the column amount of each gas component is also constant value. Let the number of layers in a vertical grid of the target gas species *gas* be *Ngas*, and a gas concentration be *Cgas* [ppm]. The subscripts *gb*, *gl*, and *lg* denote a value at a boundary, a value within the layer, and an element of the vertical grid, respectively.

The partial column amount for the target gas species w_{gas} is expressed by Eq. (4.7.5.1-10)

$$w_{gas} = \int C_{gas} \cdot n_{dry} dz = \int C_{gas} dW_{dry} \tag{4.7.5.1-10}$$

When the gas concentration within each layer of the vertical grid of gas concentration data is incrementally given by a linear function of W_{dry}, the partial column amount $w_{gas,p1\text{-}p2}$ of the target gas in a layer composed of the boundaries p_1 and p_2 that satisfy the condition $p_{gb=lg} \le p_1 < p_2 \le p_{gb=lg+1}$ is given by Eq. (4.7.5.1-11).

$$\begin{aligned} w_{gas,p1-p2} &= \int_{Wdry,p1}^{Wdry,p2} \left[\frac{C_{gas,gb=lg+1} - C_{gas,gb=lg}}{W_{dry,gb=lg+1} - W_{dry,gb=lg}} \cdot \left(W_{dry} - W_{dry,gb=lg} \right) + C_{gas,gb=lg} \right] dW_{dry} \\ &= \left[\left(1 - A_{gl=lg,p1-p2} \right) \cdot C_{gas,gb=lg} + A_{gl=lg,p1-p2} \cdot C_{gas,gb=lg+1} \right] \cdot \left(W_{dry,p2} - W_{dry,p1} \right) \end{aligned} \tag{4.7.5.1-11}$$

$$A_{gl=lg,p1-p2} = \frac{\frac{1}{2} \cdot \left(W_{dry,p2} + W_{dry,p1} \right) - W_{dry,gb=lg}}{W_{dry,gb=lg+1} - W_{dry,gb=lg}} \tag{4.7.5.1-12}$$

Accordingly, $C_{gas,ml=lm}$ the partial column-averaged dry-air mole fraction of the target gas at the layer *lm* of the Main-layer is expressed by Eq. (4.7.5.1-13) as the ratio of the partial column amount of the target gas (Eq. (4.7.5.1-14)) to the partial column amount of dry-air. However, when the range of the vertical grid of the target gas is smaller than the range of the Main-layer, the gas concentration of the insufficient area is considered to be the same as the concentration in the nearest adjacent boundary.

$$C_{gas,ml=lm} = \frac{w_{gas,ml=lm}}{w_{dry,ml=lm}} = \frac{w_{gas,ml=lm}}{W_{dry,mb=lm+1} - W_{dry,mb=lm}} \tag{4.7.5.1-13}$$

$$\begin{aligned} & w_{gas,ml=lm} \\ &= \sum_{lg=1}^{Ngas} \left[\left(1 - A_{gl=lg,p1-p2} \right) \cdot C_{gas,gb=lg} + A_{gl=lg,p1-p2} \cdot C_{gas,gb=lg+1} \right] \cdot \Delta_{p1-p2} \\ &+ C_{gas,gb=1} \cdot \Delta_0 + C_{gas,gb=Ngas+1} \cdot \Delta_{Ngas} \end{aligned} \tag{4.7.5.1-14}$$

$$\Delta_{p1-p2} = \max\left(W_{dry,p2} - W_{dry,p1}, 0 \right) \tag{4.7.5.1-15}$$

$$W_{dry,p1} = \max\left(W_{dry,gb=lg}, W_{dry,mb=lm}\right) \quad (4.7.5.1\text{-}16)$$

$$W_{dry,p2} = \min\left(W_{dry,gb=lg+1}, W_{dry,mb=lm+1}\right) \quad (4.7.5.1\text{-}17)$$

$$\Delta_0 = \max\left(W_{dry,p0} - W_{dry,mb=1}, 0\right) \quad (4.7.5.1\text{-}18)$$

$$\Delta_{Ngas} = \max\left(W_{dry,mb=lm+1} - W_{dry,p3}, 0\right) \quad (4.7.5.1\text{-}19)$$

$$W_{dry,p0} = \min\left(W_{dry,gb=1}, W_{dry,mb=lm+1}\right) \quad (4.7.5.1\text{-}20)$$

$$W_{dry,p3} = \max\left(W_{dry,gb=Ngas+1}, W_{dry,mb=lm}\right) \quad (4.7.5.1\text{-}21)$$

Rearrange the right hand side of Eq. (4.7.5.1-13) using eq. (4.7.5.1-14) with respect to each of $C_{gas,gb=1}$ to $C_{gas,gb=Ngas+1}$. Let $\mathbf{W}_{mg}$ be a matrix with each coefficient as an element; $\mathbf{C}_{gas,gb}$ be a column vector of which elements are the gas concentration at the boundaries of the vertical grid of the target gas; $\mathbf{S}_{a,gas,gb}$ be the variance-covariance matrix of $\mathbf{C}_{gas,gb}$; $\mathbf{C}_{gas,ml}$ be a column vector of which elements are the partial column-averaged concentration of each layer in the Main-layer; and $\mathbf{S}_{a,gas,ml}$ be the variance-covariance matrix of $\mathbf{C}_{gas,ml}$, then:

$$\mathbf{C}_{gas,ml} = \mathbf{W}_{mg} \cdot \mathbf{C}_{gas,gb} \quad (4.7.5.1\text{-}22)$$

$$\mathbf{S}_{a,gas,ml} = \mathbf{W}_{mg} \cdot \mathbf{S}_{a,gas,gb} \cdot \mathbf{W}_{mg}^{T} \quad (4.7.5.1\text{-}23)$$

Also for the Sub-layer, the vertical grid can be converted by using the matrix $\mathbf{W}_{sg}$ created in the same manner.

4.7.5.2 Optical thickness due to gas absorption

TANSO-FTS-2 has a wavenumber resolution capable of observing a fine wavenumber structure due to gas absorption, and thus it is necessary to simulate it also in the forward model. For the accurate calculation of column-averaged dry-air mole fractions of target gas, the line-mixing and other effects in calculating the absorption cross-section of gas molecules need to be considered, but it requires a high computational cost. For this reason, the absorption cross-section of gas molecules calculated for the specific pressures and temperatures are stored in a Look-Up-Table (LUT) beforehand (see Subsection 3.3.1), and in each analysis, the absorption cross-section at each relevant temperature, pressure, and wavenumber is obtained via linear interpolation.

As stated previously, the Sub-layer is used for calculating the optical thickness due to gas absorption. The temperature at each boundary of the Sub-layer $T_{sb=ls}$ is obtained by linearly interpolating with respect to the logarithm of pressure after adding the temperature shift to the source data of the temperature vertical profile.

The optical thickness due to gas absorption at the layer *lm* of the Main-layer $\tau_{abs,m,ml=lm}$ is given by Eq. (4.7.5.2-1), and that at the layer *lr* of the RT-layer $\tau_{abs,m,rl=lr}$ is given by Eq. (4.7.5.2-2).

$$\tau_{abs,m,ml=lm}(\nu) = \sum_{gas} \tau_{abs,gas,ml=lm}(\nu) \tag{4.7.5.2-1}$$

$$\tau_{abs,m,rl=lr}(\nu) = \tau_{abs,m,ml=lm(lr)}(\nu) \cdot frc_{RT}(lr) \tag{4.7.5.2-2}$$

$$\tau_{abs,gas,ml=lm}(\nu) = \sum_{ls \in lm} \sigma_{abs,gas,sl=ls}(\nu; p_{sl=ls}, T_{sl=ls}) \cdot w_{gas,sl=ls} \tag{4.7.5.2-3}$$

$$\sigma_{abs,gas,sl=ls}(\nu; p_{sl=ls}, T_{sl=ls}) = \begin{cases} ak_{gas}(\nu; p_{sl=ls}, T_{sl=ls}) & \\ +ak_{cnt,slf}(\nu; T_{sl=ls}) \cdot \dfrac{p_{sl=ls}}{p_0} \cdot \dfrac{T_0}{T_{sl=ls}} \cdot \dfrac{C_{H_2O,sl=ls}}{10^6 + C_{H_2O,sl=ls}} & for\ H_2O \\ +ak_{cnt,frn}(\nu; T_{sl=ls}) \cdot \dfrac{p_{sl=ls}}{p_0} \cdot \dfrac{T_0}{T_{sl=ls}} \cdot \dfrac{10^6}{10^6 + C_{H_2O,sl=ls}} & \\ ak_{gas}(\nu; p_{sl=ls}, T_{sl=ls}) + ak_{cnt,O_3}(\nu; T_{sl=ls}) & for\ O_3 \\ ak_{gas}(\nu; p_{sl=ls}, T_{sl=ls}) & others \end{cases} \tag{4.7.5.2-4}$$

$$p_{sl=ls} = \frac{p_{sb=ls} + p_{sb=ls+1}}{2} \tag{4.7.5.2-5}$$

$$T_{sl=ls} = \frac{T_{sb=ls} + T_{sb=ls+1}}{2} \tag{4.7.5.2-6}$$

where $\sigma_{abs,gas}$ [cm^2/molecules] is the absorption cross-section of a gas species *gas*, and ak_{gas} and ak_{cnt} are given by linearly interpolating from the LUT for molecular absorption cross-section according to the Eqs. (4.7.5.2-7) and (4.7.5.2-8). The subscripts *slf* and *frn* denote the components of self-continuum and foreign-continuum of the water vapor continuous absorption, respectively, where p_0 = 1013.25 hPa and T_0 = 296 K.

$$
\begin{aligned}
ak_{gas}(\nu;p,T) = & \frac{p_{i+1}-p}{p_{i+1}-p_i}\cdot\frac{T_{i,j+1}-T}{T_{i,j+1}-T_{i,j}}\cdot ak_{gasLUT,i,j}(\nu) \\
& + \frac{p_{i+1}-p}{p_{i+1}-p_i}\cdot\frac{T-T_{i,j}}{T_{i,j+1}-T_{i,j}}\cdot ak_{gasLUT,i,j+1}(\nu) \\
& + \frac{p-p_i}{p_{i+1}-p_i}\cdot\frac{T_{i+1,k+1}-T}{T_{i+1,k+1}-T_{i+1,k}}\cdot ak_{gasLUT,i+1,k}(\nu) \\
& + \frac{p-p_i}{p_{i+1}-p_i}\cdot\frac{T-T_{i+1,k}}{T_{i+1,k+1}-T_{i+1,k}}\cdot ak_{gasLUT,i+1,k+1}(\nu)
\end{aligned}
\qquad (4.7.5.2\text{-}7)
$$

where ak_{gasLUT} is a value in the LUT for molecular absorption cross-section of gas species *gas* and the subscripts *i*, *j* and *k* denote a grid point of the LUT, and each satisfies the conditions $p_i < p <= p_{i+1}$, $T_{i,j} < T <= T_{i,j+1}$ and $T_{i+1,k} < T <= T_{i+1,k+1}$, respectively.

$$
ak_{cnt,gas}(\nu;T) = \frac{T_{i+1}-T}{T_{i+1}-T_i}\cdot ak_{cnt,gasLUT,i}(\nu) + \frac{T-T_i}{T_{i+1}-T_i}\cdot ak_{cnt,gasLUT,i+1}(\nu) \qquad (4.7.5.2\text{-}8)
$$

where the subscript *i* is a grid point of the LUT and satisfies the condition $T_i < T <= T_{i+1}$.

4.7.5.3 Optical thickness due to scattering of air molecule (Rayleigh scattering)

<Partial column amount of air>

The partial column amount of air at the layer *lm* in the Main-layer is given by Eq. (4.7.5.3-1) using the partial column-averaged dry-air fraction of water vapor $C_{H2O,ml=lm}$ [ppm].

$$
w_{air,ml=lm} = w_{dry,ml=lm}\cdot\left(1 + C_{H_2O,ml=lm}\cdot 10^{-6}\right) \qquad (4.7.5.3\text{-}1)
$$

<Optical thickness due to scattering of air molecule>

The scattering of solar light by terrestrial atmosphere (Rayleigh scattering) is expressed as follows. The Rayleigh scattering cross-section for an air molecule at the layer *lm* in the Main-layer $\sigma_{sca,m,ml=lm}$ [cm^2/molecules] is given by Eq. (4.7.5.3-2).

$$
\sigma_{sca,m,ml=lm}(\lambda) = \frac{24\cdot\pi^3\cdot\left(nr_{air,ml=lm}^2 - 1\right)^2}{\lambda^4\cdot n_{air}^2\cdot\left(nr_{air,ml=lm}^2 + 2\right)^2}\left(\frac{6+3\cdot\delta_{ml=lm}}{6-7\cdot\delta_{ml=lm}}\right)\cdot 10^{16} \qquad (4.7.5.3\text{-}2)
$$

where λ is a wavelength [μm], which is the reciprocal (λ = 10000 / ν) of the wavenumber ν [cm^{-1}], nr_{air} is the refractive index of air, n_{air} = 2.546899×10^{19} [molecules/cm^3] is a number density of air, and δ is a depolarization factor.

Each variable of the right hand side of Eq. (4.7.5.3-2) is based on Bodhaine et al. (1999), and is calculated by Eqs. (4.7.5.3-3) ~ (4.7.5.3-8) as a function of the partial column-averaged dry-air mole fraction of carbon dioxide $C_{CO2,ml=lm}$ [ppm].

$$nr_{air,ml=lm} = 1 + \left(n_{300} - 1\right) \cdot \left[1 + 0.0054 \cdot \left(C_{CO_2,ml=lm} \cdot 10^{-4} - 0.03\right)\right] \tag{4.7.5.3-3}$$

$$\left(n_{300} - 1\right) = \left(8060.51 + \frac{2480990}{132.274 - \lambda^{-2}} + \frac{17455.7}{39.32957 - \lambda^{-2}}\right) \cdot 10^{-8} \tag{4.7.5.3-4}$$

$$\frac{6 + 3 \cdot \delta_{ml=lm}}{6 - 7 \cdot \delta_{ml=lm}} = F_{air,ml=lm} = \frac{78.084 \cdot F_{N_2} + 20.946 \cdot F_{O_2} + 0.934 \times 1.00 + C_{CO_2,ml=lm} \cdot 10^{-4} \times 1.15}{78.084 + 20.946 + 0.934 + C_{CO_2,ml=lm} \cdot 10^{-4}} \tag{4.7.5.3-5}$$

$$F_{N_2} = 1.034 + \frac{3.17 \cdot 10^{-4}}{\lambda^2} \tag{4.7.5.3-6}$$

$$F_{O_2} = 1.096 + \frac{1.385 \cdot 10^{-3}}{\lambda^2} + \frac{1.448 \cdot 10^{-4}}{\lambda^4} \tag{4.7.5.3-7}$$

$$\delta_{ml=lm} = \frac{6 \cdot \left(F_{air,ml=lm} - 1\right)}{7 \cdot F_{air,ml=lm} + 3} \tag{4.7.5.3-8}$$

Based on the above, the optical thickness $\tau_{sca,m,ml=lm}$ due to scattering of air molecules at the layer *lm* of the Main-layer is given by Eq. (4.7.5.3-9), and hence, the optical thickness $\tau_{sca,m,rl=lr}$ due to scattering of air molecules at the layer *lr* of the RT-layer is given by Eq. (4.7.5.3-10).

$$\tau_{sca,m,ml=lm}\left(\nu\right) = \sigma_{sca,m,ml=lm}\left(\lambda\left(\nu\right)\right) \cdot w_{air,ml=lm} \tag{4.7.5.3-9}$$

$$\tau_{sca,m,rl=lr}\left(\nu\right) = \tau_{sca,m,ml=lm(lr)}\left(\nu\right) \cdot frc_{RT}\left(lr\right) \tag{4.7.5.3-10}$$

For the depolarization factor of the Rayleigh scattering $\delta_{rl=lr}(\nu)$, the factor of the Main-layer (Eq. (4.7.5.3-8)) to which the layer *lr* of the RT-layer belongs is utilized.

4.7.5.4 A priori value of vertical profile of aerosol

To consider aerosol scattering effects in retrieving column-averaged dry-air mole fractions of target gas, aerosol parameters are simultaneously retrieved with gas. There are various aerosol

species, therefore, aerosol field simulated by the aerosol transport model SPRINTARS is utilized to take the spatiotemporal distribution of aerosol (see "GOSAT-2 TANSO-FTS-2 L2 Pre-processing Algorithm Theoretical Basis Document"). However, since the information can be obtained from the observed spectra is not sufficient to identify each of them, two mixture types of aerosol species are considered in the FTS-2 SWIR L2 processing. Although the aerosol optical thickness has a wavelength dependency, the logarithm of the aerosol optical thickness at reference wavelength for each mixture type and each layer of Main-layer is included in the state vector element. Here, the reference wavelength is set to be 1.6 μm to consider the effect on the retrieved column-averaged dry-air mole fractions of gas.

The 19 vertical profiles of mass mixing ratio [kg/kg] of soil dust (10 size bin), carbonaceous (4 species), sulfate (1 species), and sea-salt (4 size bin) aerosols are available from SPRINTARS. In the FTS-2 SWIR L2 processing, these aerosol species fall into two types as shown in Table 4.7.5.4-1. The aerosol hygroscopic growth effect is considered as different scattering properties in the LUT (see subsection 3.3.1). For a total of 75 components of all 19 species, the subscripts *aer* and *aerLUT* are used to identify each species and each component, respectively.

Table 4.7.5.4-1. The categorization of types and hygroscopicity of aerosol species in the FTS-2 SWIR L2 processing. BC and OC are black carbon and organic carbon, respectively.

aerosol species		Type	Hygroscopicity	Number of components
soil dust	0.13 μm bin	2	N/A	1
	0.20 μm bin	2	N/A	1
	0.33 μm bin	2	N/A	1
	0.52 μm bin	2	N/A	1
	0.82 μm bin	2	N/A	1
	1.27 μm bin	2	N/A	1
	2.02 μm bin	2	N/A	1
	3.20 μm bin	2	N/A	1
	5.06 μm bin	2	N/A	1
	8.06 μm bin	2	N/A	1
carbonaceous	BC / OC 0.3	1	consider	8
	BC / OC 0.15	1	consider	8
	BC / OC 0.0	1	consider	8
	pure black carbon	1	N/A	1
sulfate		1	consider	8
sea salt	0.178 μm bin	2	consider	8
	0.562 μm bin	2	consider	8

	1.780 μm bin	2	consider	8
	5.620 μm bin	2	consider	8

<Remapping of aerosol mass mixing ratio>

Convert the aerosol mass mixing ratio at the boundary of the SPRINTARS vertical grid $C_{aer,ab=la}$ [kg/kg] into the partial column mass at each layer of the Main-layer $m_{aer,ml=lm}$ [g/cm^2], where *Naer* is the number of layers of SPRINTARS, and the subscripts *ab*, *al*, and *la* denote a value at each boundary, a value within the layer, and an element of the vertical grid, respectively.

The aerosol partial column mass is given by Eq. (4.7.5.4-1) using the mass density of air and can be calculated in the same way as the gas concentration remapping.

$$m_{aerLUT} = \int C_{aerLUT} \cdot \rho_{air} dz = \int C_{aerLUT} dM_{air} \tag{4.7.5.4-1}$$

$$M_{air,ob=lo} = \begin{cases} 0 & lo = 1 \\ M_{air,ob=lo-1} + m_{air,ol=lo-1} & 1 < lo \le No+1 \end{cases} \tag{4.7.5.4-2}$$

$$m_{aerLUT,ml=lm} = \sum_{la=1}^{Naer} \left[\left(1 - A_{al=la,p1-p2}\right) \cdot C_{aerLUT,ab=la} + A_{al=la,p1-p2} \cdot C_{aerLUT,ab=la+1} \right] \cdot \Delta_{p1-p2} + C_{aerLUT,ab=1} \cdot \Delta_0 + C_{aerLUT,ab=Na+1} \cdot \Delta_{Naer} \tag{4.7.5.4-3}$$

where the coefficients A and Δ are given by the Eq. (4.7.5.1-12) and Eqs. (4.7.5.1-15) ~ (4.7.5.1-21) when replacing W_{dry} with M_{air}, and *Ngas*, *gl*, *gb*, and *lg* with *Naer*, *al*, *ab*, and *la*, respectively.

For hygroscopic aerosols, the scattering properties in the LUT are linearly interpolated with respect to the relative humidity and utilized, however, for the convenience of calculation, the aerosol partial column mass is distributed according to the relative humidity. The relative humidity *rh* is given by Eq. (4.7.5.4-4) using the water vapor pressure e and the saturated water vapor pressure $e_{sat}(T)$.

$$rh_{ml=lm} = \frac{e_{ml=lm}}{e_{sat,ml=lm}\left(T_{ml=lm}\right)} \tag{4.7.5.4-4}$$

$$e_{ml=lm} = \frac{C_{H_2O,ml=lm}}{10^6 + C_{H_2O,ml=lm}} \cdot p_{ml=lm} \tag{4.7.5.4-5}$$

The saturated water vapor $e_{sat}(T)$ is given by the Tetens equation as:

$$e_{sat}(T)=\begin{cases}6.11\times10^{\frac{7.5\cdot(T-273.15)}{237.3+(T-273.15)}} & T\geq 273.15\\ 6.11\times10^{\frac{9.5\cdot(T-273.15)}{265.5+(T-273.15)}} & T<273.15\end{cases} \tag{4.7.5.4-6}$$

Let the grid point value of relative humidity used in the LUT for scattering properties of aerosol be denoted by rh_i, (i is an element). The distribution of aerosol partial mass for the relative humidity is given by Eq. (4.7.5.4-7).

$$m_{aer,rhi,ml=lm}=\begin{cases}m_{aer,ml=lm}\cdot\dfrac{rh_{ml=lm}-rh_{irh}}{rh_{irh+1}-rh_{irh}} & i=irh\\ m_{aer,ml=lm}\cdot\dfrac{rh_{irh+1}-rh_{ml=lm}}{rh_{irh+1}-rh_{irh}} & i=irh+1\\ 0 & others\end{cases} \tag{4.7.5.4-7}$$

where irh is an element that satisfy the condition $rh_{irh} < rh_{ml=lm} \leq rh_{irh+1}$. Note that the subscript *aer,rhi* is used for convenience to make clear the correspondence to the grid point of relative humidity, but formally, it should be noted by *aerLUT*.

<Aerosol optical thickness at reference wavelength>

The aerosol optical thickness for each aerosol type at the reference wavelength λ_{ref} (the corresponding wavenumber is denoted by ν_{ref}) in the layer *lm* of the Main-layer is expressed by Eq. (4.7.5.4-8). The a priori value of aerosol vertical profile is the logarithm of it. Furthermore, the normalized optical thickness, single scattering albedo, and scattering phase matrix for each aerosol type are expressed by Eqs. (4.7.5.4-11) ~ (4.7.5.4-13).

$$\tau_{a,type,ml=lm}(\nu_{ref})=\sum_{aerLUT\in type}\sigma_{ext,aerLUT}(\nu_{ref})\cdot m_{aerLUT,ml=lm} \tag{4.7.5.4-8}$$

$$\sigma_{ext,aerLUT}(\nu)=\sigma_{ext,aerLUT,i}\cdot\left(\frac{\lambda}{\lambda_i}\right)^{\alpha} \tag{4.7.5.4-9}$$

$$\alpha=\frac{\log\left(\sigma_{ext,aerLUT,i+1}/\sigma_{ext,aerLUT,i}\right)}{\log\left(\lambda_{i+1}/\lambda_i\right)} \tag{4.7.5.4-10}$$

$$\overline{\tau}_{a,type,ml=lm}(\nu)=\frac{\tau_{a,type,ml=lm}(\nu)}{\tau_{a,type,ml=lm}(\nu_{ref})} \tag{4.7.5.4-11}$$

$$\varpi_{a,type,ml=lm}(\nu) = \frac{\tau_{sca,a,type,ml=lm}(\nu)}{\tau_{a,type,ml=lm}(\nu)} \tag{4.7.5.4-12}$$

$$\mathbf{P}_{a,type,ml=lm}(\Theta,\nu) = \frac{\sum_{aerLUT \in type} \sigma_{sca,aerLUT}(\nu) \cdot \mathbf{P}_{aerLUT}(\Theta,\nu) \cdot m_{aerLUT,ml=lm}}{\tau_{sca,a,type,ml=lm}(\nu)} \tag{4.7.5.4-13}$$

$$\tau_{sca,a,type,ml=lm}(\nu) = \sum_{aerLUT \in type} \sigma_{sca,aerLUT}(\nu) \cdot m_{aerLUT,ml=lm} \tag{4.7.5.4-14}$$

$$\sigma_{sca,aerLUT}(\nu) = \sigma_{ext,aerLUT}(\nu) \cdot \left(\frac{\sigma_{sca,aerLUT,i}}{\sigma_{ext,aerLUT,i}} \cdot \frac{\lambda_{i+1} - \lambda}{\lambda_{i+1} - \lambda_i} + \frac{\sigma_{sca,aerLUT,i+1}}{\sigma_{ext,aerLUT,i+1}} \cdot \frac{\lambda - \lambda_i}{\lambda_{i+1} - \lambda_i} \right) \tag{4.7.5.4-15}$$

$$\mathbf{P}_{aerLUT}(\Theta,\nu) = \mathbf{P}_{aerLUT,i}(\Theta) \cdot \frac{\lambda_{i+1} - \lambda}{\lambda_{i+1} - \lambda_i} + \mathbf{P}_{aerLUT,i+1}(\Theta) \cdot \frac{\lambda - \lambda_i}{\lambda_{i+1} - \lambda_i} \tag{4.7.5.4-16}$$

where λ is the wavelength corresponding to the wavenumber ν; $\sigma_{ext,aerLUT}$, $\sigma_{sca,aerLUT}$, and $\mathbf{P}_{aerLUT}$ are values in the LUT of mass extinction coefficient [cm^2/g], mass scattering coefficient [cm^2/g], and scattering phase matrix, respectively, corresponding to the aerosol component *aerLUT*; the subscript i is an element in the LUT that satisfying the condition $\lambda_i < \lambda \leq \lambda_{i+1}$.

4.7.5.5 Optical thickness, scattering optical thickness, and scattering phase matrix by aerosol type

The aerosol scattering property at the layer *lr* of the RT-layer is calculated as expressed in Eqs. (4.7.5.5-1) ~ (4.7.5.5-3) using Eqs. (4.7.5.4-8), (4.7.5.4-11), (4.7.5.4-12), and (4.7.5.4-13).

$$\tau_{a,type,rl=lr}(\nu) = \overline{\tau}_{a,type,ml=lm(lr)}(\nu) \cdot \tau_{a,type,ml=lm(lr)}(\nu_{ref}) \cdot frc_{RT}(lr) \tag{4.7.5.5-1}$$

$$\tau_{sca,a,type,rl=lr}(\nu) = \varpi_{a,type,ml=lm(lr)}(\nu) \cdot \tau_{a,type,rl=lr}(\nu) \tag{4.7.5.5-2}$$

$$\mathbf{P}_{a,type,rl=lr}(\Theta,\nu) = \mathbf{P}_{a,type,ml=lm(lr)}(\Theta,\nu) \tag{4.7.5.5-3}$$

4.7.5.6 Optical thickness, scattering optical thickness, and scattering phase matrix by cloud type

In the TANSO-FTS-2 SWIR L2 processing, one type of single-layer homogeneous ice cloud is handled. The cloud optical property at the layer *lr* of the RT-layer is given by Eqs. (4.7.5.6-1) ~ (4.7.5.6-3) using the optical thickness at the reference wavelength λ_{ref}.

$$\tau_{c,type,rl=lr}\left(\nu\right)=\frac{\sigma_{ext,cld}\left(\nu,D_{eff}\right)}{\sigma_{ext,cld}\left(\nu_{ref},D_{eff}\right)}\cdot\tau_{c,type}\left(\nu_{ref}\right)\cdot frc_{CLD}\left(lr\right) \tag{4.7.5.6-1}$$

$$\tau_{sca,c,type,rl=lr}\left(\nu\right)=\varpi_{cld}\left(\nu,D_{eff}\right)\cdot\tau_{c,type,rl=lr}\left(\nu\right) \tag{4.7.5.6-2}$$

$$\mathbf{P}_{c,type,rl=lr}\left(\Theta,\nu\right)=\mathbf{P}_{cld}\left(\Theta,\nu,D_{eff}\right) \tag{4.7.5.6-3}$$

where $\sigma_{ext,cld}$, ϖ_{cld}, and $\mathbf{P}_{cld}$ are obtained by first calculating the values at each wavelength gird from the LUT for scattering properties of cloud (see subsection 3.3.1) through the four-point Lagrange interpolation with respect to the effective particle size D_{eff}, and then interpolating the values with respect to wavelength corresponding to the wavenumber ν. The wavelength interpolation is performed by the rational function based constrained interpolation profile method (Xiao et al., 1996) for $\sigma_{ext,cld}$, and by liner interpolation for ϖ_{cld} and $\mathbf{P}_{cld}$.

4.7.5.7 Surface albedo

Let the wavenumber dependence of surface albedo be represented by a piece-wisely connected straight lines (zigzag approximation). The wavenumber range of each sub-band is divided into (*nalbSB* - 1) parts at a fixed wavenumber interval, defining the number of wavenumber boundaries as *nalbSB*. The surface albedo values at these wavenumber boundaries are included in the state vector element. Within the adjacent wavenumber boundaries, the surface albedo is expressed by a linear function of the wavenumber. The surface albedo is given by Eq. (4.7.5.7-1), where $\alpha_{SB,i}$ is the surface albedo at the i-th wavenumber boundary.

$$\alpha\left(\nu\right)=\frac{\nu_{i+1}-\nu}{\nu_{i+1}-\nu_i}\cdot\alpha_{SB,i}+\frac{\nu-\nu_i}{\nu_{i+1}-\nu_i}\cdot\alpha_{SB,i+1}\qquad\nu_i<\nu\le\nu_{i+1} \tag{4.7.5.7-1}$$

$$\nu_i=\nu_{SB,sta}+\frac{\nu_{SB,end}-\nu_{SB,sta}}{nalbSB-1}\cdot\left(i-1\right)\qquad i=1,2,...,nalbSB \tag{4.7.5.7-2}$$

where subscripts *SB*,*sta* and *SB*,*end* denote beginning and ending wavenumber of sub-band *SB*, respectively.

A priori value of surface albedo is calculated from the polarization synthesized spectrum for each sub-band by Eq. (4.7.5.7-3). The same value is set to all wavenumber boundaries for each sub-band.

$$\alpha_{prior,SB}=\overline{\alpha_{clr,SB}\left(\nu\right)}\Big|_{\alpha_{clr,SB}(\nu)\ge0.98\cdot Max\left(\alpha_{clr,SB}(\nu)\right)} \tag{4.7.5.7-3}$$

$$\alpha_{clr,SB}(\nu) = \frac{\pi \cdot D_{sun-obs}^2 \cdot S_{synth,SB}(\nu)}{\cos\theta_0 \cdot F_0(\nu)} \qquad (4.7.5.7\text{-}4)$$

where $\overline{x}\big|_{condition}$ denotes the average value of x that satisfies the condition *condition*.

4.7.5.8 Summary of the a priori value and its variance-covariance matrix of state vector

Table 4.7.5.8-1 summarizes the a priori value and its variance-covariance matrix of state vector.

Table 4.7.5.8-1. A priori value and its variance-covariance matrix of state vector.

State vector element	a priori value and its variance-covariance matrix
CO_2 profile (15 layer)	A priori value and its variance-covariance matrix are calculated by Eqs. (4.7.5.1-22) and (4.7.5.1-23), respectively, using the FTS-2 L2 pre-processing result.
CH_4 profile (15 layer)	A priori value and its variance-covariance matrix are calculated by Eqs. (4.7.5.1-22) and (4.7.5.1-23), respectively, using the FTS-2 L2 pre-processing result.
CO profile (15 layer)	A priori value and its variance-covariance matrix are calculated by Eqs. (4.7.5.1-22) and (4.7.5.1-23), respectively, using the FTS-2 L2 pre-processing result.
H_2O profile (15 layer)	A priori value and its variance-covariance matrix are calculated by Eqs. (4.7.5.1-22) and (4.7.5.1-23), respectively, using the FTS-2 L2 pre-processing result.
aerosol profile (15 layer, 2 type)	A priori value is a logarithm of the optical thickness at reference wavelength calculated by Eq. (4.7.5.4-8) using the FTS-2 L2 pre-processing result, and variance is set to $(0.2)^2$.
surface pressure	The FTS-2 L2 pre-processing result is used as a priori value, and variance is set to $(5\ [\mathrm{hPa}])^2$.
temperature shift	A priori value and its variance are set to 0.0 [K] and $(5\ [\mathrm{K}])^2$, respectively.
SIF signal at the reference wavelength	A priori value and its variance are set to 1.0×10^{-9} [W/cm^2/str/cm^{-1}] and $(1.0\times10^{-9}$ [W/cm^2/str/cm^{-1}])^2, respectively. See Eq. (4.7.4-10).
SIF slope for wavenumber	A priori value and its variance are set to 1.8×10^{-3} [cm] and $(7.0\times10^{-4}$ [cm])^2, respectively. See Eq. (4.7.4-10).
surface albedo	A priori value is calculated by Eq. (4.7.5.7-3). Variance is set to $(0.1)^2$ and $(0.01)^2$ for retrieval processing (SIF & proxy-method) and (full-physics method), respectively.
zero-level offset	A priori value and its variance are set to 0.0 [W/cm^2/str/cm^{-1}] and $(1.0\times10^{-8}$ [W/cm^2/str/cm^{-1}])^2, respectively See Eq. (4.7.4-11).
wavenumber dispersion correction factor	A priori value and its variance are set to 0.0 and $(1.0\times10^{-5})^2$, respectively See Eq. (4.7.4-12).

4.7.5.9 Summary of scattering property and input parameters of *pstar*

Table 4.7.5.9-1 summarizes the correspondence between scattering property and input variables of *pstar*.

Table 4.7.5.9-1. Correspondence between scattering property and input variables of *pstar*.

Input variables of *pstar*	Scattering property
Optical thickness for each layer of RT-layer $\tau_{rl}(\nu)$	$\tau_{rl}(\nu) = \tau_{abs,m,rl}(\nu) + \tau_{sca,m,rl}(\nu) + \Sigma\tau_{a,type,rl}(\nu) + \Sigma\tau_{c,type,rl}(\nu)$ Eqs. (4.7.5.2-2), (4.7.5.3-10), (4.7.5.5-1), and (4.7.5.6-1)
Optical thickness of Rayleigh scattering for each layer of RT-layer $\tau_{sca,m,rl}(\nu)$	Eq. (4.7.5.3-10)
Optical thickness of scattering elements other than Rayleigh scattering by type for each layer of RT-layer $\tau_{sca,p,type,rl}(\nu)$	Eqs. (4.7.5.5-2) and (4.7.5.6-2)
Scattering phase matrix of scattering elements other than Rayleigh scattering by type for each layer of RT-layer $\mathbf{P}_{p,type,rl}(\Theta,\nu)$	Eqs. (4.7.5.5-3) and (4.7.5.6-3)
Depolarization factor of Rayleigh scattering for each layer of RT-layer $\delta_{rl}(\nu)$	Eq. (4.7.5.3-8)
Surface albedo $\alpha(\nu)$	Eq. (4.7.5.7-1)

4.7.6 Jacobian

$\partial \mathbf{I}_{mono}(\nu)/\partial \mathbf{x}$ of the right hand side of Eq. (4.7.4-14) is derived for each state vector element as a function of output variables of *pstar*. The relationship $\partial \mathbf{I}/\partial \ln(x) = x \times \partial \mathbf{I}/\partial x$ is used as necessary.

(a) Layer-averaged dry-air mole fractions of gas

Jacobian with respect to the layer-averaged dry-air mole fractions of gas $C_{gas,ml=lm}$ can be calculated using $\partial \mathbf{I}_{mono}(\nu)/\partial C_{gas,ml=lm}$ in Eq. (4.7.6-1).

$$\begin{aligned}\frac{\partial \mathbf{I}_{mono}(\nu)}{\partial C_{gas,ml=lm}} &= \sum_{lr \in lm} \frac{\partial \tau_{abs,gas,ml=lm(lr)}(\nu)}{\partial C_{gas,ml=lm(lr)}} \cdot \frac{\partial \tau_{abs,gas,rl=lr}(\nu)}{\partial \tau_{abs,gas,ml=lm(lr)}(\nu)} \cdot \frac{\partial \mathbf{I}_{mono}(\nu)}{\partial \tau_{abs,rl=lr}(\nu)} \\ &= \frac{f_{\mathbf{I}} \cdot \left[\tau_{abs,gas,ml=lm}(\nu) + \Delta\tau_{ml=lm} \right]}{C_{gas,ml=lm}} \cdot \sum_{lr \in lm} frc_{RT}(lr) \cdot \frac{\partial \mathbf{I}_{RT}(\nu)}{\partial \tau_{abs,rl=lr}(\nu)}\end{aligned} \tag{4.7.6-1}$$

$$\Delta\tau_{ml=lm} = \begin{cases} C_{H_2O,ml=lm} \cdot \sum_{ls \in lm} w_{H_2O,sl=ls} \cdot \dfrac{\partial \sigma_{abs,H_2O,sl=ls}(\nu)}{\partial C_{H_2O,sl=ls}} & for\ H_2O \\ 0 & others \end{cases} \tag{4.7.6-2}$$

$$\begin{aligned}&\frac{\partial \sigma_{abs,H_2O,sl=ls}(\nu)}{\partial C_{H_2O,sl=ls}} \\ &= \left[ak_{cnt,slf}(\nu; T_{sl=ls}) - ak_{cnt,frn}(\nu; T_{sl=ls}) \right] \cdot \frac{p_{sl=ls}}{p_0} \cdot \frac{T_0}{T_{sl=ls}} \cdot \frac{10^6}{\left(10^6 + C_{H_2O,sl=ls}\right)^2}\end{aligned} \tag{4.7.6-3}$$

(b) Logarithm of aerosol optical thickness by type at reference wavelength

Jacobian with respect to the logarithm of aerosol optical thickness by type at reference wavelength $\ln(\tau_{a,type,ml=lm})$ can be calculated using $\partial \mathbf{I}_{mono}(\nu)/\partial \ln(\tau_{a,type,ml=lm})$ in Eq. (4.7.6-4).

$$
\begin{aligned}
&\frac{\partial \mathbf{I}_{mono}(\nu)}{\partial \ln\left(\tau_{a,type,ml=lm}\left(\nu_{ref}\right)\right)} \\
&= \sum_{lr \in lm} \frac{\partial \tau_{abs,a,type,ml=lm(lr)}(\nu)}{\partial \ln\left(\tau_{a,type,ml=lm}\left(\nu_{ref}\right)\right)} \cdot \frac{\partial \tau_{abs,rl=lr}(\nu)}{\partial \tau_{abs,a,type,ml=lm(lr)}(\nu)} \cdot \frac{\partial \mathbf{I}_{mono}(\nu)}{\partial \tau_{abs,rl=lr}(\nu)} \\
&+ \sum_{lr \in lm} \frac{\partial \tau_{sca,a,type,ml=lm(lr)}(\nu)}{\partial \ln\left(\tau_{a,type,ml=lm}\left(\nu_{ref}\right)\right)} \cdot \frac{\partial \tau_{sca,a,type,rl=lr}(\nu)}{\partial \tau_{sca,a,type,ml=lm(lr)}(\nu)} \cdot \frac{\partial \mathbf{I}_{mono}(\nu)}{\partial \tau_{sca,a,type,rl=lr}(\nu)} \\
&= f_{\mathbf{I}} \cdot \tau_{abs,a,type,ml=lm}(\nu) \cdot \sum_{lr \in lm} frc_{RT}(lr) \cdot \frac{\partial \mathbf{I}_{RT}(\nu)}{\partial \tau_{abs,rl=lr}(\nu)} \\
&+ f_{\mathbf{I}} \cdot \tau_{sca,a,type,ml=lm}(\nu) \cdot \sum_{lr \in lm} frc_{RT}(lr) \cdot \frac{\partial \mathbf{I}_{RT}(\nu)}{\partial \tau_{sca,a,type,rl=lr}(\nu)}
\end{aligned}
\tag{4.7.6-4}
$$

(c) Surface pressure

Jacobian with respect to the surface pressure p_{SRF} can be calculated using $\partial \mathbf{I}_{mono}(\nu)/\partial p_{SRF}$ in Eq. (4.7.6-5).

$$\frac{\partial \mathbf{I}_{mono}(\nu)}{\partial p_{SRF}} = \sum_{lr=1}^{Nr} \frac{\partial \tau_{abs,m,rl=lr}(\nu)}{\partial p_{SRF}} \cdot \frac{\partial \mathbf{I}_{mono}(\nu)}{\partial \tau_{abs,rl=lr}(\nu)} + \sum_{lr=1}^{Nr} \frac{\partial \tau_{sca,m,rl=lr}(\nu)}{\partial p_{SRF}} \cdot \frac{\partial \mathbf{I}_{mono}(\nu)}{\partial \tau_{sca,m,rl=lr}(\nu)}$$
$$+ \sum_{lr=1}^{Nr} \sum_{type} \frac{\partial \tau_{abs,a,type,rl=lr}(\nu)}{\partial p_{SRF}} \cdot \frac{\partial \mathbf{I}_{mono}(\nu)}{\partial \tau_{abs,rl=lr}(\nu)}$$
$$+ \sum_{lr=1}^{Nr} \sum_{type} \frac{\partial \tau_{sca,a,type,rl=lr}(\nu)}{\partial p_{SRF}} \cdot \frac{\partial \mathbf{I}_{mono}(\nu)}{\partial \tau_{sca,a,type,rl=lr}(\nu)}$$
$$+ \sum_{lr=1}^{Nr} \sum_{type} \frac{\partial \tau_{abs,c,type,rl=lr}(\nu)}{\partial p_{SRF}} \cdot \frac{\partial \mathbf{I}_{mono}(\nu)}{\partial \tau_{abs,rl=lr}(\nu)}$$
$$+ \sum_{lr=1}^{Nr} \sum_{type} \frac{\partial \tau_{sca,c,type,rl=lr}(\nu)}{\partial p_{SRF}} \cdot \frac{\partial \mathbf{I}_{mono}(\nu)}{\partial \tau_{sca,c,type,rl=lr}(\nu)}$$
$$= f_{\mathbf{I}} \cdot \sum_{lr=1}^{Nr} \frac{\partial \tau_{abs,m,ml=lm(lr)}(\nu)}{\partial p_{SRF}} \cdot frc_{RT}(lr) \cdot \frac{\partial \mathbf{I}_{RT}(\nu)}{\partial \tau_{abs,rl=lr}(\nu)}$$
$$+ f_{\mathbf{I}} \cdot \sum_{lr=1}^{Nr} \tau_{abs,m,ml=lm(lr)}(\nu) \cdot \frac{\partial frc_{RT}(lr)}{\partial p_{SRF}} \cdot \frac{\partial \mathbf{I}_{RT}(\nu)}{\partial \tau_{abs,rl=lr}(\nu)}$$
$$+ f_{\mathbf{I}} \cdot \sum_{lr=1}^{Nr} \frac{\partial \tau_{sca,m,ml=lm(lr)}(\nu)}{\partial p_{SRF}} \cdot frc_{RT}(lr) \cdot \frac{\partial \mathbf{I}_{RT}(\nu)}{\partial \tau_{sca,m,rl=lr}(\nu)}$$
$$+ f_{\mathbf{I}} \cdot \sum_{lr=1}^{Nr} \tau_{sca,m,ml=lm(lr)}(\nu) \cdot \frac{\partial frc_{RT}(lr)}{\partial p_{SRF}} \cdot \frac{\partial \mathbf{I}_{RT}(\nu)}{\partial \tau_{sca,m,rl=lr}(\nu)}$$
$$+ f_{\mathbf{I}} \cdot \sum_{lr=1}^{Nr} \sum_{type} \tau_{abs,a,type,ml=lm(lr)}(\nu) \cdot \frac{\partial frc_{RT}(lr)}{\partial p_{SRF}} \cdot \frac{\partial \mathbf{I}_{RT}(\nu)}{\partial \tau_{abs,rl=lr}(\nu)}$$
$$+ f_{\mathbf{I}} \cdot \sum_{lr=1}^{Nr} \sum_{type} \tau_{sca,a,type,ml=lm(lr)}(\nu) \cdot \frac{\partial frc_{RT}(lr)}{\partial p_{SRF}} \cdot \frac{\partial \mathbf{I}_{RT}(\nu)}{\partial \tau_{sca,a,type,rl=lr}(\nu)}$$
$$+ f_{\mathbf{I}} \cdot \sum_{lr=1}^{Nr} \sum_{type} \tau_{abs,c,type}(\nu) \cdot \frac{\partial frc_{CLD,type}(lr)}{\partial p_{SRF}} \cdot \frac{\partial \mathbf{I}_{RT}(\nu)}{\partial \tau_{abs,rl=lr}(\nu)}$$
$$+ f_{\mathbf{I}} \cdot \sum_{lr=1}^{Nr} \sum_{type} \tau_{sca,c,type}(\nu) \cdot \frac{\partial frc_{CLD,type}(lr)}{\partial p_{SRF}} \cdot \frac{\partial \mathbf{I}_{RT}(\nu)}{\partial \tau_{sca,a,type,rl=lr}(\nu)}$$

(4.7.6-5)

$$\frac{\partial \tau_{abs,m,ml=lm}(\nu)}{\partial p_{SRF}}$$
$$= \sum_{gas} \sum_{ls \in lm} \left[\frac{\partial p_{sl=ls}}{\partial p_{SRF}} \cdot \frac{\partial \sigma_{abs,gas,sl=ls}(\nu; p_{sl=ls}, T_{sl=ls})}{\partial p_{sl=ls}} \cdot w_{gas,sl=ls} \right] + \frac{\tau_{abs,m,ml=lm}(\nu)}{p_{SRF} - p_{TOA}}$$

(4.7.6-6)

$$\frac{\partial p_{sl=ls}}{\partial p_{SRF}} = \begin{cases} \dfrac{\left[\dfrac{ls \cdot p_{sb=ls+1}}{Nd} + \dfrac{(ls-1)\cdot p_{sb=ls}}{Nd}\right]\cdot\left(1-\dfrac{p_{mb=1}}{p_{mb=2}}\right)}{2\cdot\left(p_{SRF}-p_{TOA}\right)} & 1 \le ls \le Nd \\ \dfrac{p_{sl=ls}-p_{TOA}}{p_{SRF}-p_{TOA}} & Nd+1 \le ls \le Ns+1 \end{cases} \tag{4.7.6-7}$$

$$\frac{\partial \sigma_{abs,gas,sl=ls}\left(\nu; p_{sl=ls}, T_{sl=ls}\right)}{\partial p_{sl=ls}} = \begin{cases} \dfrac{\partial ak_{gas}\left(\nu; p_{sl=ls}, T_{sl=ls}\right)}{\partial p_{sl=ls}} \\ +ak_{cnt,slf}\left(\nu; T_{sl=ls}\right)\cdot\dfrac{1}{p_0}\cdot\dfrac{T_0}{T_{sl=ls}}\cdot\dfrac{C_{H_2O,sl=ls}}{10^6+C_{H_2O,sl=ls}} & for\ H_2O \\ +ak_{cnt,frn}\left(\nu; T_{sl=ls}\right)\cdot\dfrac{1}{p_0}\cdot\dfrac{T_0}{T_{sl=ls}}\cdot\dfrac{10^6}{10^6+C_{H_2O,sl=ls}} & \\ \dfrac{\partial ak_{gas}\left(\nu; p_{sl=ls}, T_{sl=ls}\right)}{\partial p_{sl=ls}} & others \end{cases} \tag{4.7.6-8}$$

$$\begin{aligned} \frac{\partial ak_{gas}(\nu; p, T)}{\partial p} = & -\frac{1}{p_{i+1}-p_i}\cdot\frac{T_{i,j+1}-T}{T_{i,j+1}-T_{i,j}}\cdot ak_{gasLUT,i,j}(\nu) \\ & -\frac{1}{p_{i+1}-p_i}\cdot\frac{T-T_{i,j}}{T_{i,j+1}-T_{i,j}}\cdot ak_{gasLUT,i,j+1}(\nu) \\ & +\frac{1}{p_{i+1}-p_i}\cdot\frac{T_{i+1,k+1}-T}{T_{i+1,k+1}-T_{i+1,k}}\cdot ak_{gasLUT,i+1,k}(\nu) \\ & +\frac{1}{p_{i+1}-p_i}\cdot\frac{T-T_{i+1,k}}{T_{i+1,k+1}-T_{i+1,k}}\cdot ak_{gasLUT,i+1,k+1}(\nu) \end{aligned} \tag{4.7.6-9}$$

$$\frac{\partial \tau_{sca,m,ml=lm}(\nu)}{\partial p_{SRF}} = \frac{\tau_{sca,m,ml=lm}(\nu)}{p_{SRF}-p_{TOA}} \tag{4.7.6-10}$$

$$\frac{\partial frc_{RT}(lr)}{\partial p_{SRF}} = \begin{cases} \dfrac{-Nm\cdot\left(p_{rb=lr+1}-p_{rb=lr}\right)}{\left(p_{SRF}-p_{TOA}\right)^2} & \begin{cases} p_{rb=lr}\notin p_{mb} \\ p_{rb=lr+1}\notin p_{mb} \end{cases} \\ \dfrac{\left[lm(lr+1)-1\right]\cdot\left(p_{SRF}-p_{TOA}\right)-Nm\cdot\left(p_{rb=lr+1}-p_{rb=lr}\right)}{\left(p_{SRF}-p_{TOA}\right)^2} & \begin{cases} p_{rb=lr}\notin p_{mb} \\ p_{rb=lr+1}\in p_{mb} \end{cases} \\ \dfrac{\left[1-lm(lr)\right]\cdot\left(p_{SRF}-p_{TOA}\right)-Nm\cdot\left(p_{rb=lr+1}-p_{rb=lr}\right)}{\left(p_{SRF}-p_{TOA}\right)^2} & \begin{cases} p_{rb=lr}\in p_{mb} \\ p_{rb=lr+1}\notin p_{mb} \end{cases} \\ 0 & others \end{cases} \tag{4.7.6-11}$$

$$\frac{\partial frc_{CLD,type}(lr)}{\partial p_{SRF}} = \begin{cases} \dfrac{lm(lr+1)-lm(lr)}{Nm\cdot\left(p_{rb=lrbot_{type}}-p_{rb=lrtop_{type}}\right)} & \begin{cases} lrtop_{type}\le lr\le lrbot_{type}-1 \\ p_{rb=lr}\in p_{mb} \\ p_{rb=lr+1}\in p_{mb} \end{cases} \\ \dfrac{lm(lr+1)-1}{Nm\cdot\left(p_{rb=lrbot_{type}}-p_{rb=lrtop_{type}}\right)} & \begin{cases} lrtop_{type}\le lr\le lrbot_{type}-1 \\ p_{rb=lr}\notin p_{mb} \\ p_{rb=lr+1}\in p_{mb} \end{cases} \\ \dfrac{1-lm(lr)}{Nm\cdot\left(p_{rb=lrbot_{type}}-p_{rb=lrtop_{type}}\right)} & \begin{cases} lrtop_{type}\le lr\le lrbot_{type}-1 \\ p_{rb=lr}\in p_{mb} \\ p_{rb=lr+1}\notin p_{mb} \end{cases} \\ 0 & others \end{cases} \tag{4.7.6-12}$$

(d) Temperature shift

Jacobian with respect to the temperature shift ΔT can be calculated using $\partial \mathbf{I}_{mono}(\nu)/\partial\Delta T$ in Eq. (4.7.6-13).

$$\begin{aligned} \frac{\partial \mathbf{I}_{mono}(\nu)}{\partial\Delta T} &= \sum_{lr=1}^{Nr}\frac{\partial\tau_{abs,rl=lr}(\nu)}{\partial\Delta T}\cdot\frac{\partial \mathbf{I}_{mono}(\nu)}{\partial\tau_{abs,rl=lr}(\nu)} \\ &= f_{\mathbf{I}}\cdot\sum_{lr=1}^{Nr}\frac{\partial\tau_{abs,m,ml=lm(lr)}(\nu)}{\partial\Delta T}\cdot frc_{RT}(lr)\cdot\frac{\partial \mathbf{I}_{RT}(\nu)}{\partial\tau_{abs,rl=lr}(\nu)} \end{aligned} \tag{4.7.6-13}$$

$$\frac{\partial \tau_{abs,m,ml=lm}(\nu)}{\partial \Delta T} = \sum_{gas}\sum_{ls\in lm} \frac{\partial \sigma_{abs,gas,sl=ls}(\nu; p_{sl=ls}, T_{sl=ls})}{\partial T_{sl=ls}} \cdot w_{gas,sl=ls} \tag{4.7.6-14}$$

$$\frac{\partial \sigma_{abs,gas,sl=ls}(\nu; p_{sl=ls}, T_{sl=ls})}{\partial T_{sl=ls}}$$

$$= \begin{cases} \dfrac{\partial ak_{H_2O}(\nu; p_{sl=ls}, T_{sl=ls})}{\partial T_{sl=ls}} \\ \quad + \left[\dfrac{\partial ak_{cnt,slf}(\nu; T_{sl=ls})}{\partial T_{sl=ls}} - \dfrac{ak_{cnt,slf}(\nu; T_{sl=ls})}{T_{sl=ls}} \right] \cdot \dfrac{p_{sl=ls}}{p_0} \cdot \dfrac{T_0}{T_{sl=ls}} \cdot \dfrac{C_{H_2O,sl=ls}}{10^6 + C_{H_2O,sl=ls}} \\ \quad + \left[\dfrac{\partial ak_{cnt,fln}(\nu; T_{sl=ls})}{\partial T_{sl=ls}} - \dfrac{ak_{cnt,fln}(\nu; T_{sl=ls})}{T_{sl=ls}} \right] \cdot \dfrac{p_{sl=ls}}{p_0} \cdot \dfrac{T_0}{T_{sl=ls}} \cdot \dfrac{10^6}{10^6 + C_{H_2O,sl=ls}} \\ \qquad\qquad\qquad\qquad\qquad\qquad\qquad\qquad\qquad\qquad \textit{for } H_2O \\ \dfrac{\partial ak_{O_3}(\nu; p_{sl=ls}, T_{sl=ls})}{\partial T_{sl=ls}} + \dfrac{\partial ak_{cnt,O_3}(\nu; T_{sl=ls})}{\partial T_{sl=ls}} \\ \qquad\qquad\qquad\qquad\qquad\qquad\qquad\qquad\qquad\qquad \textit{for } O_3 \\ \dfrac{\partial ak_{gas}(\nu; p_{sl=ls}, T_{sl=ls})}{\partial T_{sl=ls}} \\ \qquad\qquad\qquad\qquad\qquad\qquad\qquad\qquad\qquad\qquad \textit{others} \end{cases} \tag{4.7.6-15}$$

$$\begin{aligned} \frac{\partial ak_{gas}(\nu; p, T)}{\partial T} = & -\frac{p_{i+1} - p}{p_{i+1} - p_i} \cdot \frac{1}{T_{i,j+1} - T_{i,j}} \cdot ak_{gasLUT,i,j}(\nu) \\ & + \frac{p_{i+1} - p}{p_{i+1} - p_i} \cdot \frac{1}{T_{i,j+1} - T_{i,j}} \cdot ak_{gasLUT,i,j+1}(\nu) \\ & - \frac{p - p_i}{p_{i+1} - p_i} \cdot \frac{1}{T_{i+1,k+1} - T_{i+1,k}} \cdot ak_{gasLUT,i+1,k}(\nu) \\ & + \frac{p - p_i}{p_{i+1} - p_i} \cdot \frac{1}{T_{i+1,k+1} - T_{i+1,k}} \cdot ak_{gasLUT,i+1,k+1}(\nu) \end{aligned} \tag{4.7.6-16}$$

$$\frac{\partial ak_{cnt,gas}(\nu; T)}{\partial T} = \frac{1}{T_{i+1} - T_i} \cdot \left[ak_{cnt,gasLUT,i+1}(\nu) - ak_{cnt,gasLUT,i}(\nu) \right] \tag{4.7.6-17}$$

(e) SIF signal at the reference wavelength

Jacobian with respect to the SIF signal at the reference wavelength SIF_{ref} can be calculated using $\partial \mathbf{I}_{mono}(\nu)/\partial SIF_{ref}$ in Eq. (4.7.6-18).

$$\frac{\partial \mathbf{I}_{mono}(\nu)}{\partial SIF_{ref}} = f_{\mathbf{I}} \cdot \frac{\partial \mathbf{I}_{SIF}(\nu)}{\partial SIF_{ref}}$$

$$= \begin{cases} \begin{pmatrix} f_{\mathbf{I}} \cdot \left[1 + SIF_{slp} \cdot (\nu - 13245)\right] \cdot \exp\left[-\dfrac{\tau_{gas}(\nu)}{|\cos\theta_1|}\right] \\ 0 \\ 0 \\ 0 \end{pmatrix} & \textit{for Band 1} \\ \begin{pmatrix} 0 & 0 & 0 & 0 \end{pmatrix}^T & \textit{for Band 2,3} \end{cases}$$

(4.7.6-18)

(f) SIF slope for wavenumber

Jacobian with respect to the SIF slope for wavenumber SIF_{slp} can be calculated using $\partial \mathbf{I}_{mono}(\nu)/\partial SIF_{slp}$ in Eq. (4.7.6-19).

$$\frac{\partial \mathbf{I}_{mono}(\nu)}{\partial SIF_{slp}} = f_{\mathbf{I}} \cdot \frac{\partial \mathbf{I}_{SIF}(\nu)}{\partial SIF_{slp}}$$

$$= \begin{cases} \begin{pmatrix} f_{\mathbf{I}} \cdot SIF_{ref} \cdot (\nu - 13245) \cdot \exp\left[-\dfrac{\tau_{gas}(\nu)}{|\cos\theta_1|}\right] \\ 0 \\ 0 \\ 0 \end{pmatrix} & \textit{for Band 1} \\ \begin{pmatrix} 0 & 0 & 0 & 0 \end{pmatrix}^T & \textit{for Band 2,3} \end{cases}$$

(4.7.6-19)

(g) Surface albedo

Jacobian with respect to the surface albedo α_i can be calculated using $\partial \mathbf{I}_{mono}(\nu)/\partial \alpha_i$ in Eq. (4.7.6-20).

$$\frac{\partial \mathbf{I}_{mono}(\nu)}{\partial \alpha_i} = f_{\mathbf{I}} \cdot \frac{\partial \alpha(\nu)}{\partial \alpha_i} \cdot \frac{\partial \mathbf{I}_{RT}(\nu)}{\partial \alpha(\nu)} \tag{4.7.6-20}$$

$$\frac{\partial \alpha(\nu)}{\partial \alpha_i} = \begin{cases} \dfrac{\nu_{i+1} - \nu}{\nu_{i+1} - \nu_i} & \nu_{i-1} < \nu \le \nu_i \\ \dfrac{\nu - \nu_i}{\nu_{i+1} - \nu_i} & \nu_i < \nu \le \nu_{i+1} \\ 0 & others \end{cases} \qquad i = 1,2,...,nalbSB \tag{4.7.6-21}$$

(h) Zero-level offset

Jacobian with respect to the zero-level offset $\mathbf{I}_{ZLO}$ can be calculated using $\partial \mathbf{I}_{mono}(\nu)/\partial \mathbf{I}_{ZLO}$ in Eq. (4.7.6-22).

$$\frac{\partial \mathbf{I}_{mono}(\nu)}{\partial \mathbf{I}_{ZLO}} = 1 \tag{4.7.6-22}$$

(i) Wavenumber dispersion correction factor

Jacobian with respect to the wavenumber dispersion correction factor $\Delta\rho$ can be calculated using $\partial \mathbf{I}_{mono}(\nu)/\partial \Delta\rho$ in Eq. (4.7.6-23).

$$\begin{aligned} \frac{\partial \mathbf{I}_{mono}(\nu)}{\partial \Delta\rho} &= f_{\mathbf{I}} \cdot \frac{\partial \left[\mathbf{I}_{RT}(\nu) + \mathbf{I}_{SIF}(\nu)\right]}{\partial \nu} \\ &= f_{\mathbf{I}} \cdot C_{\nu,k-1} \cdot \left[\mathbf{I}_{RT}(\nu_{k-1}) + \mathbf{I}_{SIF}(\nu_{k-1})\right] \\ &\quad + f_{\mathbf{I}} \cdot C_{\nu,k} \cdot \left[\mathbf{I}_{RT}(\nu_k) + \mathbf{I}_{SIF}(\nu_k)\right] \\ &\quad + f_{\mathbf{I}} \cdot C_{\nu,k+1} \cdot \left[\mathbf{I}_{RT}(\nu_{k+1}) + \mathbf{I}_{SIF}(\nu_{k+1})\right] \\ &\quad + f_{\mathbf{I}} \cdot C_{\nu,k+2} \cdot \left[\mathbf{I}_{RT}(\nu_{k+2}) + \mathbf{I}_{SIF}(\nu_{k+2})\right] \end{aligned} \tag{4.7.6-23}$$

$$\begin{cases} C_{\nu,k-1} = \dfrac{(\nu - \nu_{k+1}) \cdot (\nu - \nu_{k+2}) + (\nu - \nu_k) \cdot (\nu - \nu_{k+2}) + (\nu - \nu_k) \cdot (\nu - \nu_{k+1})}{(\nu_{k-1} - \nu_k) \cdot (\nu_{k-1} - \nu_{k+1}) \cdot (\nu_{k-1} - \nu_{k+2})} \\ C_{\nu,k} = \dfrac{(\nu - \nu_{k+1}) \cdot (\nu - \nu_{k+2}) + (\nu - \nu_{k-1}) \cdot (\nu - \nu_{k+2}) + (\nu - \nu_{k-1}) \cdot (\nu - \nu_{k+1})}{(\nu_k - \nu_{k-1}) \cdot (\nu_k - \nu_{k+1}) \cdot (\nu_k - \nu_{k+2})} \\ C_{\nu,k+1} = \dfrac{(\nu - \nu_k) \cdot (\nu - \nu_{k+2}) + (\nu - \nu_{k-1}) \cdot (\nu - \nu_{k+2}) + (\nu - \nu_{k-1}) \cdot (\nu - \nu_k)}{(\nu_{k+1} - \nu_{k-1}) \cdot (\nu_{k+1} - \nu_k) \cdot (\nu_{k+1} - \nu_{k+2})} \\ C_{\nu,k+2} = \dfrac{(\nu - \nu_k) \cdot (\nu - \nu_{k+1}) + (\nu - \nu_{k-1}) \cdot (\nu - \nu_{k+1}) + (\nu - \nu_{k-1}) \cdot (\nu - \nu_k)}{(\nu_{k+2} - \nu_{k-1}) \cdot (\nu_{k+2} - \nu_k) \cdot (\nu_{k+2} - \nu_{k+1})} \end{cases} \tag{4.7.6-24}$$

4.8 Post-processing (SIF & proxy method)

Proxy method based column-averaged dry-air mole fractions and some parameters related to the degree of optical path length modification are calculated using the retrieval result (SIF & proxy method). Note: if any of the corresponding retrieval has not converged, a missing value is set.

- XCH_4 (proxy method)

XCH_4 (proxy method) $XCH4_{Proxy}$ is calculated by Eq. (4.8-1) using $XCO2_{B2,CLR}$ and $XCH4_{B2,CLR}$ retrieved by the process ID of "B2_1590" and "B2_1660", respectively.

$$XCH4_{Proxy} = \frac{XCH4_{B2,CLR}}{XCO2_{B2,CLR}} \cdot XCO2_{MDL} \tag{4.8-1}$$

where $XCO2_{MDL}$ is a priori XCO_2 value.

- XCO (proxy method)

XCO (proxy method) XCO_{Proxy} is calculated by Eq. (4.8-2) using $XCO_{B3,CLR}$ and $XCH4_{B3,CLR}$ retrieved by the process ID of "B3_2350".

$$XCO_{Proxy} = \frac{XCO_{B3,CLR}}{XCH4_{B3,CLR}} \cdot XCH4_{Proxy} \tag{4.8-2}$$

- Surface pressure difference

Surface pressure difference Δp_{SRF} is calculated by Eq. (4.8-3) using the retrieved surface pressure $p_{SRF,B1,CLR}$ by the process ID of "B1_Psrf".

$$\Delta p_{SRF} = p_{SRF,B1,CLR} - p_{SRF,prior} \tag{4.8-3}$$

where $p_{SRF,prior}$ is a priori surface pressure value.

- H_2O ratio

H_2O ratio $H2ORatio$ is calculated by Eq. (4.8-4) using the retrieved $XH2O_{B2,CLR}$ and $XH2O_{B3,CLR}$ by the process ID of "B2_1590" and "B3_2060", respectively.

$$H2ORatio = \frac{XH2O_{B3,CLR}}{XH2O_{B2,CLR}} \tag{4.8-4}$$

- CO_2 ratio

CO_2 ratio *CO2Ratio* is calculated by Eq. (4.8-5) using the retrieved $XCO2_{B2,CLR}$ and $XCO2_{B3,CLR}$ by the process ID of "B2_1590" and "B3_2060", respectively.

$$CO2Ratio = \frac{XCO2_{B3,CLR}}{XCO2_{B2,CLR}} \tag{4.8-5}$$

- CH_4 ratio

CH_4 ratio *CH4Ratio* is calculated by Eq. (4.8-6) using the retrieved $XCH4_{B2,CLR}$ and $XCH4_{B3,CLR}$ by the process ID of "B2_1660" and "B3_2350", respectively.

$$CH4Ratio = \frac{XCH4_{B3,CLR}}{XCH4_{B2,CLR}} \tag{4.8-6}$$

4.9 Output of Processing Results

The processing results by the retrievals (SIF & proxy method) and (full-physics method) are output to separate files. Detail of the items stored in these files are shown in Subsection 3.3.2.

4.10 Read of Processing Results by Retrieval Component (SIF & proxy method)

One month's worth of the processing results by the retrieval (SIF & proxy method) shown in Subsection 3.3.2 are read out.

4.11 Data Screening for SIF Radiance Correction

Since, the zero-level offset retrieved by the process ID of “B1_SIF” corresponds to the filling-in signal (FS) described in Section 4.1, the undesirable signal (US) has to be subtracted from FS to obtain SIF (SIF radiance correction). At first, the relationship between the incident radiance and US is evaluated to create the correction table, then, the evaluated table is applied to the SIF radiance correction. In this section, the screening conditions for SIF radiance correction and those for creating the correction table are presented.

<Screening conditions for SIF radiance correction>

The soundings falls in any of the following conditions are excluded from the target of the SIF radiance correction.

- When quality flag of each observation point (FTS-2 L1B Product: QualityInfo/soundingQualityflag) is “Poor” or “NG”.
- When IMC stability flag (FTS-2 L1B Product: QualityInfo/IMC_StabilityFlag) is NOT “Stable”.
- When scan stability flag (FTS-2 L1B Product: QualityInfo/scanStabilityFlag) is NOT “Stable”.

When spike flag (FTS-2 L1B Product: QualityInfo/spikeFlag) of the Band 1P or 1S used for the retrieval processing is NOT “Normal (no spike)”.

When yaw steering flag (FTS-2 L1B Product: SatelliteGeometry/yawSteeringFlag) is NOT “Execute (ON)”.

When land fraction f_{LAND} [%] (Eq. (4.6.2-1)) is less than 100%.

When SNR_{synth} (Eq. (4.5-27)) of Band 1 is less than 70.

When the process ID of “B1_SIF” has not converged.

When any of the state vector elements of the process ID of “B1_SIF” reaches to the maximum or minimum value for the constrained condition Eq. (4.7.1-2).

- When mean squared of the residual spectrum (Eq. (4.7.1-27)) of the process ID of “B1_SIF” is greater than 2.0.

<Screening conditions for creating the correction table for SIF radiance correction>

The sounding that passes the screening condition for SIF radiance correction described above and falls in any of the following conditions is treated as Non-SIF data and used to create the correction table for SIF radiance correction.

When both process ID of “B1_Psrf” and “B2_1590” have converged, and satisfies the condition $R_{B1\_Psrf} < R_{B2\_1590}$.

When both process ID of “B2_1590” and “B3_2060” have converged, and satisfies the condition $R_{B2\_1590} < R_{B3\_2060}$.

$$R_{ID} = \frac{\sum_{i=1}^{nalbSB} \alpha_{SB,i}}{nalbSB} \tag{4.11-1}$$

where subscript *ID* denotes the process ID shown in Tables 4.7.2-1 ~ 4.7.2-6.

4.12 Creating Correction Table for SIF Radiance Correction

The correction table for SIF radiance correction is created from the sounding satisfying the screening conditions for creating the correction table for SIF radiance correction as described in Section 4.11.

The incident radiance level l_r is determined from the maximum radiance $S_{synth,\max}$ within the wavenumber range used in the process ID of “B1_SIF”, minimum radiance of table $S_{tbl,\min}$, and radiance interval Δ_{rad}.

$$l_r = \mathrm{int}\left(\frac{S_{synth,\max} - S_{tbl,\min}}{\Delta_{rad}} \right) \tag{4.12-1}$$

where int(x) represents an integer obtained by truncating the decimal point of x.

The average value of US US_{ave} and its uncertainty US_{err} are calculated for each incident radiance level. When the number of soundings N_{lr} belonging to the incident radiance level l_r is zero, a missing value is set to US_{ave} and US_{err}. The table consisting of N_{lr}, US_{ave}, and US_{err} for each incident radiance level l_r is the correction table for SIF radiance correction.

$$US_{ave,lr} = \frac{\sum_{i=1}^{N_{lr}} \frac{ZLO_{ret,i}}{\sigma_{ZLO,i}^2}}{\sum_{i=1}^{N_{lr}} \frac{1}{\sigma_{ZLO,i}^2}} \tag{4.12-2}$$

$$US_{err,lr} = \sqrt{\frac{1}{\sum_{i=1}^{N_{lr}} \frac{1}{\sigma_{ZLO,i}^2}}} \tag{4.12-3}$$

where subscript i denotes i-th element, and ZLO_{ret} and σ_{ZLO} are retrieval value of zero-level offset and its uncertainty, respectively, obtained by the process ID of "B1_SIF".

4.13 SIF Radiance Correction

SIF radiance correction is conducted for each sounding satisfying the screening conditions of SIF radiance correction. At first, the incident radiance level l_r is determined by Eq. (4.12-1), then corresponding $US_{ave,lr}$ and $US_{err,lr}$ are utilized for the correction, according to the Eqs. (4.13-1) and (4.13-2). If corresponding N_{lr} is zero, a missing value is set.

$$SIF_i = fct_{SIF} \cdot \left(ZLO_{ret,i} - US_{ave,lr} \right) \tag{4.13-1}$$

$$SIF_{uncert,i} = fct_{SIF} \cdot \sqrt{\sigma_{ZLO,i}^2 + US_{err,lr}^2} \tag{4.13-2}$$

where subscript i denotes i-th element, and $fct_{SIF} = 1.7424 \times 10^8$ is the conversion factor of radiance unit from [W/cm^2/str/cm^{-1}] to [mW/m^2/nm/str].

4.14 Quality Assessment (Chlorophyll Fluorescence and Proxy Method)

Attach quality flags on a four-level scale, i.e., Good/Fair/Poor/NG, to each sounding in the following major dataset of the FTS-2 SWIR L2 Chlorophyll Fluorescence and Proxy Method Product: corrected chlorophyll fluorescence at 755 nm (FTS-2 SWIR L2 Product: SolarInducedFluorescence/SIF), XCH_4 (proxy method) (FTS-2 SWIR L2 Product: GasColumn_Proxy/XCH4_proxy), and XCO (proxy method) (FTS-2 SWIR L2 Product: GasColumn_Proxy/XCO_proxy).

<Corrected chlorophyll fluorescence at 755 nm>

Set the quality flag of the sounding that falls in any of the following conditions to "NG".

- When the sounding is excluded from the process ID of "B1_SIF" (see Subsection 4.6.1).
- When the process ID of "B1_SIF" has not converged (see Subsection 4.7.1).
- When the sounding is excluded from the target of the SIF radiance correction (see Section 4.11).

Of the remaining sounding, set the quality flag of the sounding that falls in any of the following conditions to "Poor".

- When $N_{lr} = 0$ in the SIF radiance correction (see Section 4.13).

Of the remaining sounding, set the quality flag of the sounding to "Good".

Note: The quality flag "Fair" is not currently defined.

<XCH_4 (proxy method)>

Set the quality flag of the sounding that falls in any of the following conditions to “NG”.

- When the sounding is excluded from the target of either the process ID of “B2_1590” and “B2_1660” (see subsection 4.6.1).
- When either the process ID of “B2_1590” or “B2_1660” has not converged (see subsection 4.7.1).

Of the remaining sounding, set the quality flag of the sounding that falls in any of the following conditions to “Poor”.

- When one of the average of the radiance normalized with noise level for each polarization used for FTS-2 2 μm band cloud determination is greater than or equal to 10.0.
- When the mean squared of the residual spectrum of the process ID of “B2_1590” is greater than or equal to 2.0.
- When the mean squared of the residual spectrum of the process ID of “B2_1660” is greater than or equal to 2.5.
- When DFS of XCO_2 of the process ID of “B2_1590” is less than 0.8.
- When DFS of XCH_4 of the process ID of “B2_1660” is less than 0.8.

Of the remaining sounding, set the quality flag of the sounding that falls in any of the following conditions to “Fair”.

- When DFS of XCO_2 of the process ID of “B2_1590” is less than 1.0.
- When DFS of XCH_4 of the process ID of “B2_1660” is less than 1.0.

Of the remaining sounding, set the quality flag of the sounding to “Good”.

<XCO (proxy method)>

Set the quality flag of the sounding that falls in any of the following conditions to “NG”.

- When the sounding is excluded from the target of the process ID of “B3_2350” (see subsection 4.6.1).
- When process ID of “B3_2350” has not converged (see subsection 4.7.1).
- When the quality flag for XCH_4 (proxy method) is “NG”.

Of the remaining sounding, set the quality flag of the sounding that falls in any of the following conditions to “Poor”.

- When the mean squared of the residual spectrum of the process ID of “B3_2350” is greater than or equal to 2.5.
- When either DFS of XCO or DFS of XCH_4 of the process ID of “B3_2350” is less than 0.8.
- When the quality flag for XCH_4 (proxy method) is “Poor”.

Of the remaining sounding, set the quality flag of the sounding that falls in any of the following conditions to “Fair”.

- When either DFS of XCO or DFS of XCH_4 of the process ID of “B3_2350” is less than 1.0.
- When the quality flag for XCH_4 (proxy method) is “Fair”.

Of the remaining sounding, set the quality flag of the sounding to “Good”.

4.15 Generate FTS-2 SWIR L2 Chlorophyll Fluorescence and Proxy Method Product

The processing results of the post-processing component (chlorophyll fluorescence and proxy method) are output to the daily files in HDF5 format. Detail of the items and format are shown in subsection 3.2.1 and “NIES GOSAT-2 Product File Format Description (Product edition) Vol. 4: GOSAT-2 TANSO-FTS-2 SWIR L2 Chlorophyll Fluorescence and Proxy-method Product”, respectively.

4.16 Read of Processing Results by Retrieval Component (full-physics method)

One month's worth of the processing results by the retrieval (full-physics method) shown in subsection 3.3.2 are read out.

4.17 Quality Assessment (Column-averaged Dry-air Mole Fraction)

Attach quality flags on a four-level scale, i.e., Good/Fair/Poor/NG, to each sounding in the following major dataset of the FTS-2 SWIR L2 Column-averaged Dry-air Mole Fraction Product: XCO_2 (FTS-2 SWIR L2 Product: RetrievalResult/xco2), XCH_4 (FTS-2 SWIR L2 Product: RetrievalResult/xch4), XCO (FTS-2 SWIR L2 Product: RetrievalResult/xco), and XH_2O (FTS-2 SWIR L2 Product: RetrievalResult/xh2o). On the following conditions, add "(common)" to the conditions common to all gases, and add "(unique)" to the conditions unique to each gas.

Set the quality flag of the sounding that falls in any of the following conditions to "NG".

- (Common): When the sounding is excluded from the target of the process ID of "SWFP" (see subsection 4.6.2).
- (Common): When the process ID of "SWFP" has not converged (see subsection 4.7.1).

Of the remaining sounding, set the quality flag of the sounding that falls in any of the following conditions to "Poor".

- (Unique): When DFS of each gas of the process ID of "SWFP" is less than 0.8.

Of the remaining sounding, set the quality flag of the sounding that falls in any of the following conditions to "Fair".

- (Common): When the mean squared of the residual spectrum of the sub-band 1 of the process ID of "SWFP" is greater than or equal to 1.5.
- (Common): When the mean squared of the residual spectrum of the sub-band 3 of the process ID of "SWFP" is greater than or equal to 1.6.
- (Common): When the blended albedo (Eq. (4.17-1)) of the process ID of "SWFP" is greater than 1.0.
- (Common): When the retrieved surface pressure of the process ID of "SWFP" reaches to the maximum or minimum value for the constrained condition Eq. (4.7.1-2).
- (Unique): When DFS of each gas of the process ID of "SWFP" is less than 1.0.

Of the remaining sounding, set the quality flag of the sounding to "Good".

$$blended\_albedo = 2.4 \cdot \overline{\alpha}_{SB=1} - 1.13 \cdot \overline{\alpha}_{SB=4} \tag{4.17-1}$$

$$\overline{\alpha}_{SB} = \frac{0.5 \cdot \left(\alpha_{SB,1} + \alpha_{SB,nalbSB} \right) + \sum_{i=2}^{nalbSB-1} \alpha_{SB,i}}{nalbSB - 1} \tag{4.17-2}$$

4.18 Generate FTS-2 SWIR L2 Column-averaged Dry-air Mole Fraction Product

The processing results of the post-processing component (column-averaged dry-air mole fraction), except for the sounding with its quality flag of "NG", are output to the daily files in HDF5 format. Detail of the items and format are shown in subsection 3.2.2 and "NIES GOSAT-2 Product File Format Description (Product edition) Vol. 5: GOSAT-2 TANSO-FTS-2 SWIR L2 Column-averaged Dry-air Mole Fraction Product", respectively.

5. Verification of Algorithm

The FTS-2 SWIR L2 algorithm is verified by evaluating the data quality of the retrieval results.

To evaluate the data quality of the retrieved Xgas, Xgas obtained by the Total Carbon Column Observing Network (TCCON) Project (Wunch et al., 2011) as well as Xgas calculated from the vertical profile of gas concentration observed by aircraft, such as Comprehensive Observation Network for Trace gases by Airliner (CONTRAIL) Project (Machida et al., 2008, Matsueda et al., 2008), are planned to use.

As for the retrieved SIF, its data quality is planned to evaluate through the inter-satellite comparison.

6. Precondition and Restriction

Some FTS-2 SWIR instrument characteristics are pre-processed for the FTS-2 SWIR L2 processing. See Note 2 in Table 3.3-1 for more details.

In Sections 4.4 and 4.5, the nominal values of wavenumber interval, beginning wavenumber, and ending wavenumber are assumed to be the same for P- and S-polarization components.

In Section 4.5, following assumptions are made:

- Stokes parameter V_{in} is negligibly small.
- Stokes parameters Q_{in} and U_{in} are related by the single-scattering approximation (Eq. (4.5-22)).
- Difference between ILSF for P- and S-polarization component can be ignored.
- The wavenumber dependencies denoted by $A_{P/S} \sim D_{P/S}$ in Eqs. (4.5-14) ~ (4.5-21) can be ignored in the range of the convolution integral.

In Subsection 4.7.2, following assumptions are made:

- The Lambertian surface is assumed regardless the actual land fraction within the FTS-2 IFOV-area.
- Use the polarization synthesized spectrum as the observed spectrum.
- Cloud- and aerosol-free condition is assumed for the retrieval (SIF & proxy method).
- Cloud-free condition is assumed for the retrieval (full-physics method).

In Subsection 4.7.4, following assumptions are made:

- Plane-parallel atmosphere is assumed to the radiative transfer code *pstar*.
- For the highspeed radiative transfer calculation method, the wavenumber dependencies of the cloud and aerosol scattering properties are expressed as the linear function within the wavenumber range of each sub-band. Furthermore, thermal radiation is not considered, and SIF observed by satellite can be approximated by SIF at the surface attenuated by gas absorption.

7. References

Baum, B.A., P. Yang, A.J. Heymsfield, A. Bansemer, B.H. Cole, A. Merrelli, C. Schmitt, and C. Wang (2014): Ice cloud single-scattering property models with the full phase matrix at wavelengths from 0.2 to 100 μm. J. Quant. Spectrosc. Radiat. Transf., 146, 123-139.

Bodhaine, B.A., N.B. Wood, E.G. Dutton, and J.R. Slusser (1999): On Rayleigh optical depth calculation. J. Atmos. Ocean. Tech., 16, 1854-1861.

Cox, C., and W.H. Munk (1954): Measurement of the roughness of the sea surface from photographs of the Sun's glitter. J. Opt. Soc. Am., 44, 838-850.

Devi, V.M., D.C. Benner, M.A.H. Smith, A.W. Mantz, K. Sung, L.R. Brown, and A. Predoi-Cross (2012): Spectral line parameters including temperature dependences of self- and air-broadening in the 2 ← 0 band of CO at 2.3 μm. J. Quant. Spectrosc. Radiat. Transf., 113, 1013-1033.

Devi, V.M., D.C. Benner, K. Sunk, T.J. Crawford, S. Yu, L.R. Brown, M.A.H. Smith, A.W. Mantz, V. Boudon, and S. Ismail (2015): Self- and air-broadened line shapes in the 2ν3 P and R branches of 12CH4. J. Mol. Spectrosc., 315, 114-136.

Devi, V.M., D.C. Benner, K. Sung, L.R. Brown, T.J. Crawford, S. Yu, M.A.H. Smith, A.W. Mantz, V. Boudon, and S. Ismail (2016): Spectral line parameters including line shapes in the 2ν3 Q branch of 12CH4. J. Quant. Spectrosc. Radiat. Transf., 177, 152-169.

Drouin, B.J., D.C. Benner, L.R. Brown, M.J. Cich, T.J. Crawford, V.M. Devi, A. Guillaume, J.T. Hodges, E.J. Mlawer, D.J. Robichaud, F. Oyafuso, V.H. Payne, K. Sung, E.H. Wishnow, and S. Yu (2017): Multispectrum analysis of the oxygen A-band. J. Quant. Spectrosc. Radiat. Transf., 186, 118-138.

Duan, M., Q. Min, and J. Li (2005): A fast radiative transfer model for simulating high-resolution absorption bands, J. Geophys. Res., 110, D15201, doi:10.1029/2004JD005590.

Frankenberg, C., I. Aben, P. Bergamaschi, E.J. Dlugokencky, R. van Hees, S. Houweling, P. van der Meer, R. Snel, and P. Tol (2011a): Global column-averaged methane mixing ratios from 2003 to 2009 as derived from SCIAMACHY: Trends and variability. J. Geophys. Res., 116, D04302, doi:10.1029/2010JD014849.

Frankenberg, C., J.B. Fisher, J. Worden, G. Badgley, S.S. Saatchi, J.-E. Lee, G.C. Toon, A. Butz, M. Jung, A. Kuze, and T. Yokota (2011b): New global observations of the terrestrial carbon cycle from GOSAT: Patterns of plant fluorescence with gross primary productivity. Geophys. Res. Lett., 38, L17706, doi:10.1029/2011GL048738.

Gordon, I.E., L.S. Rothman, C. Hill, R.V. Kochanov, Y. Tan, P.F. Bernath, M. Birk, V. Boudon, A. Campargue, K.V. Chance, B.J. Drouin, J.-M. Flaud, R.R. Gamache, J.T. Hodges, D. Jacquemart, V.I. Perevalov, A. Perrin, K.P. Shine, M.-A.H. Smith, J. Tennyson, G.C. Toon, H. Tran, V.G. Tyuterev, A. Barbe, A.G. Császár, V.M. Devi, T. Furtenbacher, J.J. Harrison, J.-M. Hartmann, A. Jolly, T.J. Johnson, T. Karman, I Kleiner, A.A. Kyuberis, J. Loos, O.M. Lyulin, S.T. Massie, S.N. Mikhailenko, N. Moazzen-Ahmadi, H.S.P. Müller, O.V. Naumenko, A.V. Nikitin, O.L. Polyansky, M. Rey, M. Rotger, S.W. Sharpe, K. Sung, E. Starikova, S.A. Tashkun, J. Vander Auwera, G. Wagner, J. Wilzewski, P. Wcisło, S. Yu, and E.J. Zak (2017): The HITRAN2016 molecular spectroscopic database. J. Quant. Spectrosc. Radiat. Transf., 203, 3-69.

Lamouroux, J., H. Tran, A.L. Laraia, R.R. Gamache, L.S. Rothman, I.E. Gordon, and J.-M. Hartmann (2010): Updated database plus software for line-mixing in CO2 infrared spectra and their test using laboratory spectra in the 1.5-2.3 μm region. J. Quant. Spectrosc. Radiat. Transf., 111, 2321-2331.

Liou, K.N. (2002): An Introduction to Atmospheric Radiation: Second Edition. Academic Press, New York.

Machida, T., H. Matsueda, Y. Sawa, Y. Nakagawa, K. Hirotani, N. Kondo, K. Goto, T. Nakazawa, K. Ishikawa, and T. Ogawa (2008): Worldwide measurements of atmospheric CO_2 and other trace gas species using commercial airlines. J. Atmos. Oceanic. Technol., 25, 1744-1754, doi:10.1175/2008JTECHA1082.1.

Matsueda, H., T. Machida, Y. Sawa, Y. Nakagawa, K. Hirotani, H. Ikeda, N. Kondo, and K. Goto (2008): Evaluation of atmospheric CO_2 measurements from new flask air sampling of JAL airliner observations. Pap. Meteorol. Geophys., 59, 1-17, doi:10.2467/mripapers.59.1.

Mlawer, E.J., V.H. Payne, J.-L. Moncet, J.S. Delamere, M.J. Alvarado, and D.C. Tobin (2012): Development and recent evaluation of the MT_CKD model of continuum absorption. Phil. Trans. R. Soc. A, 370, 2520-2556.

Nakagawa, T and Y. Oyanagi (1982): *Experimental data analysis by the least square method: The program SALS*. University Tokyo Press, Tokyo (in Japanese, Japanese title translated).

Nakajima, T., and M. Tanaka (1988): Algorithms for radiative intensity calculations in moderately thick atmospheres using a truncation approximation. J. Quant. Spectrosc. Radiat. Transf., 40, 51-69.

Ota, Y., A. Higurashi, T. Nakajima, and T. Yokota (2010): Matrix formulations of radiative transfer including the polarization effect in a coupled atmosphere-ocean system. J. Quant. Spectrosc. Radiat. Transf., 111, 878-894.

Parker, R., H. Boesch, A. Cogan, A. Fraser, L. Feng, P.I. Palmer, J. Messerschmidt, N. Deutscher, D.W.T. Griffith, J. Notholt, P.O. Wennberg, and D. Wunch (2011): Methane observations from the Greenhouse Gases Observing SATellite: Comparison to ground-based TCCON data and model calculations. Geophys. Res. Lett., 38, L15807, doi:10.1029/2011GL047871.

Rodgers, C.D. (2000): *Inverse Methods for Atmospheric Sounding: Theory and Practice.* World Sci., Singapore.

Suto, H., F. Kataoka, N. Kikuchi, R.O. Knuteson, A. Butz, M. Haun, H. Buijs, K. Shiomi, H. Imai, and A. Kuze (2020): Thermal and near-infrared sensor for carbon observation Fourier-transform spectrometer-2 (TANSO-FTS-2) on the Greenhouse Gases Observing Satellite-2 (GOSAT-2) during its first year on orbit. Atmos. Meas. Tech. Disscuss., https://doi.org/10.5194/amt-2020-360, in review.

Toon, G.C. (2015a): Atmospheric line list for the 2014 TCCON data release (Version GGG2014.R0). TCCON data archive, hosted by CaltechDATA, California Institute of Technology, Pasadena, CA, USA, https://doi.org/10.14291/TCCON.GGG2014.ATM.R0/1221656.

Toon, G.C. (2015b): Solar line list for the TCCON 2014 data release (Version GGG2014.R0). TCCON data archive, hosted by CaltechDATA, California Institute of Technology, Pasadena, CA, USA, https://doi.org/10.14291/TCCON.GGG2014.SOLAR.R0/1221658.

Wunch, D., Toon, G.C., Blavier, J.-F.L., Washenfelder, R.A., Notholt, J., Connor, B.J., Griffith, D.W.T., Sherlock, V., and Wennberg, P.O. (2011): The Total Carbon Column Observing Network (TCCON). Philos. T. Roy. Soc. A., 369, 2087-2112, doi:10.1098/rsta.2010.0240.

Xiao, F., T. Yabe, and T. Ito (1996): Constructing oscillation preventing scheme for advection equation by rational function. Comput. Phys. Commun., 93, 1-12.